IEC TR 63401-1

Edition 1.0 2022-11

TECHNICAL REPORT

colour inside

Dynamic characteristics of inverter-based resources in bulk power systems – Part 1: Interconnecting inverter-based resources to low short circuit ratio AC networks

IEC TR 63401-1:2022-11(en)

IEC Secretariat
3, rue de Varembé
CH-1211 Geneva 20
Switzerland

Tel.: +41 22 919 02 11
info@iec.ch
www.iec.ch

About the IEC
The International Electrotechnical Commission (IEC) is the leading global organization that prepares and publishes International Standards for all electrical, electronic and related technologies.

About IEC publications
The technical content of IEC publications is kept under constant review by the IEC. Please make sure that you have the latest edition, a corrigendum or an amendment might have been published.

IEC publications search - webstore.iec.ch/advsearchform
The advanced search enables to find IEC publications by a variety of criteria (reference number, text, technical committee, …). It also gives information on projects, replaced and withdrawn publications.

IEC Just Published - webstore.iec.ch/justpublished
Stay up to date on all new IEC publications. Just Published details all new publications released. Available online and once a month by email.

IEC Customer Service Centre - webstore.iec.ch/csc
If you wish to give us your feedback on this publication or need further assistance, please contact the Customer Service Centre: sales@iec.ch.

IEC Products & Services Portal - products.iec.ch
Discover our powerful search engine and read freely all the publications previews. With a subscription you will always have access to up to date content tailored to your needs.

Electropedia - www.electropedia.org
The world's leading online dictionary on electrotechnology, containing more than 22 300 terminological entries in English and French, with equivalent terms in 19 additional languages. Also known as the International Electrotechnical Vocabulary (IEV) online.

IEC TR 63401-1

Edition 1.0 2022-11

TECHNICAL REPORT

Dynamic characteristics of inverter-based resources in bulk power systems – Part 1: Interconnecting inverter-based resources to low short circuit ratio AC networks

INTERNATIONAL
ELECTROTECHNICAL
COMMISSION

ICS 29.020

ISBN 978-2-8322-6143-9

CONTENTS

INTERNATIONAL ELECTROTECHNICAL COMMISSION

_____

DYNAMIC CHARACTERISTICS OF INVERTER-BASED RESOURCES IN BULK POWER SYSTEMS –

Part 1: Interconnecting inverter-based resources to low short circuit ratio AC networks

FOREWORD

1) The International Electrotechnical Commission (IEC) is a worldwide organization for standardization comprising all national electrotechnical committees (IEC National Committees). The object of IEC is to promote international co-operation on all questions concerning standardization in the electrical and electronic fields. To this end and in addition to other activities, IEC publishes International Standards, Technical Specifications, Technical Reports, Publicly Available Specifications (PAS) and Guides (hereafter referred to as "IEC Publication(s)"). Their preparation is entrusted to technical committees; any IEC National Committee interested in the subject dealt with may participate in this preparatory work. International, governmental and non-governmental organizations liaising with the IEC also participate in this preparation. IEC collaborates closely with the International Organization for Standardization (ISO) in accordance with conditions determined by agreement between the two organizations.
2) The formal decisions or agreements of IEC on technical matters express, as nearly as possible, an international consensus of opinion on the relevant subjects since each technical committee has representation from all interested IEC National Committees.
3) IEC Publications have the form of recommendations for international use and are accepted by IEC National Committees in that sense. While all reasonable efforts are made to ensure that the technical content of IEC Publications is accurate, IEC cannot be held responsible for the way in which they are used or for any misinterpretation by any end user.
4) In order to promote international uniformity, IEC National Committees undertake to apply IEC Publications transparently to the maximum extent possible in their national and regional publications. Any divergence between any IEC Publication and the corresponding national or regional publication shall be clearly indicated in the latter.
5) IEC itself does not provide any attestation of conformity. Independent certification bodies provide conformity assessment services and, in some areas, access to IEC marks of conformity. IEC is not responsible for any services carried out by independent certification bodies.
6) All users should ensure that they have the latest edition of this publication.
7) No liability shall attach to IEC or its directors, employees, servants or agents including individual experts and members of its technical committees and IEC National Committees for any personal injury, property damage or other damage of any nature whatsoever, whether direct or indirect, or for costs (including legal fees) and expenses arising out of the publication, use of, or reliance upon, this IEC Publication or any other IEC Publications.
8) Attention is drawn to the Normative references cited in this publication. Use of the referenced publications is indispensable for the correct application of this publication.
9) Attention is drawn to the possibility that some of the elements of this IEC Publication may be the subject of patent rights. IEC shall not be held responsible for identifying any or all such patent rights.

IEC TR 63401-1 has been prepared by subcommittee SC 8A: Grid integration of renewable energy generation, of IEC technical committee TC 8: Systems aspects of electrical energy supply. It is a Technical Report.

The text of this Technical Report is based on the following documents:

Draft TR	Report on voting
8A/109/DTR	8A/113/RVDTR

Full information on the voting for its approval can be found in the report on voting indicated in the above table.

The language used for the development of this Technical Report is English.

This document was drafted in accordance with ISO/IEC Directives, Part 2, and developed in accordance with ISO/IEC Directives, Part 1 and ISO/IEC Directives, IEC Supplement, available at www.iec.ch/members_experts/refdocs. The main document types developed by IEC are described in greater detail at www.iec.ch/standardsdev/publications.

A list of all parts in the IEC 63401 series, published under the general title *Dynamic characteristics of inverter-based resources in bulk power systems*, can be found on the IEC website.

The committee has decided that the contents of this document will remain unchanged until the stability date indicated on the IEC website under webstore.iec.ch in the data related to the specific document. At this date, the document will be

- reconfirmed,
- withdrawn,
- replaced by a revised edition, or
- amended.

IMPORTANT – The "colour inside" logo on the cover page of this document indicates that it contains colours which are considered to be useful for the correct understanding of its contents. Users should therefore print this document using a colour printer.

INTRODUCTION

As the penetration of inverter-based energy generating resources increases, huge challenges to all sections of the power system including planning, operation, control, etc. have been created. The impact on the power grid extends from local to the whole power system. New technical solutions are needed to address the different challenges. The solutions will include the new technologies, methods and practices, to provide more flexibility and improve the efficiency of power systems, constantly balancing generation and load.

The purpose of this document (TR) is to specifically focus on information collection from regulatory agencies, including specifying low short circuit ratio AC networks and the challenges they pose for inverter-based resources, and methods, indexes, and characteristics of low short circuit ratio AC networks. This TR addresses renewable energy (RE) integration in low short circuit ratio AC networks, mainly focusing on the technology development trends, best practices of RE grid integration, and future standardization activities.

The aim of this TR is to create a strategic, technically oriented and referenced document, which presents the core and key issues of interconnecting inverter-based resources to low short circuit ratio AC networks. Renewable energy station developers and owners, transmission systems operators need to have a common understanding of the key issues based on practices and challenges between inverter-based resources and AC networks.

DYNAMIC CHARACTERISTICS OF INVERTER-BASED RESOURCES IN BULK POWER SYSTEMS –

Part 1: Interconnecting inverter-based resources to low short circuit ratio AC networks

1 Scope

As the use of inverter-based RE power generation resources increases, the use of low short circuit ratio AC networks is becoming more common. Considering the advantages of short circuit ratio in stability analysis, the low short circuit ratio is an important indication for describing weak AC networks. This document focuses on technologies and standardization aspects of interconnecting inverter-based resources to low short circuit ratio AC networks. A clear definition of low short circuit ratio AC networks with or without a high proportion of inverter-based resources and the calculation method is described. The adaptability of traditional modelling and analytical method for low short circuit ratio AC networks are discussed. Some new characteristics and challenges will be re-examined, and some adapted control strategies will be studied. This document covers the following major aspects.

In terms of defining a weak AC network, for example the (X/R) ratio, voltage sensitivity, system inertia and the short circuit ratio (SCR) are important characteristics. The definition of low short circuit ratio AC networks in IEEE Std 1204™-1997 [1][1] and in CIGRE B4.62 TB671 [2] is used. Some stability challenges for inverter-based resources in a low short circuit ratio AC network (SCR AC) will be analyzed. There are stability challenges in a low short circuit ratio (SCR) AC network, typically complex static voltage control, risk of failure in fault ride-through situations, strong control interactions and instability.

In terms of identification of low short circuit ratio (SCR) AC networks, some short circuit ratio - like index for various applications is introduced. A wind power plant (WPP) is a power station consisting of a batch of wind turbines or groups of wind turbines, collection lines, main step-up transformers and other equipment. For a single grid-connected WPP system, a fault current based calculation method and an equivalent circuit based calculation method are introduced to make an SCR calculation possible for any given WPP and network topology. For multi grid-connected WPP systems, eigenvalue decomposition based generalized short circuit ratio (gSCR) is then proposed and compared against other approaches referred to as equivalent short circuit ratio (ESCR), composite short circuit ratio (CSCR), and weighted short circuit ratio (WSCR).

In terms of large scale inverter-based resources integration, the steady-state stability analysis methods, including the P-V curve, Q-V curve, and voltage sensitivity analysis, are illustrated. The conventional control strategies of the renewable energy sources are explained. An adaptive controller designed for the photovoltaic (PV) panels, which can maximize the power output capability of PV stations under weak-grid conditions, is presented. Finally, the steady-state voltage stability problem in China that happened recently is illustrated.

[1] Numbers in square brackets refer to the Bibliography.

In terms of the transient state stability issue for low short circuit ratio AC networks after large scale inverter-based resources integration, related issues and phenomena that occur need to be discussed. Undervoltage ride-through (UVRT), overvoltage ride-through (OVRT) and multiple fault ride-through occur easily in a low SCR AC network, which bring risk of failure to fault ride-through. Electromagnetic transient simulations to supplement positive sequence root-mean-square (RMS) simulations are described, and shortfalls of the RMS models and how to identify them in simulations are considered.

In terms of the oscillatory stability issue for low short circuit ratio AC networks after large scale inverter-based resources integration, the impedance-based method is used to analyze the system stability. For the inverter modelling, three typical inverter models are established, including: a) only considering the current controller (CC); b) considering CC and phase-locked loop (PLL); c) considering CC, PLL and voltage controller (VC). Relying on the impedance analysis method, the effect of PLL, CC, number of inverters, SCR of AC grid is discussed. Finally, the additional active damping control method is proposed for suppressing the oscillation phenomenon.

This document discusses the challenges of connecting inverter-based resources to low short circuit ratio AC networks, key technical issues and emerging technologies. There are the steady-state stability issue, transient state stability issue, and oscillatory stability issue, which are the most distinct differences compared to inverter-based resources or traditional generators, and accordingly brings new challenges to operation, control, protection, etc. Therefore, technical solutions are needed. The potential solutions will include new technologies, methods and practices, in order to provide more flexibility and improve the efficiency of power systems. It is expected that this document can also provide guidance for further standardization on relevant issues.

2 Normative references

The following documents are referred to in the text in such a way that some or all of their content constitutes requirements of this document. For dated references, only the edition cited applies. For undated references, the latest edition of the referenced document (including any amendments) applies.

IEC 62934, *Grid integration of renewable energy generation – Terms and definitions*

3 Terms and definitions

For the purposes of this document, the terms and definitions given in IEC 62934 and the following apply.

ISO and IEC maintain terminological databases for use in standardization at the following addresses:

- IEC Electropedia: available at http://www.electropedia.org/
- ISO Online browsing platform: available at http://www.iso.org/obp

3.1
renewable energy
RE
primary energy, the source of which is constantly replenished and will not become depleted

Note 1 to entry: Examples of renewable energy are: wind, solar, geothermal, hydropower, etc.

Note 2 to entry: Fossil fuels are non-renewable.

[SOURCE: IEC 60050-617:2009, 617-04-11]

3.2
inverter
electric energy converter that changes direct electric current to single-phase or polyphase alternating currents

[SOURCE: IEC 60050-151:2001, 151-13-46]

3.3
point of common coupling
PCC
point in an electric power system, electrically nearest to a particular load, at which other loads are, or may be, connected

Note 1 to entry: These loads can be either devices, equipment or systems, or distinct customer's installations

[SOURCE: IEC 60050-614:2016, 614-01-12]

3.4
short circuit current of renewable energy power plant
current that a renewable energy power plant delivers to the point of connection resulting from a short circuit in the external electric power system

3.5
short circuit ratio
SCR
ratio of the three-phase short circuit power at PCC to the nominal active power of a renewable energy power plant or generating unit

Note 1 to entry: SCR is a common analytical indicator used in the industry to quantify system strength.

Note 2 to entry: There is no industry consensus on the exact definition and methodology for calculating the SCR, particularly for applications with several adjacent renewable energy power plants, or for a renewable energy power plant adjacent to HVDC terminals, see CIGRE B4.62 TB 671 [2].

3.6
voltage dip
sudden voltage reduction at a point in an electric power system, followed by voltage recovery after a short time interval, from a few periods of the sinusoidal wave of the voltage to a few seconds

[SOURCE: IEC 60050-614:2016, 614-01-08]

3.7
fault ride-through
FRT
ability of a generating unit or power plant to stay connected during specified faults in the electric power system

3.8
electrical simulation model
set of mathematical formulae or logical functions used in time or frequency domain digital simulations which describe the dynamic characteristics of a facility or certain equipment

3.9
electromechanical simulation
RMS simulation
dynamic simulation method based on the RMS model, which usually focuses on the electromechanical processes of the electric power system under disturbance, and where the typical observation time interval is from several seconds to tens of seconds after disturbance

3.10
electromagnetic transient simulation
EMT simulation
dynamic simulation method to model the electromagnetic transient behaviour of an electric power system, where instantaneous values are used in the process, and the typical observation time interval is from several microseconds to several seconds after a disturbance

3.11
steady state stability
ability of generators in a system to keep operating synchronously and transit to a new stable operating state or recover to the original stable operating state under a small power system disturbance

3.12
transient stability
ability of generators in a system to keep running synchronously and transit to a new stable operating state or recover to the original stable operating state under a large power system disturbance

3.13
sub-synchronous oscillation
electrical oscillation occurring in an electric power system at a frequency smaller than the nominal system frequency and generally sustained for a minute or more

3.14
sub-synchronous resonance
resonance between adjacent equipment in an electric power system, generating oscillations at a frequency smaller than the nominal system frequency and generally sustained for a minute or more

3.15
low-frequency oscillation
electrical oscillation occurring in an electric power system at a frequency usually between 0,1 Hz and 3 Hz

Note 1 to entry: According to an extensive survey of IEEE technical literature, the range 0,1 Hz to 3 Hz covers the majority of low-frequency oscillation events.

4 Characteristics of low short circuit ratio AC networks

4.1 Definition of low short circuit ratio

4.1.1 General

The strength of a power system is a metric used to describe the ability of a power system to maintain the core characteristics through which it interacts with a connection, namely voltage and frequency, as steadily as possible, under all operating conditions. The strength or weakness of a power system is a relative concept and needs to be addressed both in terms of the system characteristics at a given connection point as well as the size of renewable energy to be connected to the connection point.

As indications of system strength, the (X/R) ratio of the system impedance seen from the connection point and the concept of available fault level have also been used. The ability to stably transfer power over a weak transmission system, from a renewable energy station connecting point to stronger parts of a network (where generally the load is) has been quantified by using the sensitivity of the connection point's voltage to the active and reactive power outputs of the renewable energy station. The maximum stable power transfer capability has been derived, providing an insight for renewable energy station designers of the potential issues to be anticipated when power transfer reaches the maximum transfer limits.

Short circuit ratio (SCR), which is a commonly used metric for quantifying the relative power system impedance seen from a connection point, is an important indication of the strength of AC networks. The SCR seen by a generator strongly influences its ability to operate satisfactorily both in steady state and after system disturbances. While this is a very powerful and simple concept, extending its use to describe the shared impedance seen by multiple renewable energy power plants (REPPs) connecting to the same part of a network, electrically close to each other, or close to other power electronic plants such as HVDC converters, has not been unified across the industry.

4.1.2 Low SCR in IEEE Std 1204-1997

SCR is a widely used index for assessment of the strength of the connection point for HVDC links, and in particular for the line current commutated (LCC) and capacitor commutated converter (CCC) technologies. For an HVDC link it is defined as the ratio of fault level at the connection point to the nominal output active power of the link. It is commonly used at the planning stage to give an idea of the likely issues caused by integration of the HVDC link into the network. The SCR seen by a generator strongly influences its ability to operate satisfactorily both in steady state and following system disturbances. While this is a very powerful and simple concept, extending its use to describe the shared impedance seen by multiple REPPs connecting to the same part of a network, electrically close to each other, or close to other power electronic plant such as HVDC converters, has not been unified across the industry.

The SCR can be often obtained from the following formula:

$$SCR = \frac{S}{P_N} \tag{1}$$

where

S is the AC system three-phase symmetrical short circuit level in megavolt-amperes (MVA) at the convertor terminal AC bus with 1,0 p.u. AC terminal voltage;

P_N is the rated AC power in megawatts (MW).

Based on that definition and on typical inverter characteristics (such as the value of the convertor transformer reactance), the following SCR values can be used to classify an AC/DC system:

- a high SCR AC/DC system is categorized by a SCR value greater than 3;
- a low SCR AC/DC system is categorized by a SCR value between 2 and 3;
- a very low SCR AC/DC system is categorized by a SCR value lower than 2.

4.1.3 Low SCR in CIGRE B4.62 TB671

Compared to an HVDC link, a WPP has a significantly more complex topology due to the use of several wind turbines (which may or may not be identical), and the common use of static reactive support plants such as capacitor banks and dynamic reactive support plants such as STATCOMs and synchronous condensers. Additionally, it sometimes happens that several REPPs are located adjacent to each other, or even sometimes connected to the same connection point. This makes it imperative to evaluate the impact of all connected REPPs. The two aspects addressed above are difficult to account for using the conventional calculation method for the SCR. To make it applicable to any given REPP and network topology, an equivalent circuit based calculation method (ESCR) is proposed as elaborated below for various configurations. For multi REPP applications results obtained from this approach will then be compared against two other approaches referred to as composite short circuit ratio (CSCR) and weighted short circuit ratio (WSCR).

1) Composite short circuit ratio (CSCR)

Index based on short circuit ratio, which calculates an aggregate SCR for multiple renewable energy power plants by creating a common bus and tying all renewable energy power plants of interest together at that common bus.

The CSCR can be obtained from the following formula:

$$CSCR = \frac{S_{\text{kv}}}{\sum_{i=1}^{N} P_{ni}} \tag{2}$$

where

S_{kv} is the short circuit power at the virtual common bus without current contribution from the renewable energy power plants;

P_{ni} is the nominal power of renewable energy power plant i;

N is the number of the renewable energy power plants to be considered.

Composite short circuit ratio is used to estimate the equivalent system impedance seen by multiple renewable energy power plants.

2) Weighted short circuit ratio (WSCR)

Another appropriate index for the calculation of impact of adjacent REPPs is the weighted short circuit ratio (WSCR), defined by:

$$WSCR = \frac{\sum_{i=1}^{N} S_{\text{SCMVA}i} \times P_{\text{RMW}i}}{(P_{\text{RMW}i})^2} \tag{3}$$

where

$S_{\text{SCMVA}i}$ is the short circuit capacity at bus i before the connection of REPPi;

$P_{\text{RMW}i}$ is the MW rating of renewable energy station i to be connected;

N is the number of REPPs fully interacting with each other;

i is the renewable energy station index.

The proposed WSCR calculation method is based on the assumption of full interactions between renewable energy stations. This is equivalent to assuming that all renewable energy stations are connected to a virtual POI. For a real power system, there is usually some electrical distance between each renewable energy station's POI and the renewable energy stations will not fully interact with each other. The WSCR obtained with this method gives a conservative estimate of the system strength.

Based on experience obtained from commissioning, field testing, and comparison of RMS-type models against the detailed EMT-type models, the following classification is proposed when dealing with REPPs connected to weak points in the network.

a) Connection is considered to be weak if SCR at the POI is less than 5 or if SCR at the medium voltage collection grid is less than 4 (whichever of these criteria are met).

b) Connection is considered to be very weak if SCR at the POI is less than 3 of if SCR at the medium voltage collection grid is less than 2 (whichever of these criteria are met).

c) For applications with multiple REPPs, it is suggested to use the minimum value obtained from ESCR, CSCR and WSCR indices.

4.2 Stability issues posed by inverter-based resources

4.2.1 General

Low short circuit ratios may raise some instability issues in existing bulk electric systems, and the challenges this poses for inverter-based resources need to be considered in low SCRAC networks.

The example of Xinjiang power grid in China, where most wind farms are located near substations Mahuanggou east and Mahuanggou west, is presented. In these wind farms, many identical 1,5 MW direct-drive PMSGs have been deployed. These large-scale wind farms are far from the main power grid. According to the data provided by the grid company, the short circuit capacities at substation Mahuanggou west and Mahuanggou east are about 2 000 MVA and 1 450 MVA. However, the total installed wind power capacity at substation Mahuanggou east and Mahuanggou west was about 1 100 MVA at the end of 2014 and is still growing. Thus the SCR is about 1,3 or even less. In other words, these PMSG based wind farms are radially connected to a typical low SCR AC network.

In 2014, the wind power cluster in Kumul, Xinjiang, Northwest China had several accidents, where a great number of wind turbines tripped off due to the power oscillations of the power grid. Based on the PMU data, it was found that there was a sub-synchronous oscillation problem in the power grid of the Mahuanggou area. At the same time, the dynamic reactive power compensation device deployed in the region is affected by the sub-synchronous oscillation during the operation and the output power oscillation and amplification phenomenon, which seriously affects the safe and stable operation of the power grid in the Mahuanggou area.

The field recording shows that the output of the dynamic reactive power compensation device in the oscillating state has a certain regularity in Figure 2. It is found that the dynamic reactive power compensation device has an oscillation period of 40 ms when operating in the oscillation state. According to this analysis, there is a sub-synchronous oscillation of 25 Hz in the power grid. The test results show that there is a sub-synchronous oscillation of 25 Hz in the power grid of the Mahuanggou area. The sub-synchronous oscillation is a new oscillation type because of strong interactions among power electronics. The fault threatens the safe and stable operation of the power system.

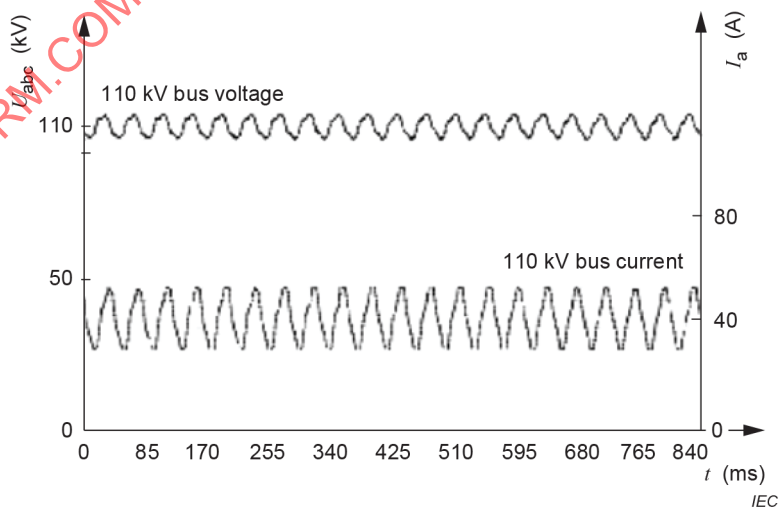

Figure 1 – Measured voltage and current curves of sub-synchronous oscillation

In order to improve the stability in the low SCR AC network, the understanding of the fault inherent mechanism is very important. The strong interactions among the wind generators, dynamic reactive power compensation device, power grid and related control strategies are the critical elements of the faults in the low SCR AC network with high proportion of inverter-based resources.

4.2.2 Static voltage control

Voltage sensitivity is very high in a low SCR AC network. With regard to renewable energy generation connected to a low short circuit ratio AC grid, small variations of active or reactive power output might bring relatively large voltage fluctuation at PCC, and the stability also might be deteriorated, which could be represented by a low stability margin.

The indication of SCR can describe the system's ability to respond to active/reactive power injections and absorptions. A low SCR system is very sensitive to active/reactive power injections (or absorptions) i.e., the system voltage changes rapidly as the amount of reactive power injected (or absorbed) changes. It is therefore difficult to stabilize the system voltage (magnitude and phase angle) in a low SCR system whereas a high SCR system is largely unresponsive to active and reactive power injections (and absorptions) and the system voltage is not significantly influenced by changes in the network. A low SCR network generally requires a voltage control system with supplementary stabilization control.

4.2.3 Fault ride-through

Renewable energy generation plants may be unable to adequately meet ride-through criteria as defined by regulatory agencies. This can manifest in several ways, but failure of the plant to regulate its terminal voltage adequately as the plant recovers its active power following a disturbance can cause the plant protections to operate inappropriately and fail to "ride-through". Further, when connected to low SCR AC networks, the ability of the controllers to adequately follow the connection point system frequency and phase immediately after a fault, is reduced significantly, causing the disconnection of the REPPs from the system.

The risk of exceeding the connection point voltage following the clearance of the faults is increased. Depending on overvoltage ride-through (OVRT) capability of individual renewable energy generation plant designs compared to others, operation of renewable energy generation plant overvoltage relays may occur upon outage conditions, especially in regions dominated by inverter based generation types like wind, with very little load or conventional generators. Loss of a plant through OVRT protection can relieve loading on the overvoltage circuits exporting the power, causing the voltage to rise further, and potentially leading to overvoltage cascading, as the system voltage rises further when generation trips.

In a low SCR network, the renewable energy generation plants may have difficulty transitioning from a reduced-power ride-through mode into its normal full power operation. The transient caused by the plant recovery and shift from control modes may be sufficient to cause the plant to re-enter its ride-through mode, causing a major transient to occur in a periodic manner. This is generally unacceptable, as the transients can be severe and can ultimately lead to plant tripping.

4.2.4 Multi-frequency oscillation

The possibility of interaction between devices is very broad. Power electronic based generators may interact with each other, or they may interact with other power electronic devices such as HVDC ties, FACTS devices such as SVCs or STATCOMs, or even with non-power electronic based devices such as series capacitors, switched shunt devices and conventional generators. Further, control instability can occur due to the interaction of the fast, high gain controllers of power electronic devices.

The weaker a system in relation to the controlled devices, the more impact of each of the devices. In general, the effect of the open loop gain as experienced by the interacting controllers is higher when they are connected and operated in weak AC systems. In power systems several phenomena are known to cause undamped or growing oscillations, and the interaction between devices and weak AC networks would cause an under damped sub-synchronous interaction (SSI) mode. Under some conditions, especially with very small short circuit ratios, the SSI can become unstable, and this causes sustained oscillations in power electronic devices as well as the whole associated grid.

4.3 Summary

With the continuous growth of installed renewable energy from inverters, large-scale connections to weak grids are becoming more common. Generally, many indications can be used to evaluate the transmission system robustness, for example the (X/R) ratio, voltage sensitivity, system inertia and so on. The short circuit ratio (SCR) is an important indication of weak AC networks, which is of importance in system stability analysis. A low SCR system usually means a weak system. There are some definitions of low short circuit ratio, but they have not been unified across the industry. At the same, in a low SCRAC networks, the static voltage controls become more complicated, the risk of failure of fault ride-through of renewable energy generation increases, the interaction between devices becomes stronger, and the risk of oscillation instability is increased.

5 Identification of low short circuit ratio AC networks

5.1 Problem statement

Connection of significant amounts of wind power to constrained power networks can result in system stability concerns, which manifest differently from those with conventional generation based on synchronous generators. Operation of the wind power plants (WPPs) under weak network could result in system and/or wind turbine converter control instabilities. Some of the interactions between transmission assets and WPPs are complex and thus special studies are needed to determine wind turbine generator (WTG) responses to such conditions. The use of simple indices for determining the likelihood of weak network conditions would be a logical step before embarking on detailed power system modelling and analysis.

In theoretical research and engineering application, short circuit ratio (SCR) is widely applied to quantitatively measure the strength of AC networks. A higher SCR leads to a stronger AC network and a more stable power system, and vice versa. The SCR has been used to assess the static voltage stability of AC-DC systems. This assessment involves two indices: the critical SCR (SCR_c) and the boundary SCR (BSCR). Usually, SCR_c≈2 is used to differentiate very weak systems from weak systems based on IEEE Standard 1204-1997. BSCR≈3 is used to differentiate weak systems from strong systems. The SCR is an indication of the AC-DC system's ability to respond to active/reactive power injections and absorptions. A low SCR (weak) system is very sensitive to reactive power injections (or absorptions). That is, the system voltage changes rapidly as the amount of reactive power injected (or absorbed) changes. Thus, it is challenging to stabilize the system voltage in a weak system. On the other hand, a high SCR (strong) system is largely insensitive to reactive power injections (or absorptions), and thus the system voltage is not significantly influenced by changes in reactive power. A weak system generally requires a voltage control system with supplementary stabilization control.

Compared to an HVDC link, an AC network integrated with multiple WPPs has a significantly more complex topology due to the use of several wind turbines (which may or may not be identical), and common use of static reactive support such as capacitor bank and dynamic reactive support such as STATCOMs and synchronous condensers. Moreover, it sometimes happens that several WPPs are located adjacent to each other, or even sometimes connected to the same connection point. This makes it imperative to appreciate the impact of all the neighbouring WPPs. The two aspects addressed above are difficult to account for using a conventional calculation method for the SCR. For a single grid-connected WPP system, a fault current based calculation method and an equivalent circuit-based calculation method are introduced to make SCR evaluation applicable to any given WPP and network topology. For a multi grid-connected WPP system, a generalized short circuit ratio (gSCR) is proposed based on eigenvalue decomposition in Clause 5 and compared against other approaches referred to as equivalent short circuit ratio (ESCR), composite short circuit ratio (CSCR), and weighted short circuit ratio (WSCR).

Without a loss of generality, the network line impedance ratio R/X is assumed to be constant and the effect of capacitance in the network is ignored. As for a WPP or WPPs, the problems discussed in this document are as follows:

a) Problem 1: Assuming that all the WPPs operate in the rated condition, how to identify whether or not the system meets the small signal stability and quantify the stability margin of the system using the gSCR.

b) Problem 2: How to understand the influence of network structure and parameters on the small signal stability of the WPPs based on the gSCR and how to evaluate the gSCR and its critical value CgSCR.

It is noted that the gSCR can be promoted by the operational gSCR for the system operating in non-rated conditions. It is worth pointing out that the gSCR-based analysis method is still applicable under these conditions, and this document will not discuss this method in detail due to space limitations.

5.2 Short circuit ratio for a single-connected REPP system

5.2.1 SCR calculation with fault current

To correctly determine the SCR, it is imperative to first calculate the fault current at the desired location, where WPPs are part of a larger power system, and hand calculations are not practicable. Short circuit calculation engines embedded into RMS-type power system simulation tools are often used for this purpose. At present, most of these tools treat wind turbines in the same fashion as synchronous generators. This would result in an overestimation of the fault current at the given point due to significantly higher fault current contribution from the synchronous generators than WPPs. Efforts are on-going in the industry to integrate appropriate fault current calculations algorithms into the RMS-type simulation tools to account for the true response of power electronic converters in the wind turbines. In the absence of such methods the following assumptions are proposed:

a) Type 1 and Type 2 wind turbines: no contribution (mentioned in CIGRE Tech. Brochure 671)

b) Type 3 and Type 4 wind turbines: 1 p.u. contribution

Type 1 and Type 2 wind turbines can therefore be removed for fault current calculations.

Type 3 and Type 4 wind turbines can be represented by fictitious synchronous generators with a fault current contribution of 1 p.u., i.e. full load current, at the turbine terminals. To this end, the transient and sub-transient reactance of the fictitious synchronous generators can be adjusted.

The following considerations should be accounted for when performing fault current calculation studies, and consequently determining the short circuit ratio:

a) Contingency conditions

It is recommended to estimate the fault level for both normal and contingency operating conditions. It is expected that the WPP will maintain its continuous uninterrupted operation for normal and credible contingency conditions. Investigating non-credible contingencies is primarily to identify the need for imposing operational constraints under such conditions. Depending on the connection agreement between the WPP owner and network owner/operator, a WPP may or may not be required to sustain non-credible contingency conditions.

b) Conventional generation dispatch

Fault level calculations should include the lowest realistic unit commitment condition of electrically close conventional synchronous generators. For planning and feasibility studies, this should include the potential retirement/mothballing of synchronous generators.

c) Number of WPPs to consider

All WPPs electrically close to the plant of interest should be considered in the calculation. A practical rule is that if adding a WPP to the calculation does not change the result, the plant can be neglected.

d) HVDC links and other power electronic devices

HVDC links and other power electronic interfaced technologies such as SVCs and STATCOMs in close proximity of WPPs should be included in the calculations of short circuit ratio.

5.2.2 SCR calculation with equivalent circuit

5.2.2.1 Equivalent circuit-based short circuit ratio (ESCR)

A simple schematic diagram of a WPP without any static and dynamic reactive support is shown in Figure 2. The WPP consists of N number of wind turbines, where the cable impedance represents the aggregate impedance of the cables for all those individual wind turbines. For simplicity only one level of voltage transformation is assumed from the MV level collection grid to the connection point. The approach presented here can be readily applied to WPP with two levels of high voltage transformations.

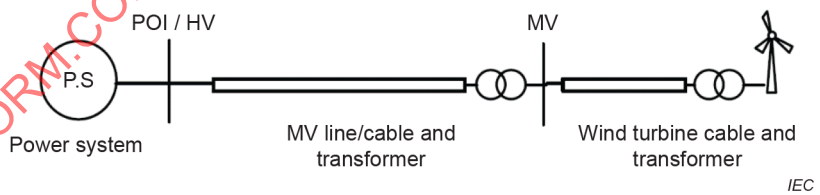

Figure 2 – Schematic diagram of a WPP with no static or dynamic reactive support

An equivalent single-phase equivalent circuit of this simple WPP is shown in Figure 3.

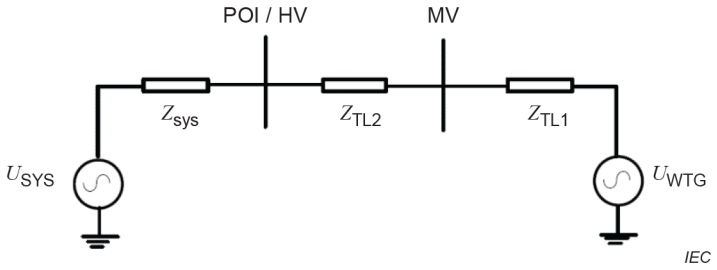

Figure 3 – Equivalent circuit representation of the WPP shown in Figure 2

The electrical network impedance is considered to be known where

Z_{TL1}: aggregate impedance of the wind turbine transformer and cable;

Z_{TL2}: aggregate impedance of the MV transformer and cable;

Z_{sys}: equivalent impedance of the system.

According to the basic definition of the short circuit ratio, SCR at the point of interconnection (POI) with the rated capacity of wind turbine (P_{WF}) can be written as:

$$SCR_{POI} = \frac{S_{POI}}{P_{WF}} \tag{4}$$

Rearranging this formula:

$$S_{POI} = SCR_{POI} \times P_{WF} \tag{5}$$

Substituting voltage (V_{POI}) and impedance (Z_{POI}) at POI for S_{POI}:

$$\frac{V_{POI}^2}{Z_{POI}} = SCR_{POI} \times P_{WF} \tag{6}$$

The per-unit impedance seen at the POI can be defined as:

$$Z_{pu,POI} = \frac{Z_{POI}}{Z_{base}} \tag{7}$$

where

$$Z_{base} = \frac{V_{POI}^2}{P_{WF}} \tag{8}$$

Substituting (7) and (8) to (6) results in:

$$SCR_{\text{POI}} = \frac{1}{Z_{\text{pu,POI}}} \tag{9}$$

This formula shows that the SCR at the POI can be calculated as the inverse of the per-unit impedance seen at the POI. For example, with $Z_{\text{pu,POI}} = 20\%$ the SCR at the POI will be 5.

The used impedance should reflect the maximum grid impedance under which the WPP is expected to operate under normal conditions.

Note that these formulae do not account for the variation of POI voltage. Further formulae will be developed by relating the SCR to steady-state voltage stability indices.

5.2.2.2 Composite short circuit ratio (CSCR)

This method primarily aims at calculating short circuit ratio at the WPP MV collection grid. Using a system base power S_{BASE} for the calculation, for example S_{BASE} = 100 MVA, the equivalent system reactance can be estimated as follows:

$$X_{\text{SYSTEM}} = \frac{S_{\text{BASE}}}{S_{\text{SC}}} \tag{10}$$

The composite short circuit level at the medium voltage collector bus CS_{SCMV} can be estimated as:

$$CS_{\text{SCMV}} = \frac{1}{(X_{\text{SYSTEM}} + X_{\text{TL2}})} \tag{11}$$

where

X_{TL2} is the HV to MV transformer impedance in p.u. on the system MVA base.

The CSCR can then be calculated as:

$$CSCR = \frac{CS_{\text{SCMV}} \times S_{\text{BASE}}}{WP_{\text{RAT}}} \tag{12}$$

where

WP_{RAT} is the nominal MVA base rating of the WPP.

In a more general approach, CS_{SCMV} could be calculated with a short circuit program by estimating the three-phase fault level at the medium voltage bus. The calculation should assume no short circuit contribution from the WPP of interest, and take into account the approach elaborated in 5.2.2 as to how to account for contribution of remote WPPs in the network. The CSCR can then be calculated as indicated in (12).

In this case with a single WPP there is no distinction between the short circuit level at the medium voltage collector bus and the composite short circuit level at the same bus. Thus, CSCR and ESCR indices will give rise to identical SCR figures for a single WPP.

5.2.2.3 Generalized short circuit ratio (gSCR)

A typical single-infeed power electronic system (SIPES) is shown in Figure 4, in which a power electronic device (PED) such as a WPP is connected to the infinite bus through the inductance. In the SIPES, it is assumed that the small signal stability of the PED can be improved when the inductance L decreases, i.e., the grid strength is improved. This assumption is valid for a SIPES with most commonly-used types of PEDs, such as the wind turbines or vector control scheme. The strength of the infeed bus connecting PED to the AC grid can be assessed by the SCR:

$$SCR = \frac{S_{ac}}{S_B} = \frac{U_N^2}{Z} \times \frac{1}{S_B} = \frac{1}{S_B Z} = \frac{B}{S_B} \tag{13}$$

where

$Z = 1/B$ is the reactance connecting the PED with the AC grid;

U_N is the rated voltage at the infeed bus in the AC grid.

In the SIPES, the small signal stability can be analyzed based on the impedance-based model, which can be constructed by the linearized equations of currents and voltages at the PED and AC grid sides, respectively.

At the AC grid terminal, the linearized equations in the s-domain can be represented as:

$$\begin{bmatrix} \Delta I_x \\ \Delta I_y \end{bmatrix} = \boldsymbol{Y}_{net\_s}(s) \begin{bmatrix} \Delta U_x \\ \Delta U_y \end{bmatrix} = B \begin{bmatrix} \beta(s) & \alpha(s) \\ -\alpha(s) & \beta(s) \end{bmatrix} \begin{bmatrix} \Delta U_x \\ \Delta U_y \end{bmatrix} \tag{14}$$

where

ΔI_x and ΔI_y are the x-axis and y-axis components of the changes of the injected current ΔI in the x-y global reference frame;

ΔU_x and ΔU_y are the x-axis and y-axis components of the changes of the terminal voltage ΔU in the x-y global reference frame;

$\boldsymbol{Y}_{net\_s}(s)$ is the admittance matrix of the AC grid, in which $\alpha(s) = \omega_0^2 / (s^2 + \omega_0^2)$, $\beta(s) = s\omega_0^2 / (s^2 + \omega_0^2)$ in the frequency domain (i.e., s-domain), and $B = 1/(\omega_0 L)$;

ω_0 is the rated angular frequency of AC system.

At the PED terminal, the linearized equations of currents and voltages in the s-domain on the rated operational point can be represented as:

$$\begin{bmatrix} \Delta I_d \\ \Delta I_q \end{bmatrix} = -\boldsymbol{Y}_{PED\_s}(s) \begin{bmatrix} \Delta U_d \\ \Delta U_q \end{bmatrix} = -S_B \begin{bmatrix} G_{dd}(s) & G_{dq}(s) \\ G_{qd}(s) & G_{qq}(s) \end{bmatrix} \begin{bmatrix} \Delta U_d \\ \Delta U_q \end{bmatrix} \tag{15}$$

where

G_{dd}, G_{dq}, G_{qd}, and G_{qq} are the port input-output transfer functions of the PED, which describe the current response to voltage perturbation;

ΔI_d and ΔI_q are the d-axis and q-axis components of the changes of the current I in the d-q local reference frame of the PED.

In (15), the components of the output current and terminal voltage are represented in the d-q local reference frame due to the control blocks such as Phase-Locked Loop (PLL) controller in a PED. To integrate (14) and (15) for small signal stability analysis of the SIPES, the d-q components in (15) are transformed into their corresponding components in the x-y global reference frame using the relationship between local and global reference frames, where it is assumed that the d-axis is aligned with the terminal voltage $\vec{U} = U\angle\theta$ of the PED in steady-state operation point. With the relationship between two reference frames, (15) can be reformulated as:

$$\begin{bmatrix} \Delta I_x \\ \Delta I_y \end{bmatrix} = -\boldsymbol{Y}_{\text{PEDxy\_s}}(s)\begin{bmatrix} \Delta U_x \\ \Delta U_y \end{bmatrix} \tag{16}$$

where

$$\boldsymbol{Y}_{\text{PEDxy\_s}}(s) = \boldsymbol{T}^{-1}\boldsymbol{Y}_{\text{PED\_s}}(s)\boldsymbol{T},\ \boldsymbol{T} = \begin{bmatrix} \cos\theta & \sin\theta \\ -\sin\theta & \cos\theta \end{bmatrix} \tag{17}$$

Based on (14) and (16), the SIPES shown in Figure 4 can be represented with an equivalent multiple-input, multiple-output (MIMO) feedback control system for the small signal stability analysis. In the control system, return deference matrix can be represented as $\left(\boldsymbol{I} + \boldsymbol{Y}_{\text{PEDxy\_s}}(s)\boldsymbol{Y}^{-1}_{\text{net\_s}}(s)\right)$. Thus, the close-loop characteristic formula of the control system is:

$$\det\left(\boldsymbol{I} + \boldsymbol{Y}_{\text{PEDxy\_s}}(s)\boldsymbol{Y}^{-1}_{\text{net\_s}}(s)\right) = 0 \tag{18}$$

where

$\boldsymbol{I}$ is a 2-by-2 identity matrix and det(·) denotes the determinant function.

Submitting (13) into (18) leads to

$$c(s) = \det\left(\begin{bmatrix} G_{\text{dd}}(s) & G_{\text{dq}}(s) \\ G_{\text{qd}}(s) & G_{\text{qq}}(s) \end{bmatrix} + SCR\begin{bmatrix} \beta(s) & \alpha(s) \\ -\alpha(s) & \beta(s) \end{bmatrix}\right) = 0 \tag{19}$$

Formula (19) shows that the relationship between grid strength and the small signal stability of the SIPES can be represented with the explicit function of SCR.

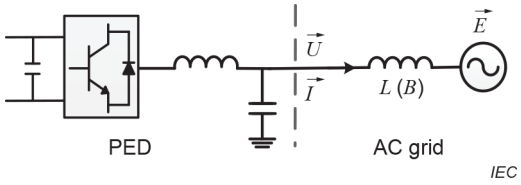

Figure 4 – A typical SIPES

The small signal stability of the SIPES depends on whether or not the solutions of (19) (i.e., system eigenvalues) are in the left-half of the complex plane. In fact, when the SCR is large, these eigenvalues are located in the left-half of the complex plane, which indicates that the system is stable. When the SCR becomes small, these eigenvalues may be located in the right-half of the complex plane, which may cause the small signal instability in the SIPES. Particularly, when the SCR is equal to a certain value, (19) has a pair of conjugate solutions located at the imaginary axis in the complex plane, which indicates that the system is critically stable. This value related to the critical stability is defined as critical short circuit ratio (SCR_c).

The relationship between the small signal stability and grid strength as well as the concept of SCR_c illustrated in Figure 5 a) shows the changes of eigenvalues' trajectories with SCR; Figure 5(b) shows the change of the damping ratio of the weakest eigenvalue with SCR.

It can be observed from Figure 5 a) that the SIPES's small signal stability increases with SCR. When SCR is smaller than 2,5, the system is unstable since it has eigenvalues in the right-half of the complex plane; when SCR is equal to 2,5, the system is critically stable since it has a pair of conjugate eigenvalues at the imaginary axis in the complex plane; and when SCR becomes larger than 2,5, the system is stable since its eigenvalues are in the left-half of the complex plane.

A similar observation can also be obtained from Figure 5 b) in terms of the relationship between the damping ratio of the system's weakest eigenvalue and SCR. It can be seen that the SCR_c can characterize the stability boundary of the SIPES: when the SCR is equal to SCR_c = 2,5, the system is critically stable since the damping ratio is zero; when the SCR is larger than SCR_c = 2,5, the system is stable since its damping ratio is larger than zero; and when the SCR is smaller than SCR_c = 2,5, the system is unstable due to the damping ratio smaller than zero.

It is worth noting that the definition and analysis of gSCR in 5.2.2.3 are the basis of those in multi-infeed power electronic system (MIPES).

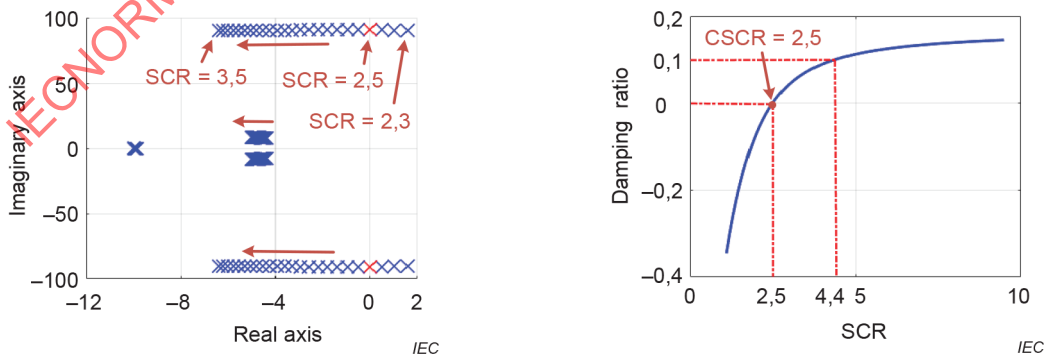

a) b)

Figure 5 – Changes of system eigenvalues, and the weakest system eigenvalue's damping ratio with SCR in a SIPES

5.2.2.4 Single WPP with static reactive power support plant (capacitor bank)

Figure 6 depicts the schematic diagram of a WPP with capacitor banks connected at the MV collection grid. The equivalent circuit can be represented as shown in Figure 7.

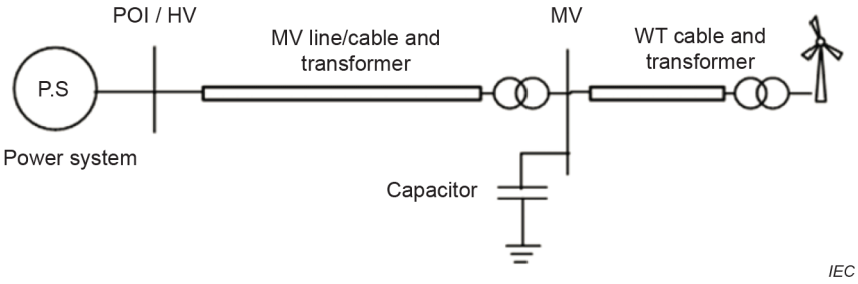

Figure 6 – Schematic diagram of a WPP with static reactive support plant (capacitor banks)

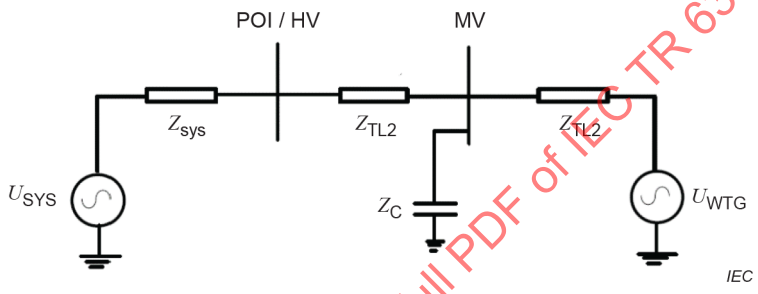

Figure 7 – Equivalent circuit representation of the WPP shown in Figure 6

Using the equivalent circuit shown in Figure 6 the following impedance relationship can be established:

$$Z_{WTG} = Z_{TL1} + \frac{Z_c \times (Z_{TL2} + Z_{sys})}{Z_C + Z_{TL2} + Z_{sys}} \quad (20)$$

Considering typical impedances of the WPP and with a static reactive compensation of 5 % to 10 % of the WPP's nominal power, one can conclude that the value of Z_C can very marginally reduce the SCR relative to the WPP configuration without capacitor banks in service. For simplicity, the shunt capacitor banks can therefore be excluded from SCR calculations.

5.2.2.5 Single WPP with dynamic reactive power support (synchronous condenser)

Figure 8 shows the schematic diagram of a WPP with synchronous condensers connected at the MV collection grid. The equivalent circuit can be represented as shown in Figure 9.

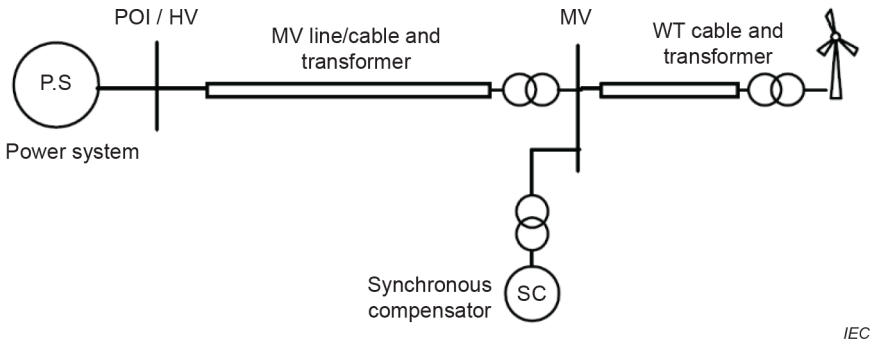

Figure 8 – Schematic diagram of a WPP with dynamic reactive support plant (synchronous condensers)

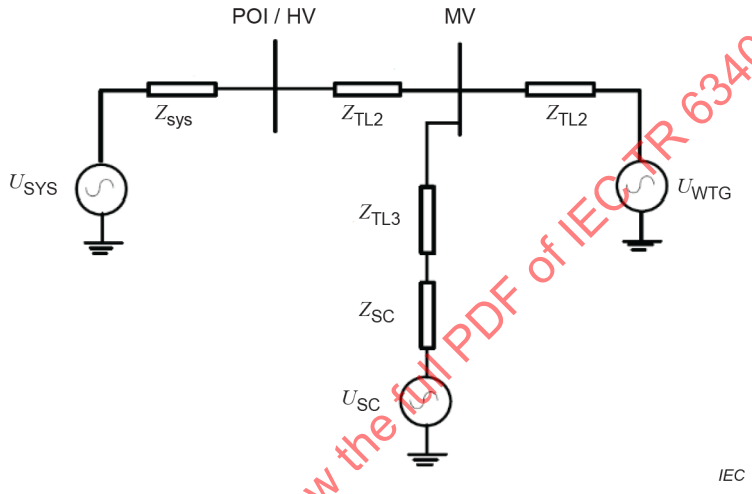

Figure 9 – Equivalent circuit representation of the WPP shown in Figure 8

Using the equivalent circuit shown in Figure 9 the following impedance relationship can be established:

$$Z_{WTG} = Z_{TL1} + \frac{(Z_{TL3} + Z_{SC}) \times (Z_{TL2} + Z_{SYS})}{Z_{TL3} + Z_{SC} + Z_{TL2} + Z_{SYS}} \quad (21)$$

Unlike with capacitor banks, the use of a synchronous condenser will allow a substantial increase in the SCR value. A numerical example describing application of synchronous condensers to increase the SCR value in a practical WPP is explained in CIGRE B4.62 TB671 report [2].

5.3 Short circuit ratio for multi grid-connected WPP system

5.3.1 General

The SCR indexes in 5.2 were proposed based on the assumption that multiple power electronic devices (PEDs) in the same renewable energy can be considered to share the same point of common coupling, which can only roughly reflect the overall voltage support strength of the AC grid. However, the above SCR indexes do not fully consider the complex dynamic coupling relationships which exist among the AC grid and multiple PEDs in the renewable energy station. Hence, the above SCR indexes are not suitable for the refined evaluation of the grid strength of the MIPES.

Similar to the SCR and CSCR in a single-infeed system, it is urgent to propose a proper and accurate multi-infeed short circuit ratio (MISCR) and critical value index for the MIPES. Nowadays, the research on the MISCR in academia and industry can be divided into two schools, which include the definition of modal decoupling method and the definition of circuit aggregation method. The former is represented by gSCR index, while the latter includes ESCR, WSCR, CSCR, etc. Subclause 5.3 provides the detailed definition and analysis of the indexes of the above.

5.3.2 Modal decoupling method

5.3.2.1 General

Subclause 5.3.2 firstly discusses the relation between the small signal stability of multi-infeed power electronic systems (MIPES) including multi-grid-connected WPPs homogeneous system and grid strength assessment. On this basis, the index generalized short circuit ratio (gSCR) is introduced to assess the grid strength of a MIPES in terms of its small signal stability while the critical gSCR (CgSCR) can characterize the stability boundary of a MIPES. Further, the definition of the index gSCR and CgSCR can still be extended to multi grid-connected WPPs heterogeneous system.

5.3.2.2 Definition of gSCR in the homogeneous system

The relationship between the grid strength and the small signal stability of a SIPES can be extended to the homogeneous MIPES to define the gSCR and CgSCR for the small signal stability analysis of the MIPES.

The characteristic formula of homogeneous MIPES can be written as:

$$\det\left(\begin{bmatrix} G_{dd}(s) & G_{dq}(s) \\ G_{qd}(s) & G_{qq}(s) \end{bmatrix} \times \boldsymbol{I}_n + \begin{bmatrix} \beta(s) & \alpha(s) \\ -\alpha(s) & \beta(s) \end{bmatrix} \times \boldsymbol{Y}_{eq}\right) = 0 \tag{22}$$

where

$\boldsymbol{Y}_{eq}=\boldsymbol{S}_B^{-1}\boldsymbol{B}$ is the diagonal matrix in which $\boldsymbol{S}_B$ = diag(S_{Bi}) is composed of the diagonal elements S_Bi (i=1…n), representing the rated capacity of each PED;

$\boldsymbol{B}$ is the reduced node susceptance matrix after eliminating passives buses and infinite buses.

As the matrix $\boldsymbol{Y}_{eq}$ is diagonalizable, there exists a matrix $\boldsymbol{W}$ that can decompose the matrix $\boldsymbol{Y}_{eq}$ into a diagonal matrix in which the diagonal elements consist of the eigenvalues (λ_i, i = 1,…,n) in the order of $0 < \lambda_1 \le \lambda_2 \le \cdots \le \lambda_n$. That is:

$$\boldsymbol{W}^{-1}\boldsymbol{Y}_{eq}\boldsymbol{W} = \boldsymbol{\Lambda} = \mathrm{diag}(\lambda_i) \tag{23}$$

Combining (22) and (23) yields:

$$\prod_{i=1,2,\ldots,n}\left[c_i(s)\right] = 0 \tag{24}$$

where

$$c_i(s) = \det\left(\begin{bmatrix} G_{dd}(s) & G_{dq}(s) \\ G_{qd}(s) & G_{qq}(s) \end{bmatrix} + \lambda_i \begin{bmatrix} \beta(s) & \alpha(s) \\ -\alpha(s) & \beta(s) \end{bmatrix}\right) = 0 \quad (25)$$

Formula (24) shows that the small signal stability of the MIPES can be analyzed by studying the stability of a set of equivalent SIPESs. The small signal stability of the MIPES depends on whether the eigenvalues of the characteristic Formula (24) are in the left-half of the complex plane. In (24), the characteristic formula of the MIPES is decoupled into a set of characteristic formulae of the equivalent SIPESs. The specific decoupling mechanism is shown in Figure 10. Thus, the small signal stability of the MIPES depends on whether or not the eigenvalues of the characteristic formula for each equivalent SIPES are in the left-half of the complex plane. In other words, the small signal stability of the MIPES depends on the small signal stability of its each equivalent SIPESs.

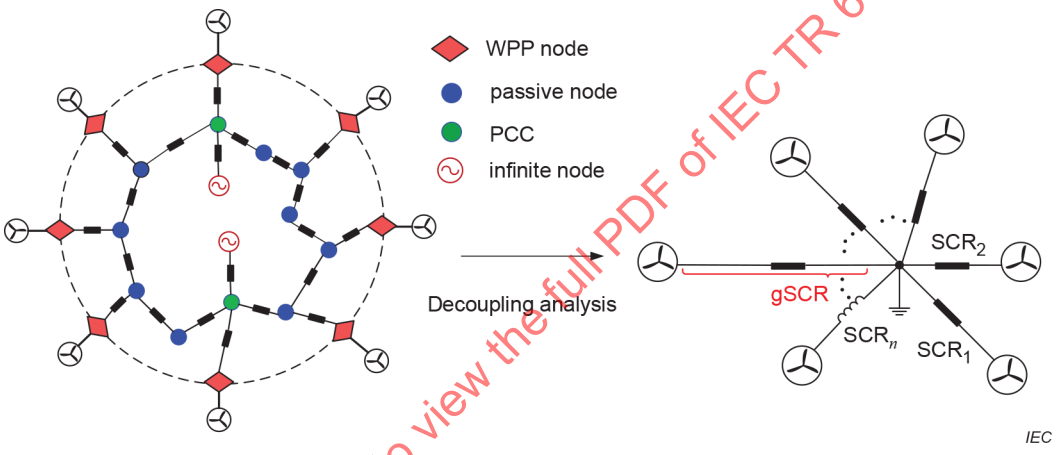

Figure 10 – Mechanism illustration of decoupling a MIPES into a set of equivalent SIPESs

In a typical homogeneous MIPES as shown in Figure 10, the gSCR is defined as the minimum eigenvalue λ_1 of extended admittance matrix $\boldsymbol{Y}_{eq}$.

$$gSCR = \min_{i=1,\ldots,n} SCR_{i\_eq} = \min \lambda\left(\boldsymbol{Y}_{eq}\right) = \min_{i=1,\ldots,n} \lambda_i = \lambda_1 \quad (26)$$

The gSCR can also be defined equivalently as:

$$gSCR = \frac{S_i}{P_{Wi} + \sum_{\substack{j=1 \\ j \neq i}}^{n} P_{Wj} \times gMIIF_{ij}} \quad (27)$$

where

S_i is the short circuit capacity observed on bus i;

$gMIIF$ is the generalized multi-infeed interaction factor, which is defined as $gMIIF_{ji}=\frac{Z_{ij}}{Z_{ii}}\frac{v_{j1}}{v_{i1}}$;

v_{i1} is the i^{th} element of the right eigenvector v_1.

Based on that definition and the relation between the gSCR and MIPES stability, the following features of gSCR can be used to analyze the small signal stability of a MIPES:

- The small signal stability of the homogeneous MIPES depends on the small signal stability of each of its equivalent SIPES. In other word, a MIPES can be decoupled into n equivalent SIPES with $SCR_{i\_eq} = \lambda_i$.
- The gSCR is the generalized representation of SCR defined in (23). When multiple PEDs are connected to the AC grid as shown in Figure 11, the gSCR is equal to the minimum SCR_{i_eq} of all equivalent SIPESs for the MIPES, (i.e., the gSCR is equal to the minimum eigenvalue λ_1 of $\boldsymbol{Y}_{eq}$). Thus, the SCR in (23) is a special case of the gSCR in (27).
- The gSCR retains the same physical interpretation of SCR defined for SIPES. Thus, the stability of the MIPES depends on the gSCR defined in (27).
- The impact of the interactions among PEDs on the stability of the MIPES can be analyzed based on the participation factors of the gSCR. Since the gSCR is defined as the minimum eigenvalue λ_1, which quantifies the grid strength and the stability of the MIPES, the impact of each PED on the stability of the MIPES can be characterized by the factor that each PED participates to λ_1. The factor p_{1j} is defined as in (28) below. When a PED has a larger participation factor, it more significantly affects the stability of the whole MIPES, and its connected bus is weaker.

$$p_{1j} = v_{1j}u_{j1} \tag{28}$$

- where p_{1j} is the participation factor of the j^{th} PED; v_{1j} is the 1st-row and j^{th}-column element of matrix $\boldsymbol{v} = \boldsymbol{W}^{-1}$, which is the left eigenvector matrix of $\boldsymbol{Y}_{eq}$;and u_{j1} is the j^{th}-row and 1st-column element of matrix $\boldsymbol{u} = \boldsymbol{W}$, which is the right eigenvector matrix of $\boldsymbol{Y}_{eq}$.

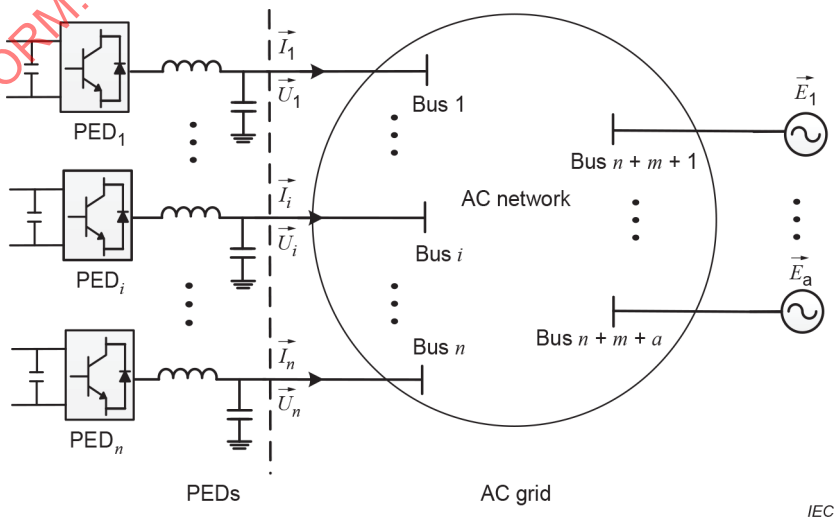

Figure 11 – A typical MIPES

CgSCR is the value of gSCR when the MIPES has a pair of conjugate eigenvalues at the imaginary axis in the complex plane. The CgSCR characterizes the stability boundary of the homogeneous MIPES. The homogeneous MIPES is stable if and only if the gSCR is greater than CgSCR. Thus, the difference between the gSCR and CgSCR indicates the stability margin of the homogeneous MIPES.

It should be noted that the CgSCR is a constant for a given PED control strategy and a given set of control parameters of the PED in the weakest equivalent SIPES for the MIPES. Thus, once the stability boundary of a SIPES is obtained, the stability boundary of a complex MIPES is also determined. As for a given system, the CgSCR is the value of gSCR when the real part of the dominant eigenvalues of the weakest equivalent SIPES is 0. Its value can be analyzed by the critical stability condition of the weakest equivalent SIPES:

$$\det\left(\begin{bmatrix} G_{dd}(s_d) & G_{dq}(s_d) \\ G_{qd}(s_d) & G_{qq}(s_d) \end{bmatrix} + \lambda_1^c \begin{bmatrix} \beta(s_d) & \alpha(s_d) \\ -\alpha(s_d) & \beta(s_d) \end{bmatrix}\right)\Bigg|_{\mathrm{Re}(s_d=0)} = 0 \tag{29}$$

where the real part of the dominant characteristic roots s_d is 0($\mathrm{Re}(s_d) = 0$). λ_1^c is defined as the critical generalized short circuit ratio (CgSCR).

More importantly, the gSCR and CgSCR can simplify the small signal stability analysis of the homogeneous MIPES. The difference between the gSCR and CgSCR indicates the stability margin of the MIPES. Both gSCR and CgSCR can be determined in the weakest equivalent SIPES that has the minimum eigenvalue λ_1 of matrix $\boldsymbol{Y}_{eq}$. Thus, the small signal stability analysis of the homogeneous MIPES can be simplified as that of its weakest equivalent SIPES.

5.3.2.3 Definition of gSCR in the heterogeneous system

In 5.3.2.3, the definition of gSCR in the homogeneous MIPES is extended to the heterogeneous MIPES. Based on the eigenvalue perturbation theory, it is proved that the dominant characteristic trajectories of heterogeneous MIPES can be approximated by the dominant characteristic trajectories of the equivalent homogeneous MIPES. It is shown that the definition of gSCR in homogeneous or heterogeneous MIPES is consistent. As for the CgSCR value of heterogeneous MIPES, it can be obtained by constructing an equivalent single-infeed system analytically or by hardwire simulation experiment. The detailed proof process is shown as follows.

Actually, the dynamics differences among different PEDs in the heterogeneous system exist. The closed-loop characteristic formula including the dynamics of MIPES and the AC network can be expressed as follows:

$$\Sigma:\ \det\left(\boldsymbol{J}_{sys1}(s)\right) = \det\left(\begin{bmatrix} \boldsymbol{\Lambda}_{11}(s) & \boldsymbol{\Lambda}_{12}(s) \\ \boldsymbol{\Lambda}_{21}(s) & \boldsymbol{\Lambda}_{22}(s) \end{bmatrix} + \begin{bmatrix} \boldsymbol{S}_B^{-1}\boldsymbol{B} & \\ & \boldsymbol{S}_B^{-1}\boldsymbol{B} \end{bmatrix}\right) = 0 \tag{30}$$

where

$$\begin{cases} \boldsymbol{\Lambda}_{11}(s) = l(s)\,\mathrm{diag}\left[\beta(s)G_{11i}(s) + \alpha(s)G_{12i}(s)\right] \\ \boldsymbol{\Lambda}_{12}(s) = l(s)\,\mathrm{diag}\left[-\alpha(s)G_{22i}(s) + \beta(s)G_{12i}(s)\right] \\ \boldsymbol{\Lambda}_{21}(s) = l(s)\,\mathrm{diag}\left[\beta(s)G_{21i}(s) + \alpha(s)G_{22i}(s)\right] \\ \boldsymbol{\Lambda}_{22}(s) = l(s)\,\mathrm{diag}\left[-\alpha(s)G_{21i}(s) + \beta(s)G_{22i}(s)\right] \end{cases} \tag{31}$$

where G_i represents the admittance transfer function matrix of MPP$_i$; The specific expressions of $G_i(s)$, $l(s)$, $\alpha(s)$, $\beta(s)$ are shown as (32).

$$\begin{gathered} l(s) = \left[\alpha^2(s) + \beta^2(s)\right]^{-1};\ \alpha(s) = \frac{\omega_0^2}{s^2 + \omega_0^2};\quad \beta(s) = \frac{s\omega_0}{s^2 + \omega_0^2} \\ G_i(s) = \begin{bmatrix} G_{11i}(s) & G_{12i}(s) \\ G_{21i}(s) & G_{22i}(s) \end{bmatrix} \end{gathered} \tag{32}$$

Then, an equivalent homogeneous system is defined, whose closed-loop characteristic formula can be represented as (33).

$$\Sigma_0:\ \det\left(\boldsymbol{J}_{\mathrm{sys0}}(s)\right) = \det\left(\bar{\boldsymbol{\Lambda}}(s) \times \mathbf{I}_{\mathbf{n}} + \boldsymbol{I}_2 \times \boldsymbol{S}_{\mathrm{B}}^{-1}\boldsymbol{B}\right) = 0 \tag{33}$$

where

$$\bar{\boldsymbol{\Lambda}}(s) = \bar{\mathbf{G}}(s)\begin{bmatrix} \beta(s) & \alpha(s) \\ -\alpha(s) & \beta(s) \end{bmatrix}^{-1} \tag{34}$$

$$\bar{\mathbf{G}}(s) = \sum_{\mathrm{i}=1}^{\mathrm{n}} p_{1i}\boldsymbol{G}_i(s) \tag{35}$$

$$p_{1\mathrm{i}} = u_{\mathrm{i}1}v_{\mathrm{i}1} \tag{36}$$

where

$u_{\mathrm{i}1}$, $v_{\mathrm{i}1}$ are the i^{th} element of the left and right eigenvectors corresponding to the minimum eigenvalues of $\boldsymbol{S}_{\mathrm{B}}^{-1}\boldsymbol{B}$, and they satisfy the relationship $\sum_{i=1}^{n} p_{1i} = 1$.

a) Proposition I: Define $\lambda_{1j}(s)$ and $\bar{\lambda}_{1j}(s)(j = 1,2)$ which are the dominant characteristic trajectories of the above heterogeneous system and its equivalent homogeneous system, respectively. Then, the loci of $\lambda_j(s)$ and $\bar{\lambda}_j(s)$ have the following relationship:

$$\lambda_{1j}(s) = \bar{\lambda}_{1j}(s) + o\left[\left\|\boldsymbol{J}_{sys1}(s) - \boldsymbol{J}_{sys0}(s)\right\|\right],\ j = 1,2 \tag{37}$$

where o(·) denotes the second-order and much higher order approximate error of a function; $\|\cdot\|$ denotes the norm of any matrix.

b) Proof: Based on the small signal stability analysis of the homogeneous system in 5.3.2.1, it is known that $\bar{\lambda}_{1j}(s)(j = 1,2)$ can be obtained from the most critical subsystem decoupled from the equivalent homogeneous system Σ_0. Thus, $\bar{\lambda}_{1j}(s)(j = 1,2)$ can be formulated as:

$$\begin{aligned}\bar{\lambda}_{1j}(s) &= \left(\bar{\boldsymbol{\kappa}}_j^T(s) \times \boldsymbol{u}_1\right)\boldsymbol{J}_{\text{sys0}}(s)\left(\bar{\boldsymbol{\pi}}_j(s) \times \boldsymbol{v}_1\right)\\ &= \left(\bar{\boldsymbol{\kappa}}_j^T(s) \times \boldsymbol{u}_1\right)\left(\bar{\boldsymbol{\Lambda}}(s) \times \mathbf{I}_{\mathbf{n}} + \boldsymbol{I}_2 \times \boldsymbol{S}_{\text{B}}^{-1}\boldsymbol{B}\right)\left(\bar{\boldsymbol{\pi}}_j(s) \times \boldsymbol{v}_1\right)\\ &= \bar{\mu}_j(s) + gSCR(j = 1,2)\end{aligned} \tag{38}$$

where

$\boldsymbol{\kappa}_j^T(s)$ and $\boldsymbol{\pi}_j(s)(j = 1,2)$ represent the normalized left and right eigenvectors of $\bar{\boldsymbol{\Lambda}}(s)$ corresponding to the characteristic function $\bar{\mu}_j(s)(j = 1,2)$, and they satisfy $\boldsymbol{\kappa}_j^T(s)\boldsymbol{\pi}_j(s) = 1, (j = 1,2)$.

In a heterogeneous MIPES, $\boldsymbol{J}_{\text{sys1}}(s)$ can be considered as a result of imposing a perturbation on $\boldsymbol{J}_{\text{sys0}}(s)$. According to matrix perturbation theory, the dominant eigenvalue function $\lambda_{1j}(s)$ $(j = 1,2)$ for $\boldsymbol{J}_{\text{sys1}}(s)$ can be represented as:

$$\begin{aligned}\lambda_{1j}(s) &= \left(\bar{\boldsymbol{\kappa}}_j^T(s) \times \boldsymbol{u}_1\right)\boldsymbol{J}_{\text{sys1}}(s)\left(\bar{\boldsymbol{\pi}}_j(s) \times \boldsymbol{v}_1\right) + o\left\|\boldsymbol{J}_{\text{sys1}}(s) - \boldsymbol{J}_{\text{sys0}}(s)\right\|\\ &= \left(\bar{\boldsymbol{\kappa}}_j^T(s) \times \boldsymbol{u}_1\right)\left(\begin{bmatrix}\boldsymbol{\Lambda}_{11}(s) & \boldsymbol{\Lambda}_{12}(s)\\ \boldsymbol{\Lambda}_{21}(s) & \boldsymbol{\Lambda}_{22}(s)\end{bmatrix} + \boldsymbol{I}_2 \times \boldsymbol{S}_{\text{B}}^{-1}\boldsymbol{B}\right)\left(\bar{\boldsymbol{\pi}}_j(s) \times \boldsymbol{v}_1\right) + o\left\|\boldsymbol{J}_{\text{sys1}}(s) - \boldsymbol{J}_{\text{sys0}}(s)\right\|\\ &= \boldsymbol{\kappa}_j^T(s)\bar{\boldsymbol{\Lambda}}(s)\bar{\boldsymbol{\pi}}_j(s) + gSCR + o\left\|\boldsymbol{J}_{\text{sys1}}(s) - \boldsymbol{J}_{\text{sys0}}(s)\right\|\\ &= \bar{\mu}_j(s) + gSCR + o\left\|\boldsymbol{J}_{\text{sys1}}(s) - \boldsymbol{J}_{\text{sys0}}(s)\right\|\ (j = 1,2)\end{aligned} \tag{39}$$

This completes the proof.

Formula (39) proved that the dominant characteristic trajectories of heterogeneous MIPES Σ can be approximated by the dominant characteristic trajectories of the equivalent homogeneous MIPES Σ_0.Therefore, the stability analysis of equivalent homogeneous system Σ_0 can be utilized to analyze heterogeneous systems Σ. Simultaneously, the stability of Σ_0 further depends on the stability of the weakest equivalent single-infeed system corresponding to the gSCR after decoupling.

Then, the study shows that the gSCR of heterogeneous system Σ and equivalent homogeneous system Σ_0 is the same, and the CgSCR of heterogeneous system Σ is also consistent with that of equivalent homogeneous system Σ_0. It is very helpful to assess the strength of the power grid and the stability margin of heterogeneous systems. Specifically, the value of CgSCR can be calculated when the most critical subsystem decoupled from the equivalent homogeneous system Σ_0 reaches the critically stable state, which can be obtained by:

$$CgSCR = \underset{gSCR}{\arg}\left\{\det\left[\left(\bar{\mu}_1(s_c)+gSCR\right)\left(\bar{\mu}_2(s_c)+gSCR\right)\right]=0\right\} \tag{40}$$

where

symbol arg{} is used to calculate the roots of the formula; $s_c = j\omega_c$ are the dominant eigenvalues of the system, which are just on the imaginary axis.

On this basis, the small signal stability and stability margin of a heterogeneous MIPES can be identified by comparing the gSCR with CgSCR.That is, the heterogeneous system is stable if and only if the smallest eigenvalue gSCR is larger or equal to its critical value CgSCR (i.e., gSCR ≥ CgSCR). Moreover, the stability margin of the heterogeneous system can be estimated by the difference between gSCR and CgSCR (i.e., gSCR-CgSCR).

5.3.2.4 Identification of gSCR for on-line stability monitoring

The generalized short circuit ratio can be obtained by an online measurement method. Consider a MIPES that contains n wind turbines. The terminals of these wind turbines are represented by nodes 1 ~ n in the graph, and the interior nodes, which are not directly connected to a wind turbine, are denoted by nodes n + 1 ~ n + m. For example, Figure 12 shows a MIPES that contains nine wind turbines, wherein nodes 1~9 are directly connected to wind turbines and nodes 10~11 are interior nodes. The AC grid is simplified as an infinite bus using the Thevenin equivalent method.

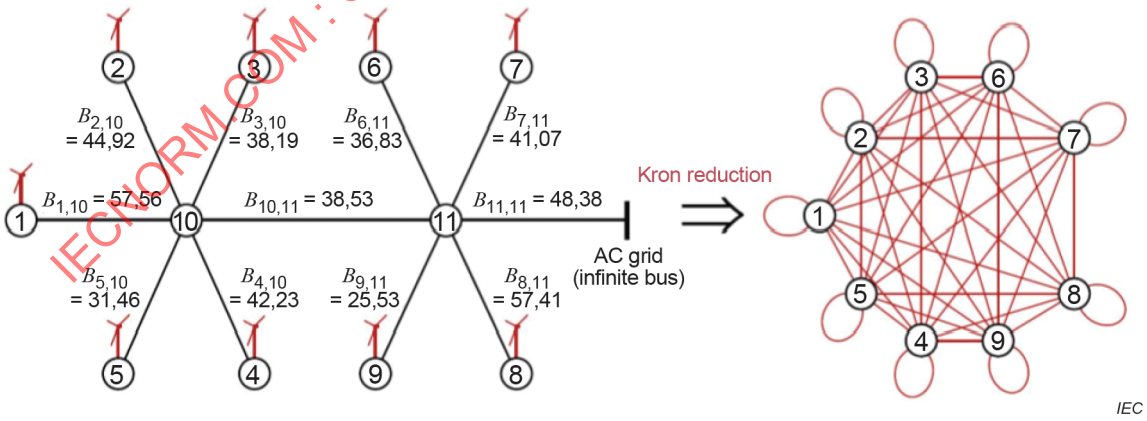

Figure 12 – A test wind farm system that contains nine wind turbines

Let $Z_{ij} = R_{ij} + jX_{ij}$ be the impedance between the i^{th} and j^{th} nodes, and $Y_{ij} = 1/Z_{ij}$ the corresponding admittance. The nodal admittance matrix $\mathbf{Y} \in R^{(n+m)\times(n+m)}$ can then be calculated

by $\mathbf{Y}_{ij} = -Y_{ij}, i \neq j$ and $\mathbf{Y}_{ii} = \sum_{j=1}^{n+m} Y_{ij}$ (Y_{ii} is the admittance between node i and the grounded node). The Kron-reduced admittance matrix can be further obtained by:

$$\overline{Y} = Y_1 - Y_2 \times Y_4^{-1} \times Y_3 \tag{41}$$

where

$\mathbf{Y}_1 \in R^{n\times n}$, $\mathbf{Y}_2 \in R^{n\times m}$, $\mathbf{Y}_3 \in R^{m\times n}$ and $\mathbf{Y}_4 \in R^{m\times m}$ are the sub-matrices of $\mathbf{Y}$ as $\mathbf{Y} = \begin{bmatrix} \mathbf{Y}_1 & \mathbf{Y}_2 \\ \mathbf{Y}_3 & \mathbf{Y}_4 \end{bmatrix}$.

When the lines are inductive, one only needs to consider the Kron-reduced susceptance matrix of the power network, which is $B = -\mathrm{Im}(\overline{\mathbf{Y}})$, where $\mathrm{Im}(R)$ denotes the imaginary part.

The grid strength and stability margin of the system can be evaluated based on the gSCR by using the current and voltage data of wind turbines measured from PMUs. The gSCR is the smallest eigenvalue of $\mathbf{S}_B^{-1}\overline{\mathbf{Y}}$, where $\mathbf{S}_B = \mathrm{diag}(S_{B1}, S_{B2}, \ldots, S_{Bn})$ is the diagonal matrix in which diagonal elements are the power of the wind turbines $S_{\mathrm{B}i}$, i=1,…,n. When the power $S_{\mathrm{B}i}$ is known, the Kron-reduced admittance matrix $\overline{\mathbf{Y}}$ can be solved by current and voltage data of wind turbines measured from PMUs. Let $\vec{I}_{i(k)}$ and $\vec{U}_{i(k)}$ respectively denote the current injection and voltage of node i measured at discrete time k, with $\Delta\vec{I}_{i(k)} = \vec{I}_{i(k)} - \vec{I}_{i(k-1)}$ and $\Delta\vec{U}_{i(k)} = \vec{U}_{i(k)} - \vec{U}_{i(k-1)}$. It can therefore be deduced that:

$$\Delta I_{(k)} = \overline{Y} \times \Delta U_{(k)} \tag{42}$$

where

$\Delta I_{(k)} = \left[\Delta\vec{I}_{1(k)} \quad \cdots \quad \Delta\vec{I}_{n(k)}\right]^T$;

$\Delta U_{(k)} = \left[\Delta\vec{U}_{1(k)} \quad \cdots \quad \Delta\vec{U}_{n(k)}\right]^T$.

Let $\overline{Y}_i$ denote the i^{th} row of $\overline{Y}$, which satisfies:

$$\Delta\vec{I}_{i(k)} = \Delta U_{(k)}^T \times \overline{\mathrm{Y}}_i^T \tag{43}$$

It can therefore be extended to the following in terms of N consecutive data sets:

$$\begin{bmatrix} \Delta\vec{I}_{i(1)} \\ \vdots \\ \Delta\vec{I}_{i(N)} \end{bmatrix} = \begin{bmatrix} \Delta U_{(1)}^{T} \\ \vdots \\ \Delta U_{(N)}^{T} \end{bmatrix} \times \overline{Y}_{i}^{T} \tag{44}$$

where

$\overline{Y}_{i}^{T}$ is an unknown parameter vector that has n dimensions.

Hence, $\overline{Y}_{i}^{T}$ can be uniquely solved by n data sets wherein $U_{(k)}^{T}(k \in \{1,\ldots n\})$ are linearly independent.

5.3.2.5 Case studies

1) A 5-infeed homogeneous system

Firstly, the gSCR of a 5-infeed power electronic homogeneous system with given network parameters is calculated in 5.3.2.5. The gSCR calculation method based on a simulation case is presented, and the validity of the gSCR theory is proved by eigenvalues comparison.

Figure 13 shows a topology of a 5-infeed power electronic system with identical converters' control and parameters. The rated capacity of PEDs and network parameters are presented in Figure 13 and Table 1 and Table 2.

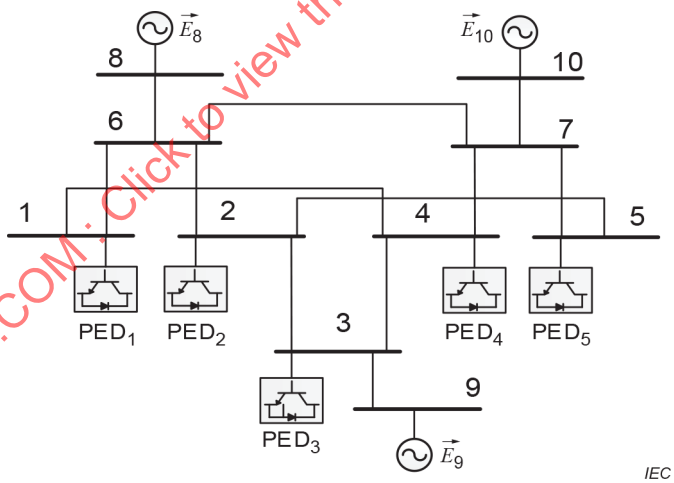

Figure 13 – One-line diagram of 5-infeed PES

Table 1 – Rated capacity of PEDs in 5-infeed PES in p.u.

No. of PEDs	1	2	3	4	5
S_B	1	2	3	1	2

Table 2 – Network parameters of 5-infeed PES in p.u.

L_{14}	0,1	L_{16}	0,2	L_{23}	0,2
L_{25}	0,1	L_{26}	0,1	L_{34}	0,15
L_{47}	0,16	L_{7}	0,08	L_{67}	0,3
L_{68}	0,1	L_{39}	0,05	$L_{7,10}$	0,2

The 5-infeed homogeneous PES is decoupled into its 5 equivalent SIPESs, and the SCR_{i_eq} values of each equivalent SIPES are presented in Table 3, and Figure 13 shows the eigenvalues of the 5-infeed homogeneous PES and its 5 equivalent SIPESs. The comparison results show that all eigenvalues of the 5-infeed PES are consistent with those of its 5 equivalent SIPESs. Thus, the stability of the 5-infeed system can be analyzed by studying the stability of each equivalent SIPES.

Table 3 – Relationship between equivalent SIPESs and eigenvalues of Y_{eq} in 5-infeed PES

SIPES	1	2	3	4	5
λ_i	2,564 1	7,293 7	10,853 2	15,115 5	29,319 2

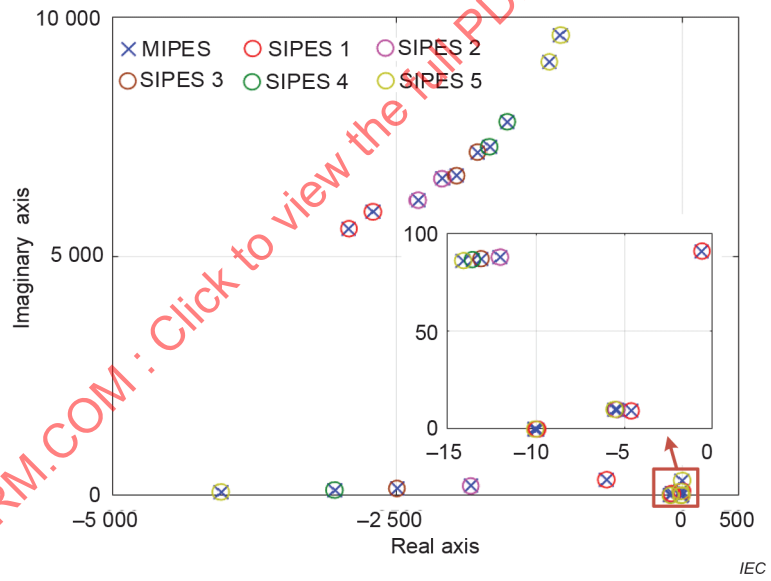

Figure 14 – Eigenvalue comparison of 5-infeed PES and its 5 equivalent SIPESs

2) IEEE 39-bus heterogeneous system

Figure 15 shows a heterogeneous system with 9 grid-following converters interconnected via an IEEE 39-bus meshed network. In such a 9-converter system, converters 1~6 use the DC voltage outer-loop control mode (U_{dc} control), and converters 7~9 adopt power outer-loop control mode (P control). The control parameters of converters 1~9 are shown in Table 4.

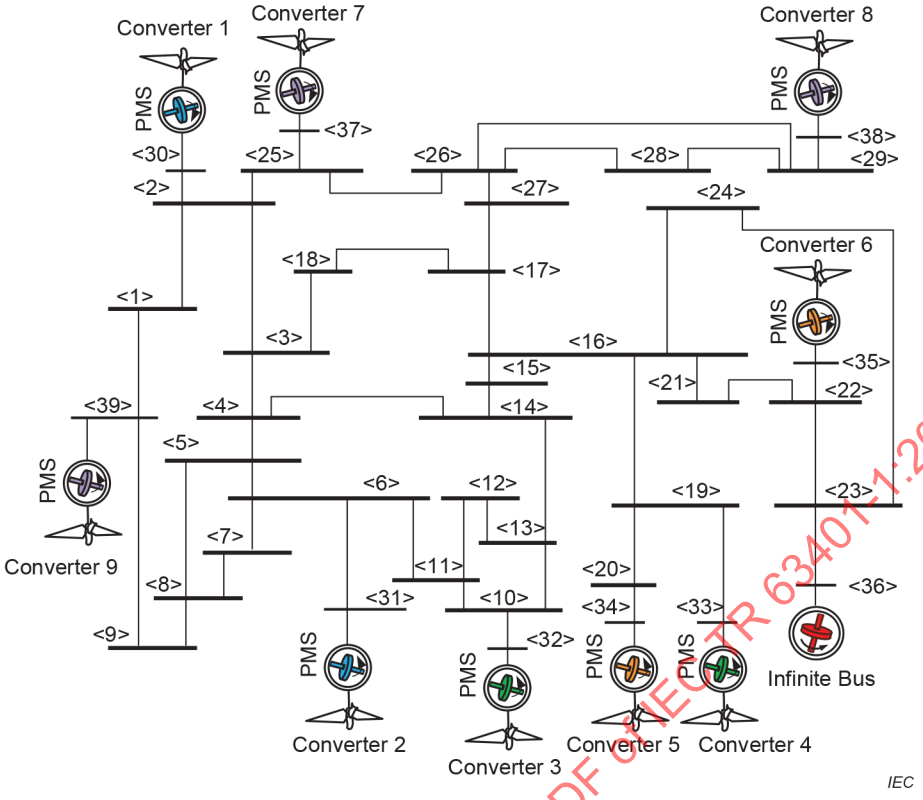

Figure 15 – The 9-converter heterogeneous system with a IEEE 39-bus network topology

Table 4 – Control parameters of converters

Filter inductance / filter capacitance / DC capacitance	0,05 / 0,05 / 0,038
PI parameters of current control loop	1 / 10
PI parameters of the constant active power control loop	1 / 10
PI parameters of the constant DC voltage control loop	0,5 / 5
Parameters of the voltage feed forward filter	0,01
PI parameters of the PLL in converter 1~2	29 / 7 500
PI parameters of the PLL in converter 3~4	35 / 7 200
PI parameters of the PLL in converter 5~6	40 / 7 000
PI parameters of the PLL in converter 7~9	26 / 7 800

In the 9-converter heterogeneous system, the proposed method in 5.3.2.2 is first validated by modal analysis. To this end, several cases are created in the system by equally proportionally changing coefficient k, which is proportional to the line length in the per-unit system. When increasing coefficient k from 0,5 to 1,0, the value of gSCR, the dominant eigenvalues, and the damping ratios of the dominant eigenvalues in the 9-converter heterogeneous system, which are shown in Figure 16 (a) and Figure 16 (b) are evaluated. Also, Figure 16 (a) and Figure 16 (b) show the dominant eigenvalues and the damping ratios of the dominant eigenvalues in the most critical subsystem decoupled from the equivalent homogeneous system of the 9-converter heterogeneous system when increasing coefficient k from 0,5 to 1,0.

It can be observed from Figure 16 that the small signal stability and stability margin of the 9-converter heterogeneous system can be assessed based on gSCR and its critical value CgSCR. Based on (46), the critical value CgSCR of 2,208 can be obtained. As shown in Figure 16 (a), when gSCR = CgSCR (i.e. gSCR – CgSCR = 0), the dominant eigenvalues in the 9-converter heterogeneous system are exactly at the imaginary axis, which indicates the system is critically stable. When gSCR is larger than CgSCR (i.e. gSCR – CgSCR > 0), the dominant eigenvalues in the 9-converter heterogeneous system are in the left-half of the complex plane, which suggests the system is stable and has a certain stability margin. When gSCR is smaller than CgSCR (i.e. gSCR – CgSCR < 0), the dominant eigenvalues in the 9-converter heterogeneous system are in the right-half of the complex plane, which means the system is unstable. The similar observation can also be obtained from Figure 16(b) in terms of the damping ratio. Thus, the small signal stability and stability margin of the 9-converter heterogeneous system can be identified by comparing the gSCR with CgSCR.

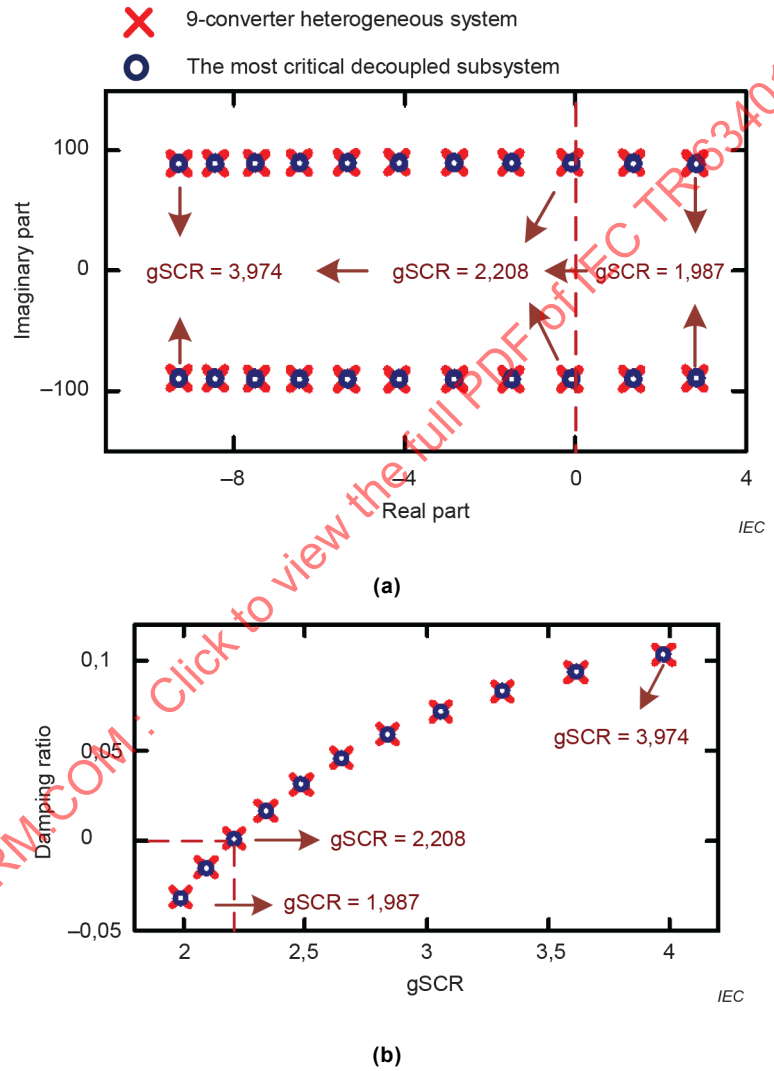

Figure 16 – The dominant eigenvalues and the damping ratios

5.3.3 Circuit aggregation method

5.3.3.1 Equivalent circuit-based short circuit ratio (ESCR)

The ESCR approach is based on assessment of the observed voltage change at one WPP bus (e.g., bus 1 shown in Figure 17) for a small voltage change at another WPP bus (e.g., bus 2 shown in Figure 17). The ESCR is an approximate indicator of the interactions between the WPPs. The interaction factor, termed here as wind plant interaction factor (WPIF), is defined as:

$$WPIF_{ij} = \frac{\Delta V_i}{\Delta V_j} \tag{45}$$

where

ΔV_i is the voltage change observed on bus i for a small voltage change at bus j.

WPP buses electrically far apart will have WPIF values closer to zero, whereas for buses very close, WPIF should be closer to unity.

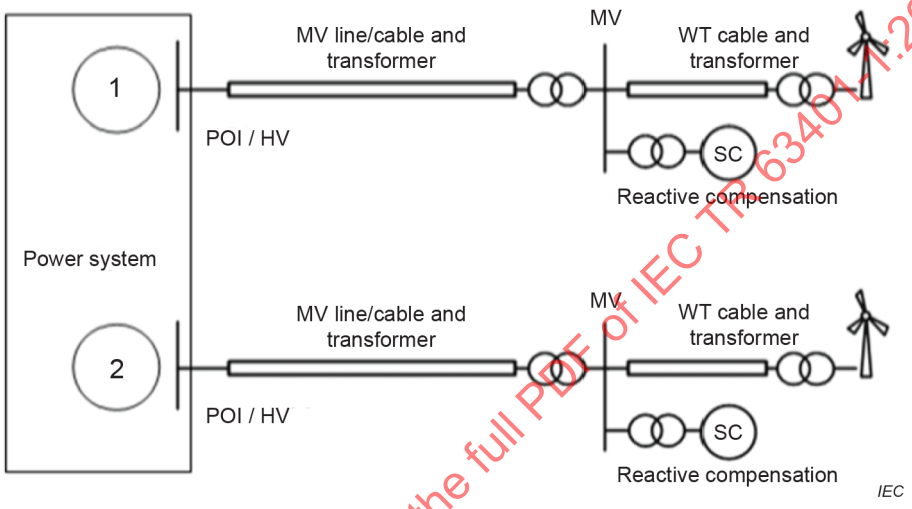

Figure 17 – Nearby WPP connected to the same region in a power system

When more than one WPP is connected to a power system, electrically close to each other, the short circuit level of the network in the region is shared between these WPPs. Hence the network strength, seen from one WPP is significantly less than the network short circuit level calculated at the bus. The following definition of ESCR extends the concept of SCR for a given WPP, approximately considering the sharing of the network strengths by the other nearby WPPs:

$$ESCR_i = \frac{S_i}{P_{\mathrm{WF}i} + \sum_j (WPIF_{ji} \times P_{\mathrm{WF}j})} \tag{46}$$

An advantage of the use of ESCR is that it can be readily amended to cater to any conceivable configuration for connection of multiple WPPs.

The above (46) can also be expressed in terms of the elements of the impedance matrix Z, of the network, connecting the wind farms. Equivalent representation of multiple wind farms connecting to a power system with its Z matrix is shown in Figure 18.

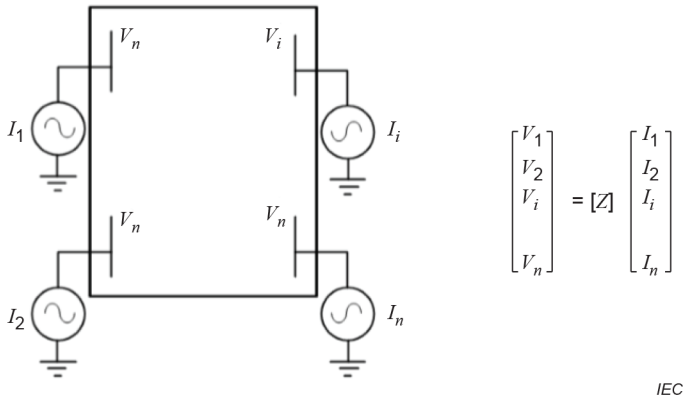

Figure 18 – Equivalent representation of multiple windfarms connecting to a power system with its *Z* matrix

Assuming a small change of current at the i^{th} node:

$$\Delta V_j = Z_{ji} \Delta I_i \tag{47}$$

$$\Delta V_i = Z_{ii} \Delta I_i \tag{48}$$

Resulting in a WPIF of:

$$WPIF_{ji} = \frac{\Delta V_j}{\Delta V_i} = \frac{z_{ji}}{z_{ii}} \tag{49}$$

Also noting, if the system is represented in p.u., on the base power of $P_{\mathrm{WF},i}$:

$$SCR_{\mathrm{POI},i} = \frac{S_{\mathrm{POI},i}}{P_{\mathrm{WF},i}} = \frac{1}{Z_{ii}} \tag{50}$$

Hence, when all quantities are represented in p.u., on a base power of $P_{\mathrm{WF},i}$, Formula (39) can be written as:

$$ESCR_i = \frac{S_i}{P_{\mathrm{WF}i} + \sum_j (WPIF_{ji} \times P_{\mathrm{WF}j})} = \frac{P_{\mathrm{WF}i} / Z_{ii}}{P_{\mathrm{WF}i} + \sum_{j=1,m,j\neq i} \frac{Z_{ji}}{Z_{ii}} P_{\mathrm{WF}j}} = \frac{1}{\sum_{j=1,m} Z_{ji} P_{\mathrm{WF}j,\mathrm{pu}}} \tag{51}$$

In considering a common situation where two WPPs connecting to one bus, or electrically close to each other, when there is no appreciable impedance between the WPPs, and all are connected to the same point in the network (as shown in Figure 19), SCR calculations can be modified as follows:

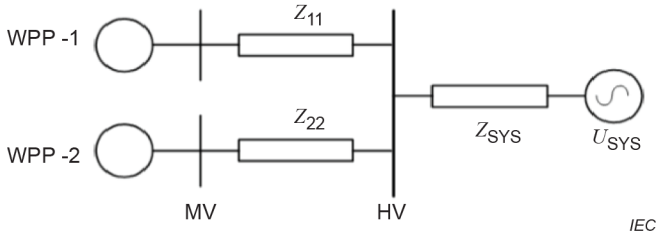

Figure 19 – Equivalent circuit representation of two WPPs connected to the same connection point-configuration 2

$$ESCR_{WF1}=\frac{1}{(P_{WF1}\times z_{11})+Z_{sys}\times(P_{WF1}+P_{WF2})} \tag{52}$$

$$ESCR_{WF2}=\frac{1}{(P_{WF2}\times z_{22})+Z_{sys}\times(P_{WF1}+P_{WF2})} \tag{53}$$

where

Z_{11} and Z_{22} primarily represent transformer impedances in each of the WPPs, and all quantities are expressed in p.u., with the base power of the respective wind farm rated power.

5.3.3.2 Weighted short circuit ratio (WSCR)

Another appropriate index for the calculation of the impact of adjacent WPPs is the weighted short circuit ratio (WSCR), defined by:

$$\begin{aligned} WSCR&=\frac{Weighted\quad S_{SCMVA}}{\sum_{i}^{N}P_{RMWi}}\\ &=\frac{(\sum_{i}^{N}S_{SCMVAi}\times P_{RMWi})/\sum_{i}^{N}P_{RMWi}}{\sum_{i}^{N}P_{RMWi}}\\ &=\frac{\sum_{i}^{N}S_{SCMVAi}\times P_{RMWi}}{(\sum_{i}^{N}P_{RMWi})^{2}} \end{aligned} \tag{54}$$

where

S_{CMVAi} is the short circuit capacity at bus i before the connection of WPP i;

R_{MWi} is the MW rating of WPP i to be connected;

N is the number of WPPs fully interacting with each other;

i is the WPP index.

A small sample system with four WPPs, as shown in Figure 20, is used to demonstrate the proposed WSCR concept. The subsystem, consisting of four WPPs in close proximity, connects to the main system with weak links. Table 5 shows the WPP sizes and SCR values calculated for assuming no interaction.

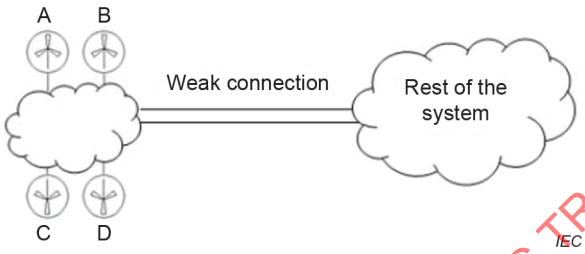

Figure 20 – Four WPPs integrated into the system with weak connections

Table 5 – Wind capacity and SCR values assuming no interaction

WPP	Rating MW	Short circuit capacity	SCR
a	1 200	6 500	5,42
b	1 000	8 000	8
c	800	8 500	10,63
d	2 000	7 000	3,5

The WSCR index can then be calculated as follows:

$$WSCR = \frac{1200 \times 6500 + 1000 \times 8000 + 800 \times 8500 + 2000 \times 7000}{(1200 + 1000 + 800 + 2000)^2} = 1{,}46 \quad (55)$$

5.3.3.3 Composite short circuit ratio (CSCR)

In this method, the multiple WPPs connecting to the same HV bus or HV busses in closed electrical proximity are approximated as single aggregated WPPs connected to the common MV bus as shown in Figure 21.

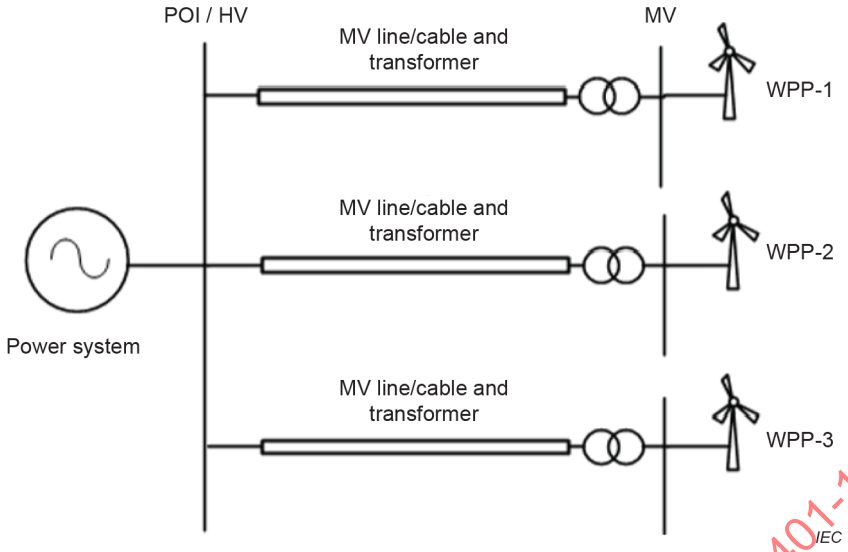

Figure 21 – Multiple WPPs connecting to the same HV bus or HV buses in close proximity

The equivalent circuit for the WPP connections is shown in Figure 22.

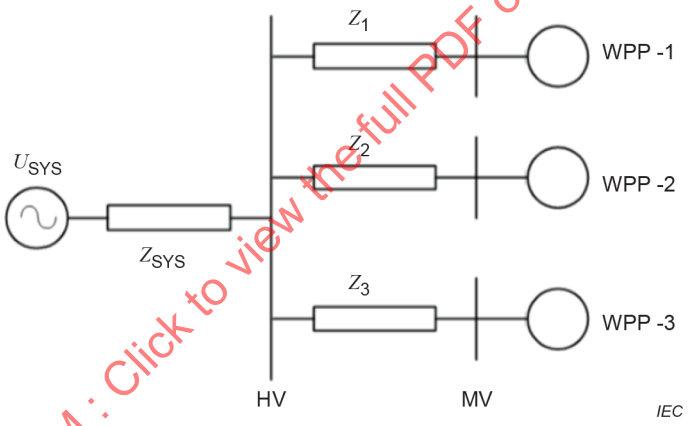

Figure 22 – Equivalent circuit representation of WPPs connecting to the same HV bus

In the CSCR method, all the WPPs are assumed to be connected to the same MV bus. The approximate equivalent circuit representation is shown in Figure 23.

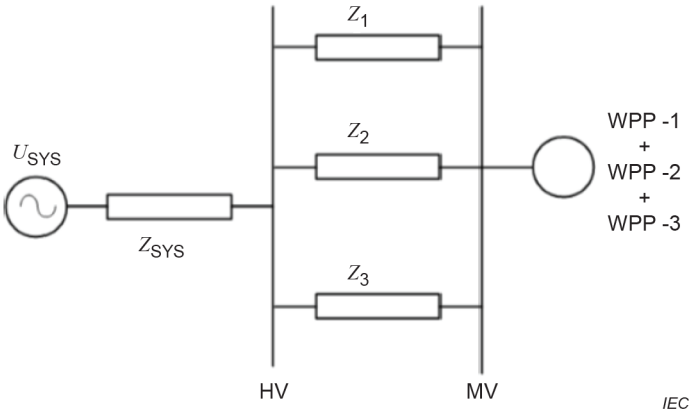

Figure 23 – Approximate equivalent representation assumed for CSCR method

It is assumed that all the impedances are represented as p.u. values, based on an MVA base of S_{BASE}.

The approximate short circuit level at the MV bus in p.u. is given by (assuming U_{SYS} is approximately unity):

$$S_{MV,pu} = \frac{U^2_{SYS,pu}}{Z_{SYS} + \frac{1}{\frac{1}{z_1} + \frac{1}{z_2} + \frac{1}{z_3}}} = \frac{1}{Z_{SYS} + \frac{1}{\frac{1}{z_1} + \frac{1}{z_2} + \frac{1}{z_3}}} \quad (56)$$

The approximate short circuit level in MVA is given by:

$$S_{MV} = S_{MV,pu} \times S_{BASE} \quad (57)$$

The CSCR is defined as:

$$CSCR = \frac{S_{MV}}{(WP1_{RAT} + WP2_{RAT} + WP3_{RAT})} \quad (58)$$

where

$WP1_{RAT}$, $WP2_{RAT}$, and $WP3_{RAT}$ are the rating of WPP1, WPP2, and WPP3.

Substituting Formula (57) and Formula (58) in Formula (56), CSCR is calculated as:

$$CSCR = \frac{S_{BASE}}{(WP1_{RAT} + WP2_{RAT} + WP3_{RAT})} \times \frac{1}{Z_{SYS} + \frac{1}{\frac{1}{z_1} + \frac{1}{z_2} + \frac{1}{z_3}}} \quad (59)$$

In a more general approach, SMV can be calculated with a short circuit program. The medium voltage buses should be connected to a branch of negligible impedance and the three-phase fault level of the joint buses should be calculated. The calculation should assume no short circuit contribution of the WPPs. The CSCR can be calculated as indicated in (59).

In this case, there is an important distinction between the short circuit level at the medium voltage collector bus and the composite short circuit level with the medium voltage buses connected. Unlike the ESCR index, which calculates the short circuit ratio for each of the adjacent WPPs, the CSCR approach calculates an aggregate SCR for a fictitious WPP comprising all those adjacent WPPs.

5.4 Summary

The strength of a power system is a metric used to describe the ability of a power system to maintain the core characteristics through which the system interacts with a connection, namely voltage and frequency, as steadily as possible, under all operating conditions. The strength or weakness of a power system is a relative concept and needs to be addressed both in terms of the system characteristics at a given connection point as well as the size of the WPP(s) to be connected to the connection point. SCR is a commonly used metric for quantifying the relative power system impedance seen from a connection point. The SCR seen by a generator strongly influences its ability to operate satisfactorily both in steady state and following system disturbances. While there are several methods for calculating the SCR, eigenvalue decomposition-based generalized short circuit ratio (gSCR) is presented for calculation of the short circuit ratio for any given WPP and power system. Three other approaches referred to as equivalent circuit-based short circuit ratio (ESCR), composite short circuit ratio (CSCR), and weighted short circuit ratio (WSCR) are presented and compared with gSCR. The definition of different MISCRs is shown in Table 6.

Table 6 – The definition of different MISCRs

Different types of SCRs	Definitions	Interaction factors	Critical values
gSCR	$\frac{1/Z_{ii}}{\sum_{j=1}^{n} P_j \times \frac{Z_{ij}}{Z_{ii}} \frac{v_{j1}}{v_{i1}}}$	$\frac{Z_{ij}}{Z_{ii}} \frac{v_{j1}}{v_{i1}}$	Obtained from a WPP
ESCR	$\frac{1/Z_{ii}}{\sum_{j=1}^{n} P_j \times \frac{Z_{ij}}{Z_{ii}}}$	$\frac{Z_{ij}}{Z_{ii}}$	Try and error
WSCR	$\frac{\sum_{i}^{N} S_{\mathrm{SCMVA}i} * P_{\mathrm{RMW}i}}{(\sum_{i}^{N} P_{\mathrm{RMW}i})^2}$	$\frac{P_{\mathrm{RMW}i}}{\sum_{i}^{N} P_{\mathrm{RMW}i}}$	Try and error
CSCR	$\frac{1/Z_{ii}}{\sum_{j=1}^{n} P_j \cdot \left(Z_{sys} + Z_1 \parallel Z_2 \parallel \cdots \parallel Z_n\right) / Z_{ii}\right)}$	$(Z_{\mathrm{sys}} + Z_1 \parallel Z_2 \parallel \cdots \parallel Z_n) / Z_{ii}$	Try and error

Each of the methods described in the preceding subclauses has benefits and drawbacks as a screening tool to identify weak grid conditions and potential issues with inverter-based resources. Table 7 provides an illustrative description of the similarities, differences, benefits, and drawbacks of these metrics. The '×' represents that the metric cannot be applied for the described purpose. One star '※'represents that the metric can be applied with some additional effort or processing, or can be applied to a limited extent, and two stars '※※' represents that the metric is easily or directly applied for these purposes.

Table 7 – Comparison of SCR methods

Metric		Simple calculation using short circuit program	Accounts for nearby inverter-based equipment	Provides common metric across a larger group of VER	Accounts for weak electrical coupling between plants within larger group	Considers non-active power inverter capacity	Able to consider individual sub-plants within larger group
SCR	Short circuit ratio	※※	×	×	×	×	×
CSCR	Composite SCR	※	※※	※※	×	×	×
WSCR-MW	Weighted SCR using MW	※	※※	※※	※	×	×
WSCR-MVA	Weighted SCR using MVA	※	※※	※※	※	※※	×
SCRIF	Multi-infeed SCR	×	※※	×	※※	※※	※※
gSCR	Generalized short circuit ratio	×	※※	※※	※※	※※	※※

Each metric has benefits and drawbacks in its application for assessing system strength and potential weak grid issues. These may include:

1) Simple calculation using short circuit programs: The metric utilizes positives sequence short circuit program for primary results. Some simple additional manipulation or post-processing may be required.
2) Accounting for nearby inverter-based equipment: The metric inherently considers the presence of nearby inverter-based equipment, particularly if the equipment is very close.
3) Common metric across a large group of inverter-based resources: The metric provides a single consolidated value for all the plants within the selected group.
4) Accounts for weak coupling between plants within larger group: The metric is able to consider the isolating effect of impedance between inverter-based resource plants, or to consider that each plant may be obtaining system strength from different sources (as opposed to assuming plants are perfectly coupled, essentially a single plant).
5) Considers non-active power inverter capacity: The metric accounts for the capacity of inverters nearby which may require a strong system, but do not generate active power. Examples could be curtailed wind plants, static compensators (STATCOMs), or SVCs.
6) Considers individual sub-plants within larger group: The metric provides a system strength value at any number of individual buses within a group, accounting for the presence of the others.

6 Steady state voltage stability issue for low short circuit ratio AC networks

6.1 Problem statements

With the rapid development of science and technology, the excessive consumption of conventional energy such as coal, oil, and natural gas has made energy shortages and environmental pollution the main bottleneck for the development of various countries. The development and utilization of renewable energy represented by wind energy and photovoltaic power has become one of the energy strategic decisions for sustainable development. However, the increasing use of the inverter-based renewable resources introduces new challenges in assessing the steady-state stability in weak-grids. The distribution of renewable energy is often far from the load centre, and it often requires long-distance power transmission lines to be integrated into the power grid. Therefore, the grid becomes weaker, and the power output of the inverter-based resources is limited by the grid conditions. The high grid impedance usually makes the inverters more prone to instability. On the other hand, the access to the renewable energy sources generally increases the active power output and decreases the voltage near the busbar, which causes a decreasing of the weak grid steady-state stability.

In Clause 6, the analysis methods of the steady state stability issues are illustrated. The mechanism of the instability which is caused by the inverter-based resources integration under weak-grid conditions is specified. Moreover, some improved control algorithms of the inverters are proposed to handle the weak-grid grid stability degradation which is caused by the large-scale inverter-based resources integration.

6.2 Steady state stability analysis method

6.2.1 *P-V* curve

Voltage stability is in power systems. It is usually associated with weak grids and heavy-load grids. The *P-V* curve method is a classical method for analyzing the static voltage stability of power systems. The *P-V* curve method analyses the static voltage stability problem of the system by plotting the relationship between the voltage and the active power output.

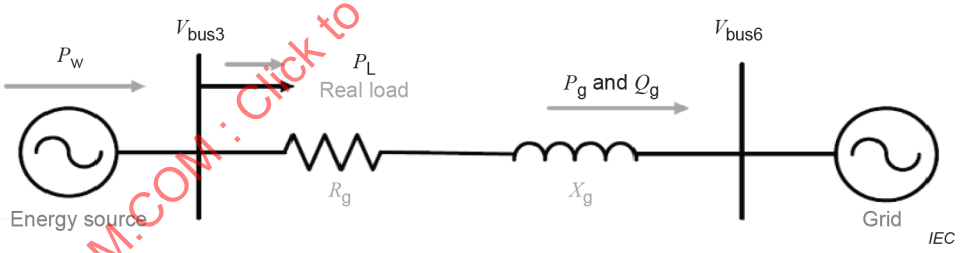

Figure 24 – System topology

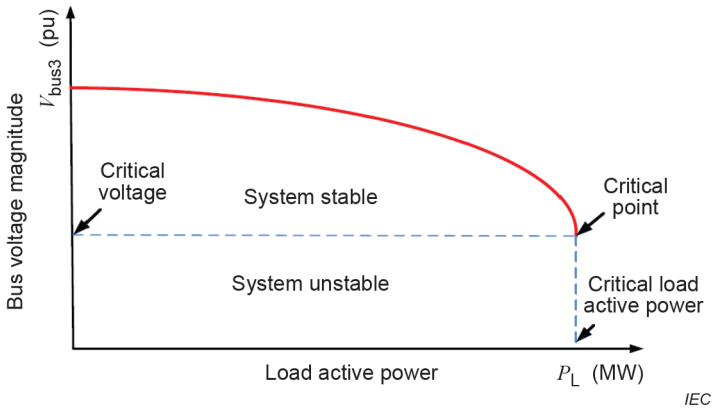

Figure 25 – Typical *P-V* curve

The system topology is illustrated in Figure 24. Figure 25 shows a typical P-V curve, where the abscissa denotes P_L and the ordinate denotes V_{bus3}. It can be seen that as the load active power increases, the voltage gradually decreases. When the critical point is reached, the voltage drops become faster when the load demand is increased. Also, when the curve crosses the critical point, the current will no longer converge, meaning that the system will be unstable. Consequently, the P-V curve can be used to analyze the stable operating range of the system.

6.2.2 Q-V curve

The Q-V curve method is also a powerful tool to analyze the static voltage stability of power systems. It reflects the relationship between the busbar voltage and the reactive power injected into the grid node. The busbar is connected with a virtual synchronous generator; therefore, different target voltage values can be set and the reactive power of the synchronous generators output corresponding to different voltage values through the power flow can be calculated. The curve between the busbar voltage and the reactive power of the synchronous generators output can be drawn.

The system topology is illustrated in Figure 26. Figure 27 is a typical Q-V curve. The reactive power output set to zero corresponds to the actual operating point of the system. The difference value between the operating point and the Q-V curve critical point is the reactive power stability margin of this node. If the Q-V curve of a node is above the abscissa axis, it means that the reactive power of the system is insufficient. If there is no additional reactive power injection, the grid will not operate. At this time, the vertical distance between the critical point and the horizontal axis represents a negative stability margin. At least the extra reactive power is required when the system is running. In addition, the operating point reflects the node voltage strength of the system. With the stronger intensity, the voltage change of the same magnitude requires more reactive power. For different strength grids, draw their Q-V curves and analyse the reactive margin and node voltage strength of different strength grids.

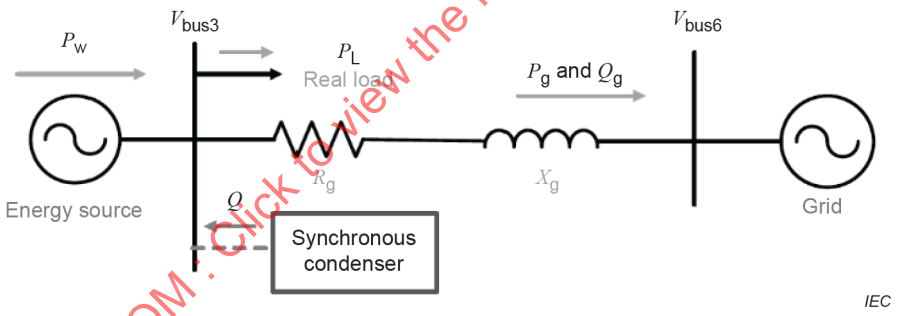

Figure 26 – System topology

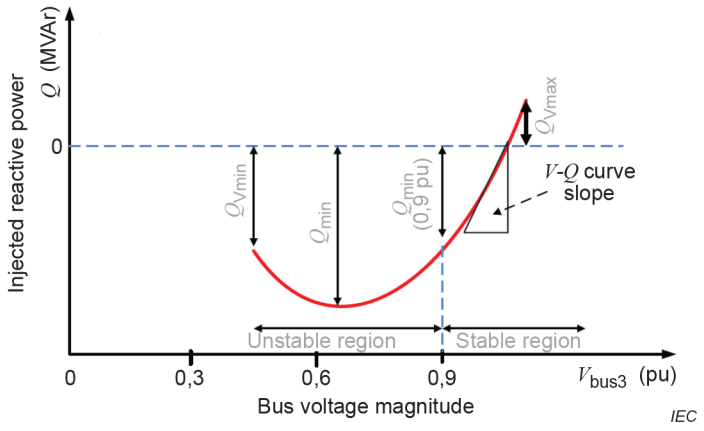

Figure 27 – Typical Q-V curve

6.2.3 Voltage sensitivity analysis

6.2.3.1 General

The large-scale wind power integration system can be simplified to an equivalent circuit, where a wind farm is integrated into an infinite bus power system via a transmission line. The generating powers of the wind farm can be expressed as $S = P_W + jQ_W$. Suppose the resistance of the transmission line is small enough to be ignored, the impedance of transmission line can be represented by X. The static reactive power compensation capacity of the wind farm is equivalent to the capacitance value (B) of the capacitor. The simplified equivalent circuit of a large-scale wind power integration system is shown in Figure 28.

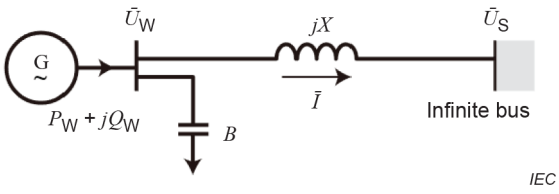

Figure 28 – Simplified equivalent circuit of large-scale wind power integration system

The transmission powers of the wind power integration system in Figure 26 are expressed as follows:

$$P_W + jQ_W = \dot{U}_W \dot{I}^* = (U_W \cos\delta + jU_W \sin\delta)[\frac{U_W \cos\delta + jU_W \sin\delta - U_S}{jX} + (U_W \cos\delta + jU_W \sin\delta)jB]^* \\ = \frac{U_W U_S \sin\delta}{X} + j(\frac{U_W^2 - U_W U_S \cos\delta}{X} - U_W^2 B) \quad (60)$$

The above formula can be expressed as follows:

$$\begin{cases} P_W = \dfrac{U_W U_S \sin\delta}{X} \\ Q_W = \dfrac{U_W^2 - U_W U_S \cos\delta}{X} - U_W^2 B \end{cases} \quad (61)$$

where $U_S$is the grid voltage, and the power angle in Formula (61) meets the following formula:

$$\sin^2\delta + \cos^2\delta = 1 \quad (62)$$

Nowadays, in order to use maximally wind energy, the power factor of variable speed wind turbines is usually set to 1. Therefore, there is no reactive power from the wind farm. Referring to Formula (61) and Formula (62), wind power integration system meets the following formula:

$$(P_W X)^2 + U_W^4 (1 - BX)^2 = U_W^2 U_S^2 \quad (63)$$

6.2.3.2 Voltage/reactive power sensitivity (dU_W/dQ)

Referring to Formula (63), the reactive power compensation capacity (Q) of a wind farm can be expressed as follows:

$$Q = U_W^2 B = \frac{U_W^2 - \sqrt{U_W^2 U_S^2 - (P_W X)^2}}{X} \tag{64}$$

P_W is considered as a constant, therefore the partial derivatives of Formula (64) can be expressed as follows:

$$\frac{dU_W}{dQ} = \frac{X\sqrt{U_S^2 U_W^2 - P_W^2 X^2}}{2U_W\sqrt{U_S^2 U_W^2 - P_W^2 X^2} - U_W U_S^2} \tag{65}$$

The voltage/reactive power sensitivity can be expressed by dU_W/dQ. According to Formula (65), P_W, X, U_S, U_W and B should meet Formula (63) simultaneously.

6.2.3.3 Voltage/active power sensitivity (dU_W/dP_W)

Referring to Formula (63), P_W can be written as:

$$P_W = \frac{\sqrt{U_W^2 U_S^2 - U_W^4 (1 - BX)^2}}{X} \tag{66}$$

If B is a constant, the partial derivatives of Formula (66) are expressed as follows:

$$\frac{dU_W}{dP_W} = \frac{X\sqrt{U_S^2 - U_W^2 (1 - BX)^2}}{U_S^2 - 2U_W^2 (1 - BX)^2} \tag{67}$$

where

dU_W/dP_W represents the voltage/active power sensitivity.

According to Formula (67), P_W, X, U_S,U_W and B should meet Formula (65) simultaneously.

If the voltage of the infinite bus power system, U_S = 220 kV and the parameters of the transmission line, L = 200km, then the unit impedance is 0,41 Ω/km. If the reference voltage, U_B = 220 kV, and the reference apparent power, S_B = 1 000 MVA, then the impedance of transmission line,X = 1,694p.u. The voltage (U_W) of PCC, the voltage/reactive power sensitivity (dU_W/dQ) and voltage/active power sensitivity (dU_W/dP_W) shall meet Formula (68):

$$\begin{cases} U_{\text{min}} \le U_{\text{W}} \le U_{\text{max}} \\ \left| \frac{dU_{\text{W}}}{dQ} \right| < \mu_{\text{q}} \\ \left| \frac{dU_{\text{W}}}{dP_{\text{W}}} \right| < \mu_{\text{p}} \end{cases} \tag{68}$$

where

U_{min} and U_{max} are the minimum and maximum voltage values, which are usually set to 0,9 p.u. and 1,1 p.u., respectively, according to the grid code.

The maximum voltage/reactive power sensitivity ($|dU_{\text{W}}/dQ|$) is μ_{q} = 0,5 kV/Mvar, and the maximum voltage/active power sensitivity ($|dU_{\text{W}}/dP_{\text{W}}|$) is μ_{p} = 0,5 kV/MW. Referring to Formula (63), Formula (65), Formula (67) and Formula (68), the voltage/reactive power sensitivity ($|dU_{\text{W}}/dQ|$) of the PCC is shown in Figure 29, and the voltage/active power sensitivity ($|dU_{\text{W}}/dP_{\text{W}}|$) of the PCC is presented in Figure 29 b). It can be observed that the control response of DFIG based on the power electronic technology is fast, which leads to a dynamic interaction between the DFIG and the voltage of the PCC. There are various instability operation risks. Firstly, the higher voltage sensitivity may cause power oscillation under the active power or reactive power disturbance. Secondly, the power grid becomes weaker when the fault line is removed, and the power oscillation of power grid is more likely to occur. For example, assume that the DFIG based wind turbines operate at point A. There is a power oscillation at point B when the DFIG based wind turbines operate at point B because of active power disturbance. There is a power oscillation at point C, when the DFIG based wind turbines operate at point C because of reactive power disturbance.

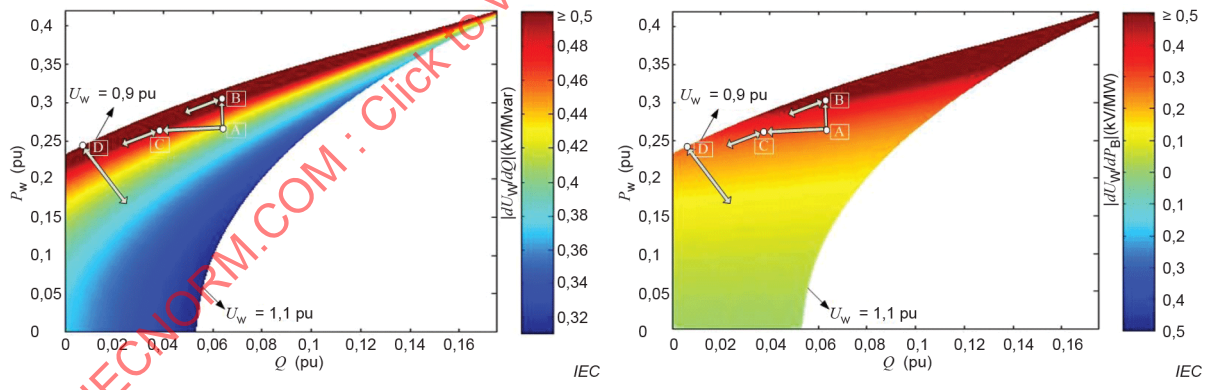

a) Voltage sensitivity (kV/Mvar) at PCC **b) Voltage sensitivity (kV/MW) at PCC**

Figure 29 – Voltage sensitivity at PCC of large-scale wind power integration system

Figure 30 depicts a single generator (or aggregate of many smaller generators) connected to an infinite bus through an equivalent network impedance.

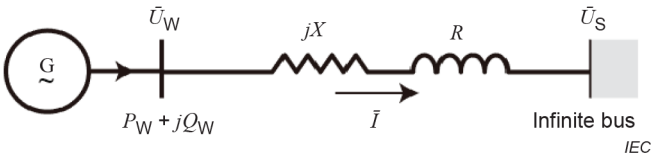

Figure 30 – Single generator connected to an infinite bus via grid impedance

According to the first principles, the voltage magnitude U_W at the generator bus in Figure 30 is found to satisfy the Formula (69) in terms of the generator power output (P_W, Q_W), the network impedance components (R, X) and the infinite bus voltage U_S:

$$U_S{}^4 - \left[2(RP_w + XQ_w) \mp U_S^2\right] U_S{}^2 + \left(R^2 + X^2\right)\left(P_W{}^2 + Q_W{}^2\right) = 0 \tag{69}$$

This is a quadratic formula in U^2 and thus has an exact analytical solution. It is most easily expressed in terms of the voltage ratio $\rho = U_W / U_S$:

$$\rho^2 \overset{\text{def}}{=} \left(\frac{U_W}{U_S}\right)^2 = \frac{1}{2}(1 + 2\lambda \pm \sqrt{1 + 4\left(\lambda - \mu^2\right)})$$
$$\lambda = \frac{RP_W + XQ_W}{U_S^2}, \mu = \frac{XP_W - RQ_W}{U_S^2} \tag{70}$$

Observe that the quantities λ and μ appearing in this solution are dimensionless. They are respectively the real and imaginary parts of the complex quantity $ZS^* / U_S^2, Z = R + jX$.

The relation of the terminal voltage magnitude to the generated power may be visualized in a number of ways. For the study of generator connections, the most convenient is the P-V curve obtained by plotting V (or ρ) against active power P for fixed reactive power Q. A typical family of P-V curves for a weak-grid connection is shown in Figure 31.

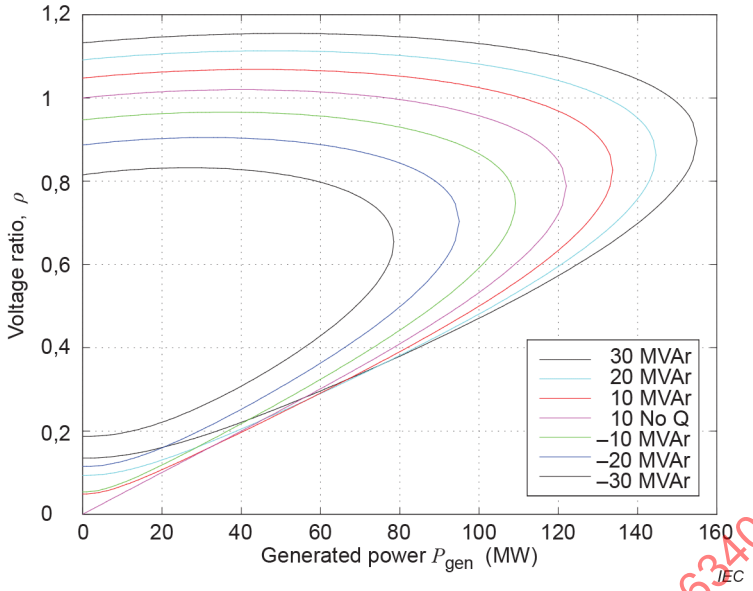

Figure 31 – *P-V* curves for a typical generator in a weak grid

Note that the usual generator sign convention is observed here, where Q is taken as positive for reactive power export to the grid and negative for reactive power import from the grid.

As Figure 31 shows, a typical P-V curve is nonlinear and tends toward a "knee point" at an ultimate value of P where the stable and unstable branches meet. This is the voltage collapse point, and corresponds to the point where the quantity under the square root in the above solution becomes zero:

$$1 + 4\left(\lambda - \mu^2\right) = 0 \tag{71}$$

Once again, this is a quadratic formula in each of the system quantities (P_W, Q_W, R, X, U_S^2) and in particular can be solved for the limiting power P_{max} at voltage collapse:

$$P_{max} = \frac{U_S^2}{2X} \times \left(\frac{|Z|}{X} \sqrt{1 + \frac{4XQ}{U_S^2}} + \frac{R}{X}\left(1 + \frac{2XQ}{U_S^2}\right)\right) \tag{72}$$

As is evident from both Formula (72) and Figure 31, increasing the reactive power export Q increases P_{max} and thus boosts the power export capacity of the connection, while reducing Q has the opposite effect. The formula also shows that the amount by which P_{max} increases or decreases for each 1 Mvar of reactive power export or import is sensitive to the X/R ratio of the network. When R is negligible, then to a good approximation P_{max} increases by 1 MW for every 1 Mvar of reactive power injection. On the other hand if $R \approx X$, then an additional 1 Mvar of reactive power injection can theoretically increase P_{max} by $\sqrt{2}+1 = 2{,}4$ MW at the generator terminals (keeping in mind that the network losses will also increase accordingly).

Provided $P_W \ll P_{max}$, simpler approximate formulae for the stable branch of the voltage solution are available. Applying the standard approximation $\sqrt{1+\varepsilon} \approx 1+\varepsilon/2\sqrt{1+\varepsilon} \approx 1+\varepsilon/2$ twice in succession to the exact solution formula above gives the following quadratic rule:

$$\rho = \frac{U}{U_W} \approx 1 + \lambda - \frac{\mu^2}{2} \tag{73}$$

Frequently the μ^2 term is also dropped, leading to the commonly-used rule of thumb (linear rule):

$$\frac{U}{U_S} \approx 1 + \lambda \quad \text{or} \quad U \approx U_S + \frac{RP_W + XQ_W}{U_S} \tag{74}$$

The linear rule should be used with caution as a first estimate only of voltage rise or drop, as its validity relies on the product XP_W (the largest term in μ) being at least an order of magnitude smaller than U_s^2.

6.2.4 Relation to short circuit ratio

The above formulae for voltage sensitivity to power flow are broadly applicable to all generator connections capable of being reduced to the simplified model. However, it is the defining characteristic of weak connections that the voltage sensitivity dU_W/dP_W or dU_W/dQ implied by these formulae is substantially greater than what is seen at a traditional generating centre within a large power system. This is typically explained in terms of the generating centre having a much greater fault level or short circuit ratio than the weak generator connection.

The key relation between SCR and voltage sensitivity stems from the following entity, alluded to above, for the dimensionless quantities λ and μ:

$$\lambda + j\mu = \frac{ZS^*}{U_S^2} = \frac{1}{U_S^2}(R + jX)(P_W - jQ_W) \tag{75}$$

Let the generator now operate at its rated MVA output: that is, let P_W and Q_W be such that. $|S| = \sqrt{P_W{}^2 + Q_W{}^2} = S_{gen}$ Then, taking the magnitude of the above expression one has:

$$|\lambda + j\mu|_{\text{Rated MVA}} = \frac{|Z|S_{gen}}{U_S^2} = |Z|\left(\frac{S_{gen}}{s_b}\right)\left(\frac{U_b^2}{U_S^2}\right)\left(\frac{s_b}{u_b^2}\right) = |Z_{pu}|\left(\frac{s_{gen}}{s_b}\right)\left(\frac{u_b}{U_S}\right)^2 \tag{76}$$

noting that U_b^2 / S_b is the base impedance for the per-unit system. But comparing this with the formula above for SCR, and employing the approximation $U_S \approx U_b$ usual for fault calculations, it is apparent that:

$$| \lambda + j\mu |_{\text{RatedMVA}} = \frac{1}{\text{SCR}} \left(\frac{U_b}{U_S} \right)^2 \approx \frac{1}{\text{SCR}} \tag{77}$$

One sees then that the quantities λ and μ central to voltage sensitivity are very closely related to the reciprocal of the SCR. It follows that the smaller the SCR, the greater the tendency toward high voltage sensitivity. The numbers λ and μ help to quantify this relationship, but they do not do so with equal force: it is seen above that λ has a first order effect on local voltage while μ has only a second order effect (at least when $P_W < P_{max}$). To separate the influences via λ and μ one shall know not just the SCR, but also the X/R ratio that good practice recommends quoting alongside SCR figures.

Returning again to the identity $\lambda + j\mu = ZS^* / U_S^2 \lambda + j\mu = ZS^* / U_S^2$ and focusing on the angles of the complex quantities involved, there results the formula:

$$\arctan \frac{\mu}{\lambda} = \arctan \frac{X}{R} - \arctan \frac{Q_W}{P_W} = \arctan \frac{X}{R} - \phi \tag{78}$$

where $= \pm \arccos(pf)$ is the power factor angle for the generator, with positive sign for Q_W export and negative for Q_W import. Applying standard trigonometric identities, one arrives at:

$$\frac{\mu}{\lambda} = \frac{X / R - \tan\phi}{1 + (X / R)\tan\phi} \tag{79}$$

where

$$\tan\phi = \frac{Q_W}{P_W} = \pm \sqrt{\frac{1}{pf^2} - 1}, \frac{\mu}{\lambda} = \frac{X / R - \tan\phi}{1 + (X / R)\tan\phi}.$$

Note that this formula applies for any amount of active and reactive power at the generator: in particular the ratio μ/λ is seen to depend only on the network X/R ratio and the operating power factor of the generator. (This also follows directly from the original definition of λ and μ above.)

One finally has (subject to the approximation $U_S \approx U_b$) the following alternative definitions of λ and μ giving their values directly from the calculated SCR and the network X/R ratio, without first calculating the network impedance Z:

$$\lambda = \frac{1}{SCR} \times \frac{(X / R)q + p}{\sqrt{1 + (X / R)^2}}, \quad \mu = \frac{1}{SCR} \times \frac{(X / R)p - q}{\sqrt{1 + (X / R)^2}} \tag{80}$$

where

$p = P_{\mathrm{w}} / S_{\mathrm{gen}}$ and $q = Q_{\mathrm{w}} / S_{\mathrm{gen}}$ are the generator power outputs in per-unit on the generator MVA rating.

Calculating the parameters λ and μ in this manner from the basic data for a generator connection allows for rapid high-level estimation of voltage stability issues and impacts based on the theory of 6.2.3.

6.3 Control strategy for inverter-based resource

6.3.1 Active power and reactive power control

The mathematical model of DFIG in the synchronous rotating reference frame (dq) can be expressed as follows:

$$\begin{cases} E = \mathrm{j} I_{\mathrm{m}} X_{\mathrm{m}} \\ U_{\mathrm{s}} = E - I_{\mathrm{m}}(R_{\mathrm{s}} + \mathrm{j} X_{\delta \mathrm{s}}) \\ \dfrac{U_{\mathrm{r}}}{s} = E + I_{\mathrm{r}}\left(\dfrac{R_{\mathrm{r}}}{s} + \mathrm{j} X_{\delta \mathrm{r}}\right) \\ I_{\mathrm{m}} = I_{\mathrm{r}} + I_{\mathrm{s}} \end{cases} \tag{81}$$

where

R_{s} is the stator resistance;

R_{r} is the rotor resistance;

$X_{\delta \mathrm{s}}$ is the stator reactance;

$X_{\delta \mathrm{r}}$ is the rotor reactance;

X_{m} is the excitation reactance;

I_{s} is the stator current;

I_{r} is the rotor current;

I_{m} is the excitation current;

s is the slip rate;

U_{s} is the stator voltage;

U_{r} is the rotor voltage;

E is the induced electromotive force of air gap magnetic field;

P_{s} is the stator active power;

Q_{s} is the stator reactive power;

P_{r} is the rotor active power;

Q_{r} is the rotor reactive power.

In order to design an optimization control strategy for a grid-integration wind farm, the active and reactive power control capabilities of the stator and grid-side converter of DFIG should be studied. According to (82), the expression of the stator of the DFIG is as follows:

$$(P_s + \frac{3U_s^2 R_s}{R_s^2 + X_s^2})^2 + (Q_s + \frac{3U_s^2 X_s}{R_s^2 + X_s^2})^2 = \frac{9U_s^2 X_m^2 I_r^2}{R_s^2 + X_s^2} \tag{82}$$

The active and reactive power control capability of the DFIG is mainly limited by the rotor current. Assuming I_{rmax} is the maximum rotor current, and the stator resistance can be ignored, then the relation between the stator reactive power limit value and the active power can be given as:

$$\begin{cases} Q_{smax} = -\frac{3U_s^2}{X_s} + \sqrt{\frac{9U_s^2 X_m^2 I_{rmax}^2}{X_s^2} - P_s^2} \\ Q_{smin} = -\frac{3U_s^2}{X_s} - \sqrt{\frac{9U_s^2 X_m^2 I_{rmax}^2}{X_s^2} - P_s^2} \end{cases} \tag{83}$$

The stator resistance, rotor resistance and converter losses are ignored. According to (81), the expression of the active power of the grid-side converter is as follows:

$$\begin{cases} P_g = P_r = sP_s \\ P_E = P_g + P_r \end{cases} \tag{84}$$

where

P_E is the total active power of the WT;

P_g is the active power of the grid-side converter.

The reactive power control capability of the grid-side converter is mainly limited by the converter capacity P_{gmax}. The constraint relation between active power and reactive power of the grid-side converter is as follows:

$$P_g^2 + Q_g^2 \leq P_{gmax} \tag{85}$$

According to (84) and (85), the reactive power limit of the grid-side converter can be given as:

$$\begin{cases} Q_{gmax} = \sqrt{P_{gmax}^2 - (sP_s)^2} \\ Q_{gmin} = -\sqrt{P_{gmax}^2 - (sP_s)^2} \end{cases} \tag{86}$$

Considering the reactive power control capability of the stator and grid-side converter, the relation between the reactive power limit and the active power regulation range of the DFIG can be obtained:

$$\begin{cases} Q_{\max} = -\dfrac{3U_s^2}{X_s} + \left(\sqrt{\dfrac{9U_s^2 X_m^2 I_{rmax}^2}{X_s^2} - P_s^2} + \sqrt{P_{gmax}^2 - (sP_s)^2}\right) \\ Q_{\min} = -\dfrac{3U_s^2}{X_s} - \left(\sqrt{\dfrac{9U_s^2 X_m^2 I_{rmax}^2}{X_s^2} - P_s^2} + \sqrt{P_{gmax}^2 - (sP_s)^2}\right) \end{cases} \tag{87}$$

According to (87), the active power and reactive power operation range of the DFIG is given. The dotted line in Figure 32 describes the active and reactive power operation range of the stator, and the solid line describes the active and reactive power operation range of the DFIG.

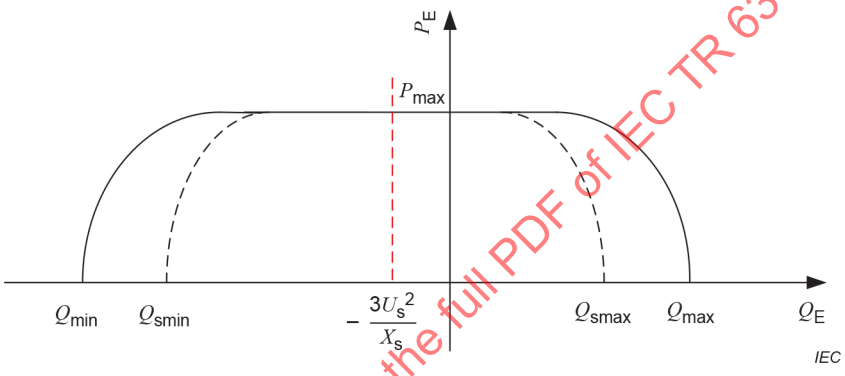

Figure 32 – Power limit curve of DFIG

Figure 32 and (73) show that the absorbed and released reactive power of the DFIG is asymmetric. The ability to absorb reactive power is stronger than the releasing reactive power, and the reactive power limit is changed with the change of active power.

6.3.2 Voltage control

Also, similar to the synchronous generator excitation system, the reactive-voltage controller for distributed power generation is shown in Formula (88):

$$E = E_{set} - D_q Q_{out} + (Q_{ref} - Q_{out})\left(k_{p1} + \frac{k_{i1}}{s}\right)\frac{1}{1+T_a s} \tag{88}$$

where

Q_{ref} is the reactive power input setting value;

D_q is the reactive power droop coefficient;

T_a is the time constant of the delay link;

E_{set} is the distributed power generation terminal voltage reference value;

k_{p1} and k_{i1} are proportional integral coefficients.

The voltage control block diagram of a DFIG is shown in Figure 33. When the grid voltage fluctuates, the doubly-fed electric turbine is controlled by the rotor-side converter to generate reactive power to participate in the voltage control of the system, so as to ensure the stability of the terminal voltage.

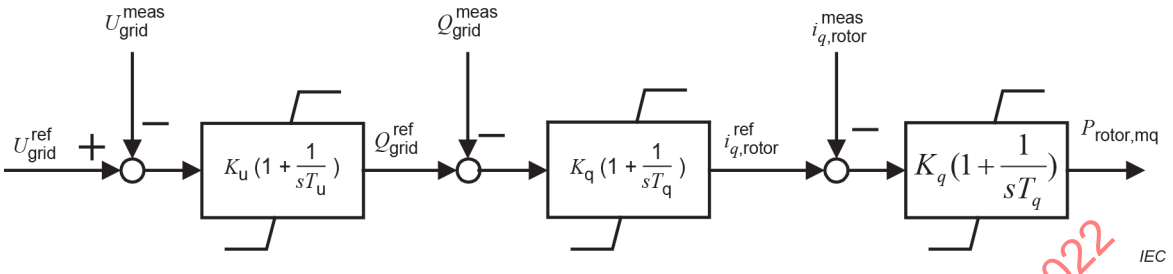

Figure 33 – Voltage control block diagram of the doubly-fed wind turbine

According to the given voltage reference value and the actual measured voltage value during the fault, the error signal passes through the PI controller to determine the reactive power reference value that the rotor-side converter needs to send, and then regulates the wind power through the inner loop current control. The turbine actually sends reactive power to help the doubly-fed induction motor rebuild the terminal voltage to a given reference value after a fault.

6.4 Case study

6.4.1 Steady state voltage stability problem – China

Concerning wind farms connected to a weak AC grid, small variations of active or reactive power output might bring relatively large voltage fluctuation at PCC, and the stability also might be deteriorated which could be represented by a low stability margin.

The installed capacity of Tuanjie wind farm, located in Baicheng County, Jilin Province in China, is 250 MW, equipped with DFIG based wind turbines. The wind farm is connected to 220 kV Taonan substation with a 100 km long AC transmission line. The network structure of Baicheng is shown in Figure 34, with the backbone mesh grid of the 220 kV system.

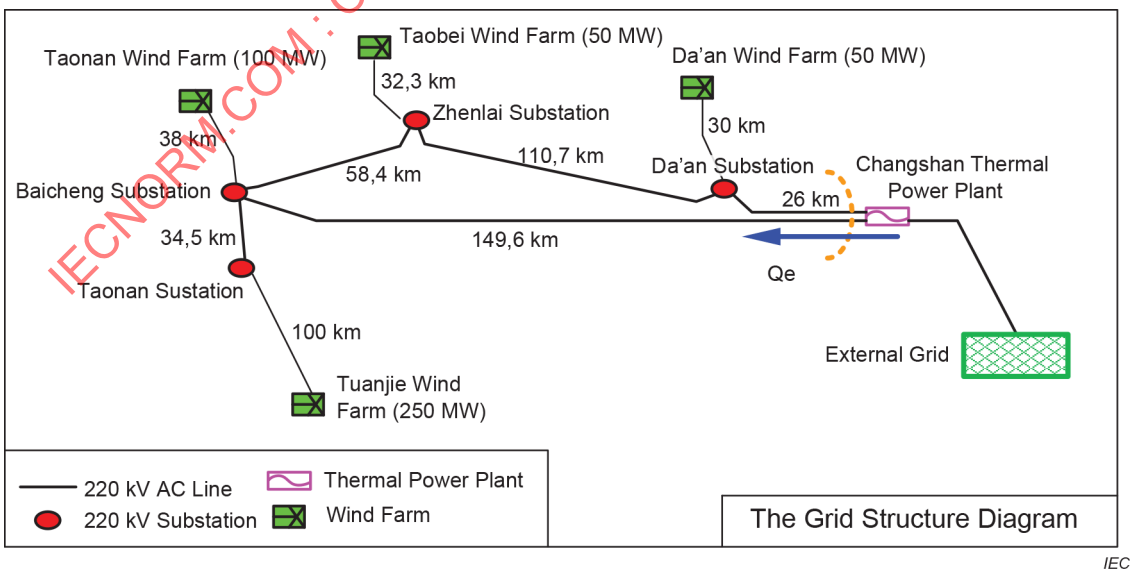

Figure 34 – Network structure of Baicheng grid

Changshan thermal power plant, with a total of 600 MW installed capacity, operates as the main synchronous power source in this area. Besides the Tuanjie wind farm, the Taonan wind farm, Taobei wind farm, and Da'an wind farm have also been developed and connected to the lower voltage level grid with 66 kV. When local load demands are met, the surplus wind power can be transmitted to the external grid. The short circuit capacity of the Baicheng networks is shown in Figure 35, without considering wind power's contribution; the PCC's short circuit capacity of Tuanjie wind farm is 521 MVA.

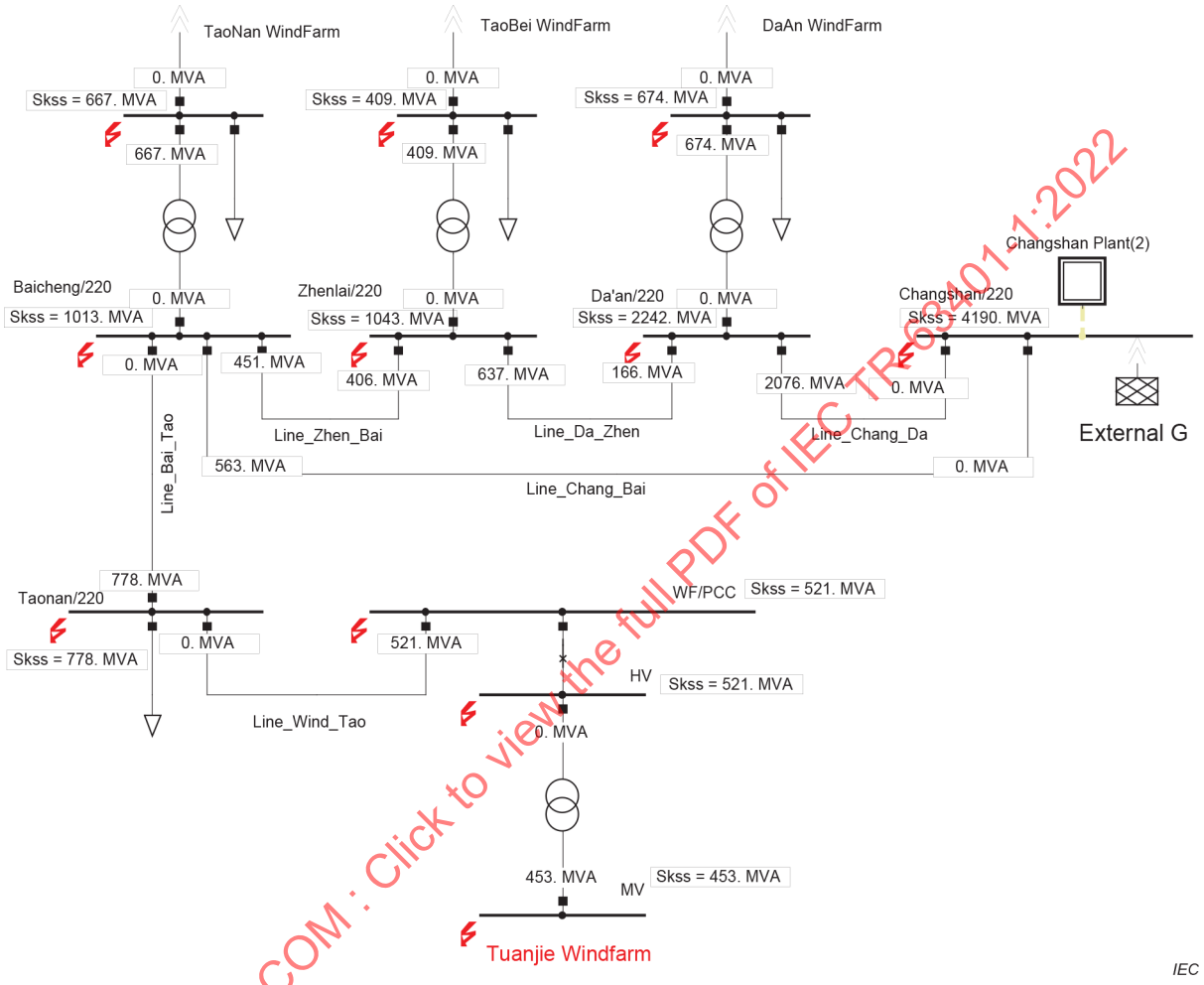

Figure 35 – Short circuit capacity of Baicheng network

The SCR of Tuanjie wind farm equals 2,08, and that could be deemed as the case of a wind farm connected to a weak AC network.

With the inherent fluctuating and intermittent characteristics, the active power output of the wind farm varies as wind speed changes, and the power variation could lead to the grid voltage fluctuation, especially at the busbars very close to the wind farm. As shown in Figure 36, P-V curves and V-Q curves are plotted to illustrate the impact of power injection on the grid voltage. During the calculation, a constant power factor is applied to DFIG based wind turbines and fixed capacitor banks are also used.

Relying on the capacitor banks compensation, the voltage level at the PCC could be controlled within the range from 1,00 p.u. to 1,03 p.u.

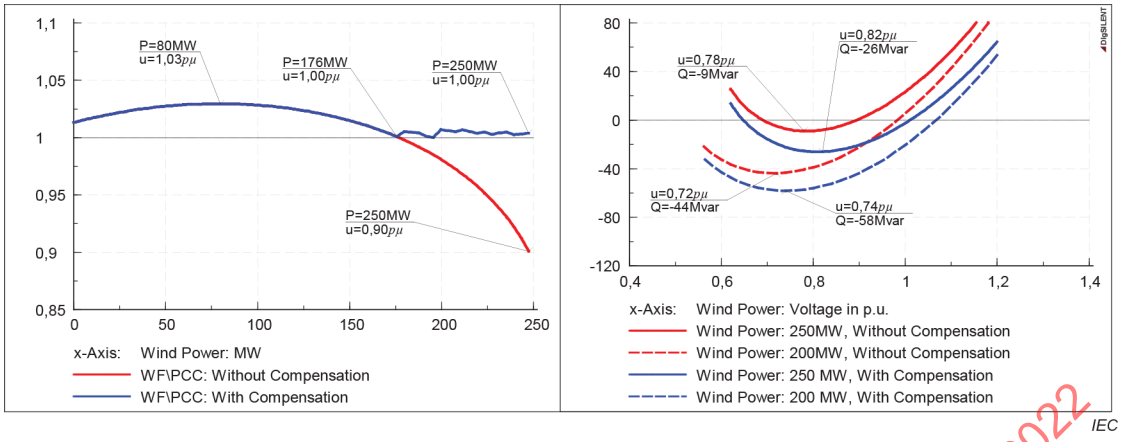

Figure 36 – *P-V* curves and *V-Q* curves

It can be seen that:

1) When the output of a wind farm is relatively high, large active power transmission could lead to high reactive power consumption along the line. If the reactive power capacity of the wind farm is insufficient, the regional network needs to absorb more reactive power from the main grid, which results in a comparatively lower voltage level. In the case of full output operation (250 MW) of the wind farm, the voltage at the PCC is only maintained in a very lower level at 0,89 p.u.
2) As a result of being connected to a weak grid, the output variation of the wind farm will lead to larger voltage fluctuation at the PCC. If no reactive power compensation facilities are installed in the wind farm, the PCC voltage will vary from 0,89 p.u. to 1,03 p.u. under different active power output levels; and if reactive power compensation facilities are adopted in the wind farm, the voltage could be maintained in the range from 1,0 p.u. to 1,03 p.u. under different output levels.
3) As the output of the wind farm increases, the reactive power margin will decrease gradually. Considering that the output of the wind farm is at 200 MW, the reactive power margin will be 44 Mvar, and if the output rises up to 250 MW, the reactive power margin will be getting lower only with 9 Mvar.

The short circuit capacities at the PCC of Tuanjie wind farm and maximum power generations under different grid conditions are shown in Table 8:

Table 8 – Wind farm's maximum power under different conditions

Operation conditions		Short circuit capacity at PCC (MVA)	Wind farm maximum power (MW)
Normal condition		521	260
Line N-1	Baicheng-Zhenlai	398	205
	Zhenlai-Da'an	398	190
	Changshan Plant-Da'an	398	170
	Changshan Plant-Baicheng	350	155

It can be seen from Table 8 that when Line Changshan Plant-Baicheng is out of service, the regional network will be shaped from a mesh grid to a radial structure, namely, Changshan Plant-Da'an-Zhenlai-Baicheng-Taonan. In this case, the electrical distance between Tuanjie wind farm and the main grid is getting much bigger. The main grid's reactive power support to Tuanjie wind farm is comparatively weak, the short circuit capacity at the PCC of Tuanjie wind farm is the smallest case, and the maximum power generation of Tuanjie wind farm is decreased to a very low level only with 155 MW. When the wind farm is connected to a weak grid, the voltage at the PCC will have a comparatively high sensitivity to wind farm's reactive power output variation, and a small change of the reactive power might bring a noticeable impact on the voltage at the PCC. As shown in Figure 37, whether the wind farm absorbs 45 Mvar reactive power from the external grid (0,966 capacitive power factor) or injects 33 Mvar reactive power to the external grid (0,982 inductive power factor), these two different operating conditions will both bring 20 % change to voltage at the PCC, which means that 1 Mvar variation of the wind farm's reactive power will result in 0,25 % change of voltage at the 220 kV PCC. In the actual operation, appropriate control of the reactive power compensation devices is also necessary according to the operation mode and the voltage level.

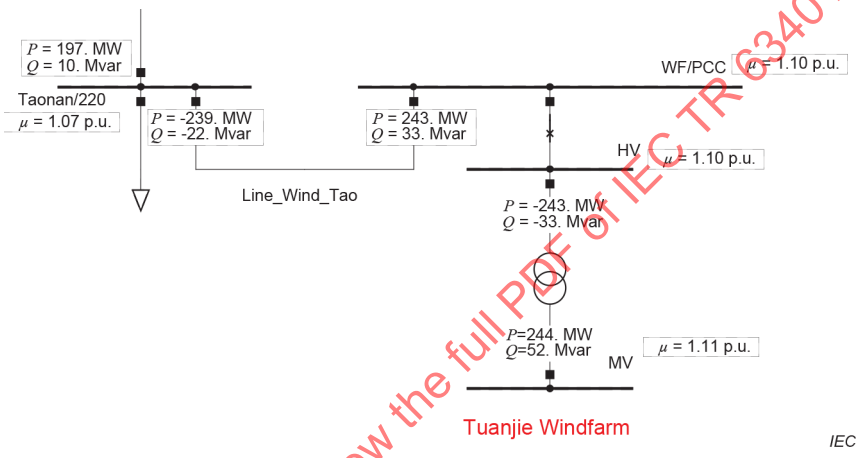

Figure 37 – Reactive power of the wind farm and voltage level at the PCC

6.4.2 Low SCR interconnection experience – Vestas

A wind power plant (WPP) connecting to the bulk electrical system (BES) where the minimum fault level MVA at the WPP's medium-voltage collector system bus divided by the WPP's MW capacity is 3-to-1 or less can be considered as a weak grid interconnection. Such a weak connection is often caused by a long radial transmission line, in a remote section of the BES that extends to the WPP. The subject of this example is a 265 MW WP with a 33 kV collector system, including such a radial line of 270 km, resulting in an SCR of 1,79 under normal grid operations and 0,79 under an N-1 condition. These low SCR values lead to stability limits for the WPP to only 148 MW and 74 MW, respectively.

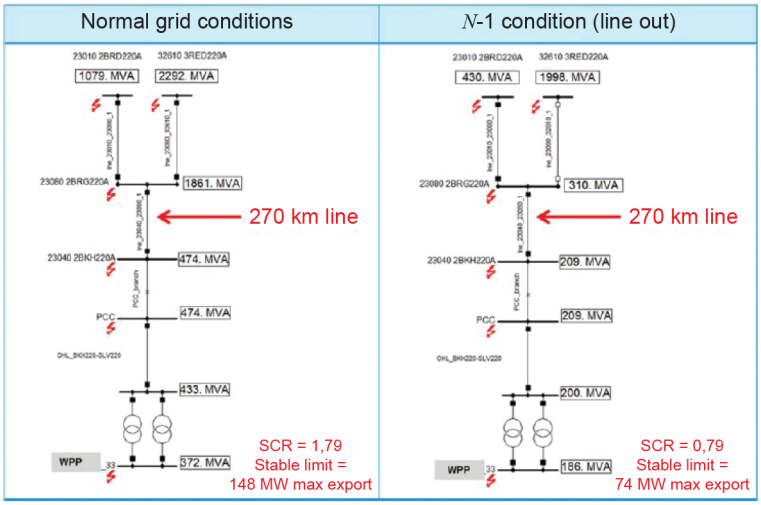

Figure 38 – Schematic representation of the study system

Without further mitigations, issues that may arise from operations under these conditions are:

1) WPP's inability to comply with transmission system operator (TSO) requirements for power factor capability.

2) Voltage constraints lead to poor voltage regulation along the line as WPP P and Q vary.

3) High sensitivity to reactive power changes, meaning small changes in Q can lead to large variations of voltage on the BES.

6.5 Summary

In the technical field of RE integration to low short circuit ratio AC networks, the existing needs and gaps include:

1) According to the P-V curve and Q-V curve analysis, in the case of a weak power grid, the maximum output power of the wind farm is limited by the weak-grid condition.
2) When the grid the SCR decreases, the voltage sensitivity of the PCC point increases, i.e., the power fluctuation will have a greater impact on the voltage of the PCC point.
3) The electrical strength (SCR) of the PCC point should be increased, so as to increase the total output capacity of the inverter-based resources and ensure the safe operation of the system.

The optimized coordination of the active and reactive power should be studied since it reveals that the power transfer capacity of the renewable power plant can be maximized by outputting the reactive power as much as possible until the PCC voltage achieves its limitation. Moreover, the reactive power droop control method can be improved to maximize the power transfer capacity of the renewable power plant under low SCR conditions.

7 Transient issue for low short circuit ratio AC networks

7.1 Problem statement

Inverter-based resources under weak grid conditions face the following situations:

1) The fault ride-through of the renewable energy grid-connected system can be divided into two phases. The voltage drop process and voltage recovery process are shown in Figure 39. In traditional studies, the effect of the inverter-based resource's dynamic behaviours on grid voltage is usually ignored, but it should be considered when the inverter-based resource is integrated into the grid with low SCR. When grid fault occurs and clears, the voltage amplitude is greatly affected by the grid condition and unit control due to the high voltage sensitivity of the grid-connected point in a weak grid with low SCR. In the process of the voltage drop, the active and reactive power injection of the renewable energy power generation unit is effective to resist the voltage drop. During the voltage recovery process, the voltage fluctuation of the grid point is enhanced by the active and reactive power injection of the renewable energy power generation unit.

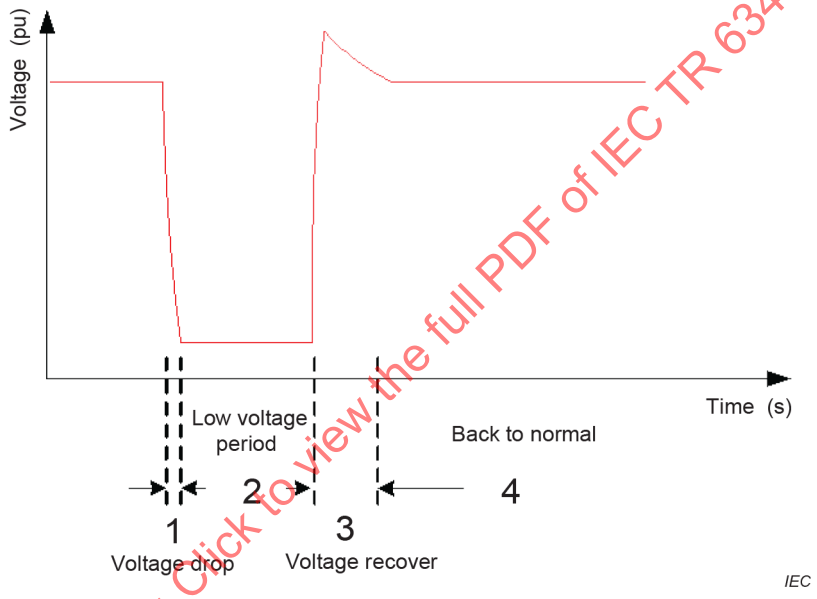

Figure 39 – Fault characteristics

2) Weak grids with low SCR experience a high impedance of the transmission line. The static power is limited. Attempting to push real current is going to consume more reactive power, which could further degrade system voltage and result in collapse. Reactive current should be given priority during fault conditions in these weak grid conditions.
3) Weak grids experience a high sensitivity of voltage to changes in power (i.e., higher dV/dP, dV/dQ). Tripping of inverter-based resources or excessive reactive current injection could result in voltage overshoot or other problems, which could result in cascading fault of inverter-based resources and further voltage rise, especially during grid voltage recovery.
4) The fault characteristics and dynamic behaviours of wind power depend on the control strategy in the whole process of grid faults, which is quite different from traditional power source. In a weak grid, the fault behaviours become more complicated due to the interaction between the inter-based resource and grid, which will affect grid protection and control.
5) The high sensitivity produces higher gain through phase locked loop and reactive power/voltage control, and even some small-signal and transient instability issue.

7.2 Transient characteristic modelling and analysis

7.2.1 Transient stability analysis tools and limitations

Transient stability simulation tools are widely used in planning applications to evaluate the stability of the BPS. These tools are effective in predicting disturbance response, generator stability, voltage stability, load dynamics, and many other phenomena for most applications. However, as VER penetration grows and there is a prevalence of weak grid interconnections, these tools may encounter limitations, which should be well understood by those who use them. Some considerations that should be made with respect to weak grids studies using transient stability tools include:

1) Positive sequence based: positive sequence RMS quantities are typically calculated in these tools. The effect of DC current components, as well as zero and negative sequence components are usually neglected in these calculations. Some of the limitations of these approximations are commonly understood for unbalanced conditions (for example, the negative sequence aspects may become relevant for evaluating limitation of overvoltage in un-faulted phases during unbalanced faults). Zero sequence aspects may not be critical because the transformer connection group in the VER systems often isolates the zero sequence system in the VER from the BPS, but this may require additional review.
2) RMS based: phasor-based tools require that the power system electrical quantities be represented as three-phase RMS quantities. The operation of protection systems is highly dependent on how measurement is modeled; there may be limitations in transient stability tools on measurement delays. Measurement, in general, shall be approximated in these models, as the RMS quantities are inherent to the transient stability tools (instantly available), while in the real controls they shall be calculated from phase quantities. Additionally, the unique individual phase dynamics implicit in a severe contingency event such as a fault may not be captured, and this can result in different behaviours from control elements which use these phase quantities, such as instantaneous phase-based protection circuits and synchronization controls (PLL details).
3) Large simulation time step: a typical power electronic converter contains control loops and algorithms with fast response times – faster than can be represented with the relatively large simulation time steps used in transient stability programs. These control loops include PLL controllers and inner current loop controllers, and are often key drivers of instability modes in weak systems (such as small signal instability modes), and govern the ability of the plant to quickly provide grid support.
4) Convergence issues: the iterative nature of the transient stability and power flow calculations can be challenging in weak systems, manifesting in convergence problems as the system becomes very weak. This aspect in some cases is driven by limitations of specific models and not the tool itself, but can prevent proper analysis.
5) Limited converter electrical representation: depending on the sophistication of the model, internal converter electrical representation is simplified. For example, the converter DC bus (including associated bus voltage protections, choppers, and controls) may be assumed to be infinitely strong. Likewise, interfaces and controls relating to the VER energy source are often approximated or ignored, where these elements can in some circumstances influence the converter behaviours.

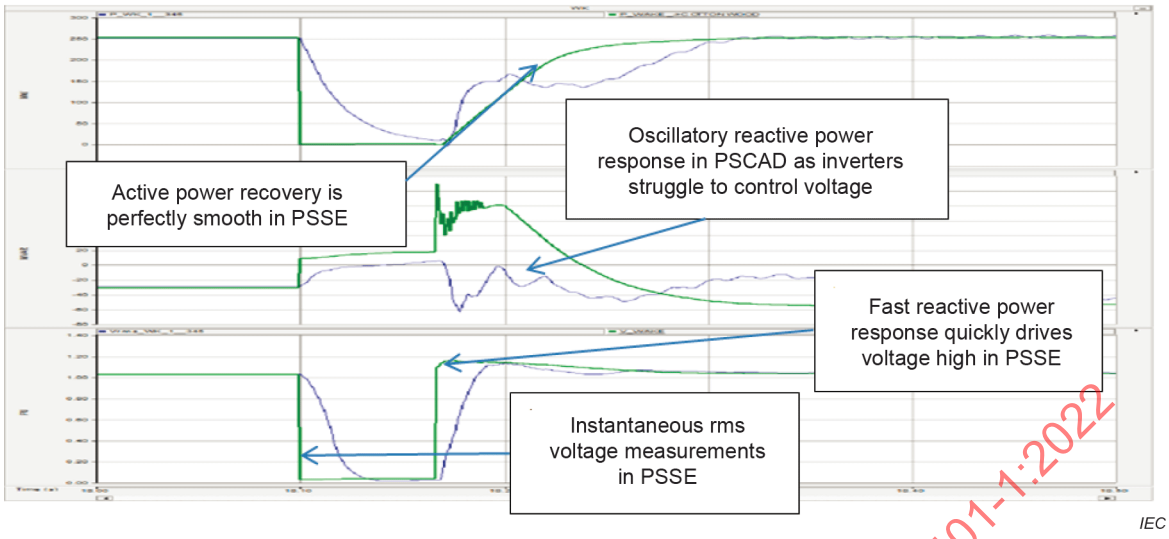

Figure 40 – Comparison of VER fault response between transient stability and EMT models

Manufacturers of modern VER equipment have in some cases gone to considerable lengths to overcome some of the above limitations and often use creative approximations to provide the best possible representation of their specific equipment using user-defined models. However, for some phenomena these tools are not appropriate, and as interconnecting systems become very weak, most manufacturers will recommend using EMT tools to confirm equipment behaviours or validate the transient stability results.

7.2.2 Electromagnetic transient (EMT) type models

In very weak system interconnections, planners and manufacturers may deem more detailed analysis to be necessary using electromagnetic transient tools. EMT simulation programs have in common a key distinction from phasor-based transient stability models. Power-flow and transient stability programs iteratively solve a system of formulae to satisfy a set of constraints in the phase domain. EMT software solves systems of differential formulae which describe the three-phase electrical network in the time domain, allowing unbalanced faults, harmonics, fast transients, and other effects to be modelled. In addition, extremely high levels of detail may be used in modelling the fast controllers which are used in real equipment converters, capable of capturing the very fast time constants used in current controls and switching algorithms. In many cases, the actual firmware code used in the power electronic devices may be inserted as-is into the model, eliminating most modelling approximations and approaching perfectly accurate control representation under transient conditions.

If it is determined that the EMT studies are required, the very high level of control details is necessary, as the control modes lead to some issues described above in weak systems which are critically dependent on the specific control implementation (including PLL, inner current controls, specific protection implementation, etc.). Use of “generic” or “typical” EMT models is usually not recommended, as they cannot predict with accuracy the specific issues which may be encountered. If conventional transient stability models are not sufficiently accurate, detailed EMT models are required. In some cases, it is useful to validate transient stability using detailed EMT models (particularly in systems which are “marginally weak”, in order to provide comfort for planners that their standard transient stability models and studies are accurate enough to predict performance.

In some cases, it is useful to validate transient stability models using detailed EMT models (particularly in systems which are marginally weak), in order to provide comfort for planners that their standard transient stability models and studies are accurately predicting performance.

7.2.3 Transient stability analysis model requirements

The increasing penetration of VER and potential weak grid issues drives the need to ensure accurate and representative models are available to planning engineers to study the impacts VER may have on grid reliability, and vice versa. Planners are recommended to use the screening methods outlined in this document to identify areas where weak grid conditions may be a concern. Once these areas are understood, modelling requirements should be put in place that clearly define the types of models, list of acceptable models, and intended use of these models. The following concepts should be considered when developing these requirements:

1) Generic positive sequence stability model: a generic model used for interconnection-wide modelling should be required for every resource seeking interconnection to the BES. Generic models are expected to accurately represent the general dynamic behaviours of the VER, and should be benchmarked to more detailed models to the extent possible. These generic models should be part of the standard model library within the commercial software platforms, and should also conform to the data requirements.
2) Detailed positive sequence stability model: interconnection stability studies (e.g., system impact studies) should use the most detailed model available for the study being performed. These studies are often positive sequence transient stability analyses. Detailed models from the VER manufacturer should be provided for these studies to ensure stability and security of the BES prior to connection of these resources. It is very important that these models be developed to a sufficient quality, with appropriate documentation, to allow for dependable use in system studies.
3) Electromagnetic transient model: in the event that a weak grid condition has been identified, or a possible weak grid condition may occur in the future, EMT models should also be required from the GO.

EMT usually requires confidentiality agreements between the manufacturer and data owners and users. These types of models are used for detailed local studies; however, the data sharing and software support for these models create challenges from an interconnection-wide modelling perspective. Transient stability models typically do not have the same degree of confidentiality restrictions (i.e., user-defined transient stability models may still require a confidentiality agreement). Hence, these models, particularly the generic models, are used for larger system modelling purposes.

7.3 Fault ride-through protection and control issue

7.3.1 General

When the grid voltage drops, the various electrical quantities of the wind turbine will undergo a series of electromagnetic transient processes.

a) Due to the direct connection between the stator and the grid, the fault of the grid causes the terminal voltage to drop, resulting in an increase in the stator current of the generator. Due to the strong coupling between the rotor and the stator, a rapidly increasing stator current causes a sharp rise in the rotor current. In addition, due to the reduced voltage at the terminal, it is not possible to normally deliver active power to the grid. These energies will cause a series of problems such as a rapid rise in DC capacitor voltage and acceleration of the rotor of the motor.
b) Since the full-power conversion wind turbine is isolated from the grid by a full-power converter, the main problem is the rapid rise of the DC capacitor voltage and the acceleration of the rotor of the motor caused by the unbalanced power of the wind turbine side and the grid-side converter.

Similar to the voltage drop, the voltage swell will also trigger a series of electromagnetic transient changes.

1) For the direct connection between the stator and the grid, the stator side of the doubly-fed wind turbine is directly connected to the grid. The sudden rise of the grid voltage will cause changes in the stator and rotor flux linkages of the doubly-fed motor. Since the flux linkage cannot be abruptly changed, transient DC components will appear in the stator and rotor windings. In the case of asymmetric faults, there will also be a negative sequence component, and the flux linkage generated by the transient current will cancel the flux linkage change caused by the sudden rise of the stator voltage. Due to the high-speed rotation of the rotor of the induction motor, the DC transient component will cause an increase in the induced voltage and current in the stator-rotor circuit. In severe cases, it will exceed the safety limits of the power electronics and the motor, causing damage to the equipment. At the same time, the transient process will cause fluctuations in the electromagnetic torque of the doubly-fed wind turbine, which will cause mechanical shock to the gearbox and affect the life of the wind power system.
2) The full-power conversion wind turbine is connected to the grid through the converter, and the change on the grid side does not directly affect the permanent magnet motor. When the grid voltage rises rapidly, the output current of the grid-side converter will decrease due to the power limitation of the converter. The power imbalance causes the excess energy of the grid to charge the DC bus capacitor through the grid side, causing the DC bus voltage to rise. When the asymmetry rises, it will also cause fluctuation with twice the fundamental frequency on the DC side, which not only threatens the safety of the converter and the capacitor parts, but also affects the quality of the output power.

7.3.2 Hardware protection of inverter-based resource during fault

7.3.2.1 AC side crowbar circuit

In the case of a weak grid, it is necessary to improve the fault ride-through capability of the renewable energy unit, and the most important thing is to improve the immunity of the grid-connected point voltage. Taking the doubly-fed wind turbine as an example, the rotor-side crowbar protection scheme is currently a mainstream protection method for realizing undervoltage ride-through of the doubly-fed wind turbine. The basic principle is that when the rotor-side current rises to a preset threshold, the switching element is triggered to conduct, and at the same time, all switching devices in the rotor-side converter are turned off, so that the rotor fault current flows into the crowbar resistor, which is a surge on the rotor-side. The current provides an unloading path. With the increasingly strict regulation of grid-connected wind power, crowbar protection circuits use diode rectifier bridges with the topology of self-shutdown devices such as GTO or IGBT, as shown in Figure 41. This structure can turn off the crowbar protection circuit at any time, so that the rotor-side converter can be put back into operation when the wind turbine is not off-grid, and the necessary reactive power support is provided to the faulty grid. From the perspective of topology, the rotor-side crowbar can effectively suppress the rotor-side overcurrent caused by the voltage drop, so that the RSC can be effectively protected and realize the uninterrupted operation of the DFIG unit during the fault. As long as the control strategy is appropriate, theoretically any degree of voltage fault traversal can be achieved. However, it is worth noting that during the crowbar conduction period, the RSC stops working and the generator is in an uncontrollable state. The DFIG needs to absorb a certain amount of reactive power from the power grid, which is not conducive to the rapid recovery of the faulty power grid.

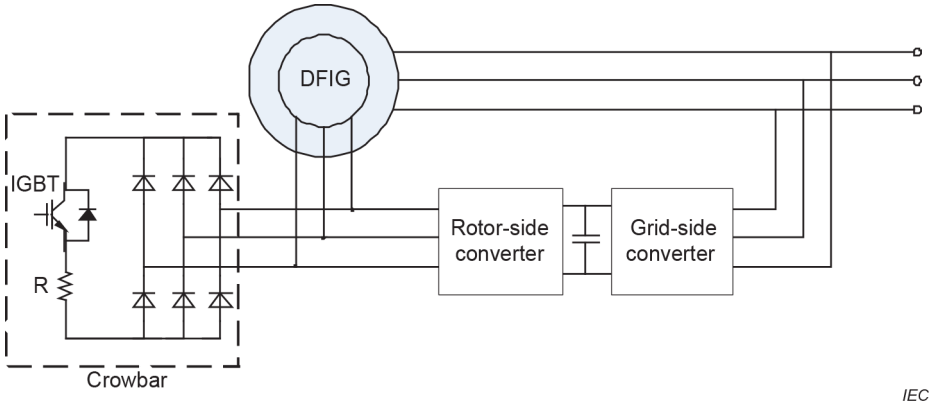

Figure 41 – Doubly-fed wind turbine rotor-side crowbar protection circuit topology

The selection of the resistance R in the crowbar is subject to certain principles. According to the literature, the approximate expression of the rotor current after the crowbar action is:

$$I_s(t) \approx I_r(t) = \frac{U_s}{\sqrt{(\omega_1 L_\sigma)^2 + R^2}}\left[(1-p)e^{-t/\tau_z} - (1-s)(1-p)(1-\sigma)e^{-t/\tau_r} + pe^{j\omega_1 t}\right] + I_{r0}e^{-t/\tau_r} \quad (89)$$

where:

L_σ is the sum of the stator and rotor leakage reactance;

p is the voltage drop depth;

$\tau_s \approx \frac{L_\sigma}{R_s}, \tau_r \approx \frac{L_\sigma}{R_r + R}$;

I_{r0} is the initial value of the rotor current that is converted to the stator side when the DFIG is in steady state operation before the fault.

The greater the resistance of the resistor R, the faster the rotor current decays, so the amplitude of the current and torque oscillations is smaller. However, the resistance of R is not as large as possible. If R is too large, overvoltage of the RSC switching device and rotor winding will happen, and the DC bus voltage oscillation will be aggravated. Therefore, the value of the resistor R mainly depends on two factors. One is that R shall be large enough to suppress the short circuit current; the other is that the voltage across R should not exceed the DC bus voltage when flowing through the maximum current of the rotor.

The literature has made a detailed analysis of the mathematical model of DFIG after crowbar connection, and gives a formula for calculating the reasonable range of crowbar resistance:

$$R_{\min} = \frac{\omega_r}{I_{\text{safe}}}\sqrt{\left(\frac{U_s}{\omega_s}\right)^2 - (L_\sigma I_{\text{safe}})^2} \quad (90)$$

$$R_{\max} = \frac{V_{\text{dc}}\omega_t L_\sigma}{\sqrt{3(U_s\omega_t / \omega_s)^2 - V_{\text{dc}}^2}} \quad (91)$$

Different crowbar resistance values will have an impact on the turbine's fault ride-through capability. When the current safety is limited to 2 p.u., when the resistance value is 0,4 p.u. or more, the rotor current amplitude can be controlled within the safety limit. As the resistance increases, the smaller the rotor current amplitude, the faster the attenuation. However, as the resistance increases further, for example, when 0,8 p.u. or more is reached, the influence of different resistance values on the rotor fault current is hardly different. According to the above principle, and considering that a larger value is more conducive to reducing the time of crowbar operation, the resistance value of crowbar can be taken as 1 p.u.

In addition, the choice of input and cutting time of the crowbar is also very important. Improper selection will cause the crowbar to act multiple times on the one hand, and may cause large current surges on the other hand. If properly selected, it can effectively reduce the number of switchings and working times and as far as security is concerned, the WT is in a controllable state.

7.3.2.2 DC side chopper circuit

The principle of the DC side chopper circuit is similar to that of the crowbar circuit. The resistor is connected to the DC bus and controlled by a controllable switch to provide a release channel for excess energy when turned on. Chopper protection usually adopts the hysteresis control of the DC bus overvoltage and the low voltage return. When the DC bus voltage is higher than the set upper limit, the conduction reduces its overvoltage; when the DC bus voltage is lower than the set lower limit, it will be turned off.

The advantage of the DC chopper is that the RSC is still in a controllable state during operation without being cut off, so that the converter can be used to send a certain reactive power to support the recovery of the grid voltage. However, its drawback is that it is difficult to effectively protect against overcurrent. Therefore, in order to achieve effective protection against overcurrent, the RSC current capacity should be appropriately expanded when the chopper circuit is used alone to achieve undervoltage ride-through.

During the input of the chopper circuit, the bleeder power and energy of the chopper circuit resistor are as follows:

$$P_{\mathrm{dc}} = \frac{V_{\mathrm{dc}}^2}{R_{\mathrm{dc}}}. \tag{92}$$

$$W_{\mathrm{dc}} = \int P_{\mathrm{dc}} dt \tag{93}$$

The greater the unbalanced power on both sides of the DC bus, the more severe the DC bus overvoltage, and the unbalanced power is released by the chopper circuit. As can be seen from Formula (92), the smaller the R_{dc} is, the better the P_{dc} is.

In order to provide effective reactive power support as much as possible, the wind turbine should avoid the input of the crowbar protection circuit as much as possible during the fault, so that the wind turbine is in the fault ride-through control mode under the controlled state. Wherein, the reference value of the reactive current (the q-axis component of the rotor current) can be dynamically determined according to the voltage change of the wind turbine terminal and the reference value of the active current (the d-axis component of the rotor current) can be set based on the active output level and the reactive current before the fault.

7.3.3 Unbalancing-voltage ride-through issue

Due to the limited control ability of the grid-side and rotor-side converters of the doubly-fed wind turbine and its close relationship and mutual influence with the electromagnetic and electromechanical aspects of the generator, the control and operation under asymmetric faults are more complicated. When the grid is unbalanced, the traditional vector control strategy of the grid-side and rotor-side converter based on the stator voltage orientation under the balanced grid voltage cannot accurately control the positive and negative sequence currents in the synchronous speed rotating dq coordinate system. As a result, the current control failure of the grid-side and rotor-side converters under unbalanced faults is triggered. The unbalanced power grid fault causes the height of the three-phase AC current to be unbalanced, which is prone to an overcurrent phenomenon, causing the DFIG converter to output active power, reactive power and DC link voltage twice the grid frequency fluctuation. Not only will the rotor excitation current harmonics be affected, as well as the accuracy of the rotor-side converter control implementation, but also the overvoltage and overcurrent of the entire PWM excitation inverter, especially affecting the service life of the DC bus capacitor. At the same time, the unbalanced grid voltage causes the DFIG stator current height imbalance, which will cause unbalanced heating of the stator windings, and the generator torque will pulsate, causing the power transmitted to the grid to oscillate.

Since the controllable variables of the grid-side and rotor-side converters for DFIG excitation are limited, the grid-side and rotor-side converters need to be controlled in a coordinated way under the grid voltage imbalance fault to maximize the overall control capability of the entire wind turbine. The collaborative control target can be set to:

1) In addition to the independent decoupling control of the average active and reactive power of the DFIG output stator, the rotor-side converter also needs to control the electromagnetic torque constant to eliminate the generator electromagnetic torque double frequency pulsation and reduce the wind turbine shafting mechanical stress.
2) In addition to the DC bus voltage and the average reactive power's inherent independent decoupling control function, the grid-side converter needs to realize the control DFIG output active power constant to compensate the double frequency pulsation of the DFIG stator output active power, so that the entire DFIG power generation system loses. The active power double-frequency pulsation to the grid is zero, ensuring grid power supply and demand balance, safety and stability.

The d^+ axis positive sequence stator (grid) voltage vector orientation is used, that is, the positive sequence stator voltage u^+_{sd+} is fixed on the d^+ axis of the forward rotation synchronous speed coordinate system, and the positive and negative sequence currents of the rotor-side converter under constant electromagnetic torque The control instruction formula is as follows:

$$\begin{bmatrix} i^{+*}_{rd+} \\ i^{+*}_{rq+} \\ i^{-*}_{rd-} \\ i^{-*}_{rq-} \end{bmatrix} = \begin{bmatrix} \dfrac{L_s u^+_{sd+}}{L_m D_3} P_{s0} \\ -\dfrac{L_s u^+_{sd+}}{L_m D_4}\left(Q_{s0} + \dfrac{D_4}{L_s}\right) \\ k_{dd} i^{+*}_{rd+} + k_{qd} i^{+*}_{rq+} \\ k_{qd} i^{+*}_{rd+} - k_{dd} i^{+*}_{rq+} \end{bmatrix} \tag{94}$$

where,

the subscripts "+" and "-" are represented as positive and negative sequence components;

the superscripts "+" and "-" are expressed as positive and negative synchronous speed coordinate systems.

Considering that the DFIG stator and the grid-side converter in the actual wind power system are directly connected to the grid, that is, $U_{gdq}^{+}=U_{sdq}^{+}$, the positive-sequence d^{+} axis grid (stator) voltage orientation is used, $u_{gd+}^{+}=u_{sd+}^{+}$, $u_{gq+}^{+}=u_{sq+}^{+}=0$. The negative sequence current control command formula is as shown in Formula (95).

$$\begin{cases} i_{gd-}^{-*}=-\dfrac{2P_s\cos 2}{3u_{sd+}^{+}}-k_{dd}i_{gd+}^{+*}-k_{qd}i_{gq+}^{+*} \\ i_{gq-}^{-*}=-\dfrac{2P_r\sin 2}{3u_{sd+}^{+}}-k_{qd}i_{gd+}^{+*}+k_{dd}i_{gq+}^{+*} \end{cases} \tag{95}$$

Calculate the corresponding positive and negative sequence current command values of the grid-side and rotor-side converters. A 100 Hz generalized integrator is embedded in the traditional current control under balanced grid conditions to achieve uniform and precise control of positive and negative sequence currents. The schematic diagram of the positive and negative sequence current control of the DFIG converter under the asymmetric fault of the power grid is shown in Figure 42.

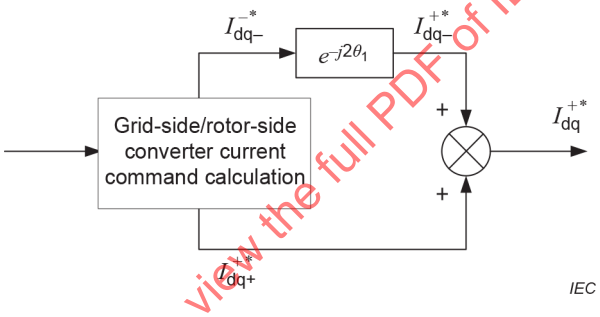

Figure 42 – Schematic diagram of positive and negative sequence current control of DFIG converter under grid unbalanced fault

Figure 43 compares the effect of the DFIG converter before and after the positive and negative sequence current control under the asymmetrical fault of the power grid. During the simulation operation, the two-phase grounding short circuit fault occurred within 8 s. Then the fault recovery is 8,5 s, the grid voltage steady-state unbalance degree was δ = 0,135, the DFIG unit speed command was set to 1,2 p.u. (synchronous speed was 1,0 p.u.). The active and reactive power settings are 0,6 p.u. and 0 p.u. respectively, and the average reactive power of the grid-side converter is 0 p.u. As a result of the simulation, the additional negative sequence control scheme can effectively suppress the double frequency components such as stator and rotor current, grid-side control current, and electromagnetic torque.

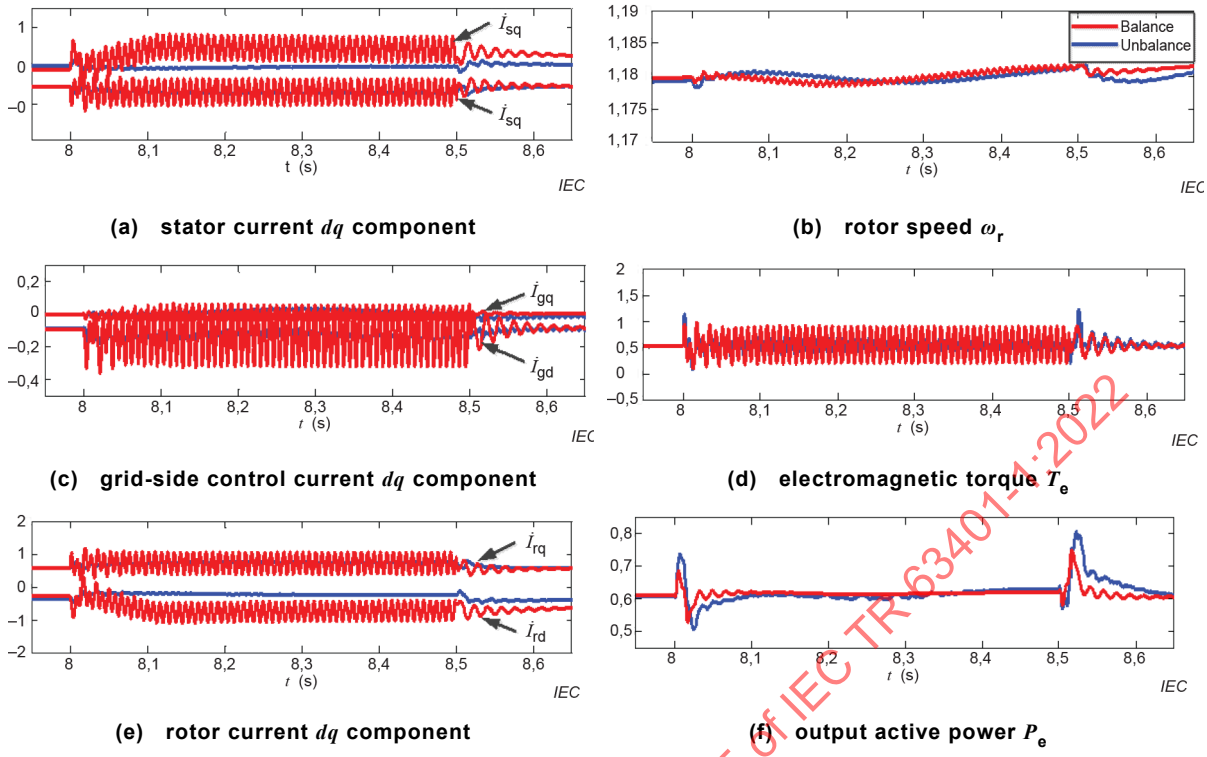

Figure 43 – Comparative analysis of simulation results

7.3.4 Overvoltage ride-through control strategy

The wind turbine realizes the fault ride-through and needs the cooperation of the main control system and the converter. After receiving the grid voltage rise fault signal given by the converter, the main control system needs to shield the faults related to overvoltage ride-through (such as: high grid voltage, converter output power deviation from the command value, etc.), and give up the power control of the master control system. Then set a reasonable grid overvoltage ride-through protection curve; the wind turbine output active and reactive power during high voltage crossing is determined by the converter control. After receiving the grid voltage recovery signal given by the converter, the main control system restores the previously shielded fault or alarm signal, restores control of the wind turbine power, and the wind turbine operates normally.

By analyzing the transient characteristics of the doubly-fed wind turbine under the grid voltage swell fault, combined with the existing scheme of realizing the high voltage ride though of the doubly-fed wind turbine by adding hardware equipment, the grid-side and rotor-side converters are based on the overvoltage ride-though period. On the basis of the power adaptation principle, it is necessary to consider the dynamic reactive power support of the unit to achieve overvoltage ride-through control.

The stability of the bus voltage when the grid voltage rises is a prerequisite for ensuring that the wind turbine is not off-grid. Taking a 2 MW doubly-fed wind turbine as an example, the rated working voltage of the unit is 690 V, and the normal working voltage of the DC bus capacitor is 1 050 V. Under normal grid conditions, the peak value of the grid line voltage is $690 \times \sqrt{2} = 976$ V. However, when the grid voltage suddenly rises to 1,3 times the nominal value, if the grid-side converter continues to use power factor control, the bus voltage will rise above 1 269 V, far beyond DC. The maximum continuous operating voltage of the bus bar is 1 150 V, which will cause damage to the device.

Therefore, in order to ensure the normal operation of the grid-side converter and the stable control of the bus voltage during the grid voltage rise, it is necessary to increase the withstand voltage level of the converter switching device and the bus capacitor while using the grid-side converter line reactance. The pressure causes the grid-side converter to output a certain inductive reactive current. The proposed optimal control strategy is not only economical and practical, but also provides a certain dynamic reactive power support capability for the faulty power grid. The relationship between the minimum value of the reactive current and the peak voltage and active current of the grid phase during normal operation of the grid-side converter is:

$$I_{gq\min} = \frac{1}{\omega_s L_g}\left[\sqrt{U_{dc}^2/3 - \left(-\omega_s L_g I_{gd}\right)^2} - U_g\right] \quad (96)$$

Formula (96) shows that the value of the inductive reactive current of the grid-side converter during the voltage surge of the grid depends on the size of the grid phase voltage U_g on the one hand and the active current of the output on the other hand. The reactive output capability of the grid-side converter during the sudden voltage rise of the grid is mainly determined by the voltage swell amplitude and is hardly affected by the output current of the converter.

Figure 44 is a block diagram of the high voltage ride-through control of a doubly-fed wind turbine after considering the power constraints of the converter. The specific control strategy is: when the grid voltage is lower than 1,1 p.u., the grid-side converter operates in the unit power factor control mode, and the rotor-side converter operates in the maximum wind energy tracking mode. Once the grid voltage is detected to rise to 1,1 p.u. and above, the grid-side converter is immediately switched to the bus voltage control mode, and the rotor-side converter is switched to the reactive power support mode. At the same time, in order to suppress the voltage rise of the bus voltage which may occur at the moment of sudden voltage change, the parallel DC unloading chopper circuit on the DC bus line triggers conduction at the voltage upper limit U_{dcmax} to ensure the safety of the DC link.

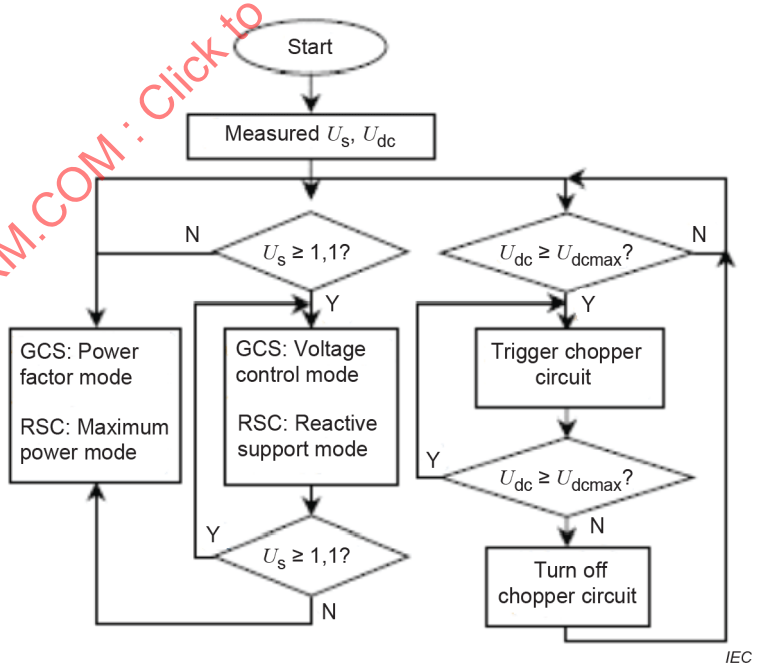

Figure 44 – Overvoltage ride-through control flow diagram

7.3.5 Multiple fault ride-through

7.3.5.1 General

Multiple fault ride-through refers to the ability of the wind turbine to maintain continuous operation in the grid when the system is subjected to two or more disturbances in succession. Under a single grid short circuit fault, the voltage drop or recovery causes the stator flux to generate a DC component, and the magnetic circuit coupling between the stator and rotor causes the rotor-side overcurrent and overvoltage. When the grid voltage drops, the electromagnetic torque decreases, the captured mechanical power cannot be sent out in time, and the power imbalance causes the speed to rise. Under multiple fault ride-through, the stator flux linkage DC component attenuation caused by the first fault ride-through and the power recovery after fault removal require time. At this time, the second fault ride-through occurs, and there will be a transient superposition effect, which will lead to multiple fault ride-through. Overvoltage and overcurrent problems are more serious, and speed control and power control are more difficult.

7.3.5.2 Speed characteristics analysis

The formula of motion of the motor rotor can be expressed by the following formula:

$$\omega = \omega_0 + \frac{1}{T_j}\int_{t1}^{t2}\left(P_{\mathrm{m}}/\omega - P_{\mathrm{e}}/\omega - D_{\omega}\right)dt \tag{97}$$

where:

ω_0 is the steady state value of the speed at the start of the fault;

P_{m} is the mechanical power of the motor;

P_{e} is the electromagnetic power of the motor;

D is the mechanical damping of the motor;

T_J is the motor rotor inertia time constant.

Considering the more serious multiple fault conditions, as shown in Figure 45, both voltages fall to 0,2 p.u. and the voltage drop duration is 625 ms. The interval between the first fault recovery and the second fault is 1 s.

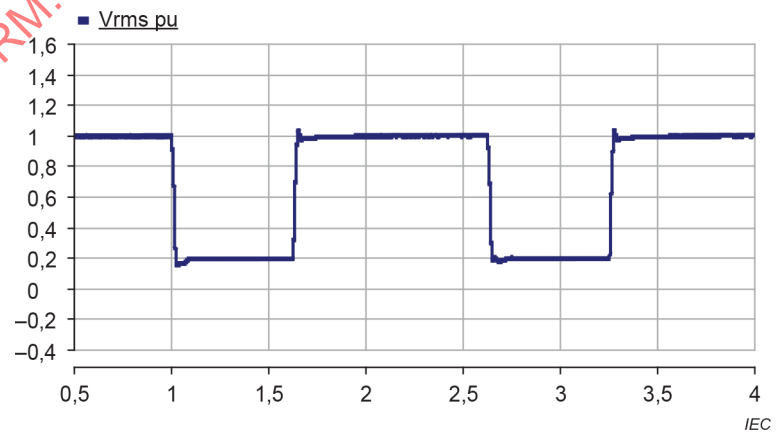

Figure 45 – Multiple fault conditions

The mechanical power P_m of the motor can be calculated by:

$$P_m = \frac{\pi}{2}\rho C_p R^2 V_w^3 \tag{98}$$

where

$C_p = f(\lambda, \beta)$, $\lambda = R\omega / V_w$.

According to a typical pitch angle control strategy, during fault crossing, as the speed increases, the pitch angle β will increase, thereby reducing the captured mechanical power, as shown in Figure 46. Typical adjustment characteristics for the pitch angle are typically 6 °/s.

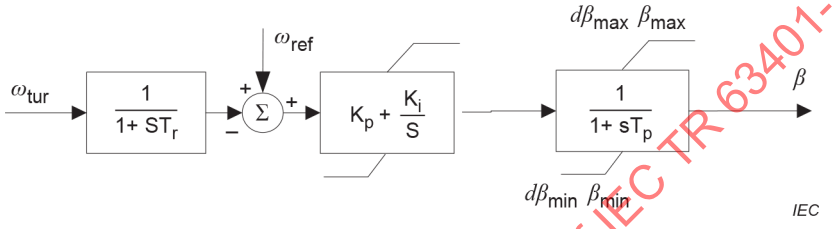

Figure 46 – Pitch angle control strategy

According to the requirements of the grid-connected technical guidelines, the wind turbine needs dynamic reactive current injection during the fault. Under the premise of meeting the reactive current injection, the residual capacity of the converter can be used to generate the active current. After the fault is removed, the active power needs to recover to at least the steady-state value before the fault within 10 s. The smaller the P_e, the more serious the rotor over speed problem. Therefore, considering the most serious situation, when the voltage drops to 0,2 p.u., the converter capacity is all used to generate reactive current, and the active current output is 0. After the fault is removed, the active power is recovered at a speed of 0,1 p.u./s.

Based on the typical characteristic analysis of P_m and P_e, the maximum value of the speed change under multiple fault ride-through can be approximated by calculating the shaded area as shown in Figure 47. It can be seen that compared with a single voltage drop, the continuous motor traverses the motor speed further, and there is a risk of motor overspeed.

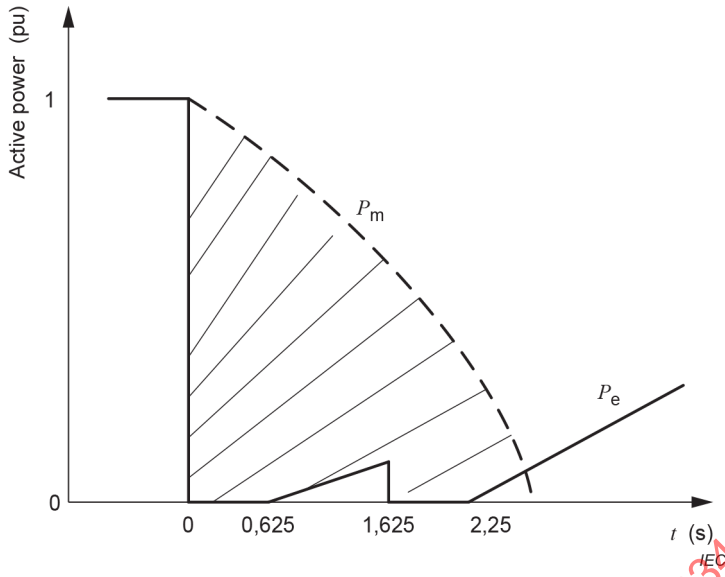

Figure 47 – Typical characteristics of P_m and P_e under multiple fault ride-through

7.3.5.3 Control strategy

In order to reduce the increase in the motor speed under the multiple fault ride-through, it is necessary to reduce the mechanical power captured by the wind turbine or increase the electromagnetic power of the output. The mechanical power can be reduced by increasing the adjustment speed of the wind turbine pitch angle. However, considering the mechanical constraints of the pitch system, the response speed of the pitch angle control is slow, and it is necessary to combine the flux linkage attenuation control and active power after fault removal. The recovery strategy is combined to achieve multiple fault ride-through.

1) After the fault is removed, the flux linkage attenuation control is quickly input to attenuate the DC component of the stator flux linkage.
2) Active power recovery control combines fast recovery and slow recovery. The active power is quickly restored to partial power, and then slowly restored to the pre-fault steady state value.

The power control loop of a wind turbine is typically implemented by a PI regulator. If the active power recovery slope limit after fault removal is directly increased, it may cause a pit phenomenon after active power recovery. Therefore, it is necessary to quickly recover the active power of the wind turbine to a partial power value by using the transient characteristic that the voltage of the terminal is rapidly increased after the fault is removed, and then perform the slope limitation of the active power recovery. Approximate analysis of the maximum value of the speed change under multiple fault ride-through is shown in the shaded area in Figure 48.

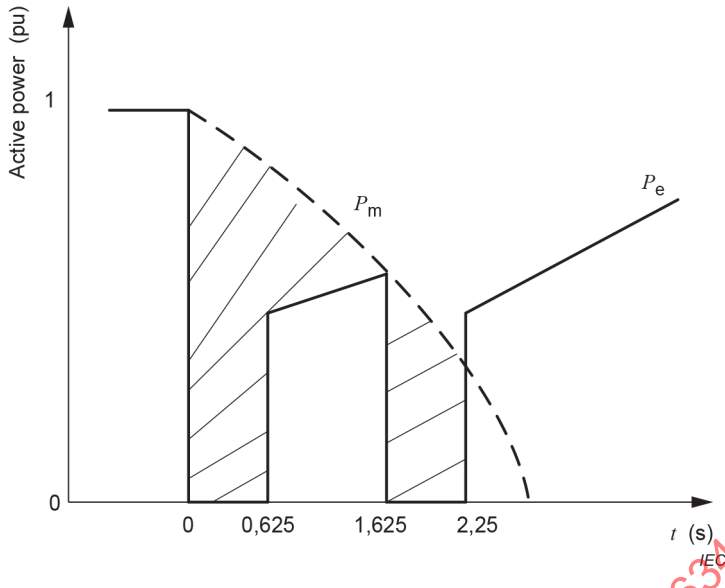

Figure 48 – Characteristics of P_m and P_e under multiple fault ride-through

7.3.6 Under and over -voltage ride-through in time sequence

Large-scale wind power transmission via HVDC has become one of the typical scenarios. Among various types of DC faults, commutation failure is one of the most common faults.

When the DC commutation fails, the AC voltage transient process of the sending end system is divided into three stages. Stage 1 (low voltage): the commutation failure causes the DC current to rise rapidly, and the converter station absorbs large-scale reactive power from the system, resulting in the voltage drop. Stage 2 (high voltage): the DC current decreases, and the inverter reactive power consumption decreases. There is an excess of reactive power, and there is an AC transient overvoltage. Stage 3 (voltage recovery): DC power gradually recovers to pre-fault level, the converter reactive power consumption gradually increases, and the reactive power is gradually balanced; the process can be represented by Figure 49. The DC near-zone's new energy units quickly transition from the low-voltage stage to the high-voltage stage, the grid-connected point voltage of the wind farm is within the contour line shown by the shadow, and the wind turbines in the wind farm should be guaranteed to operate continuously without going off the grid.

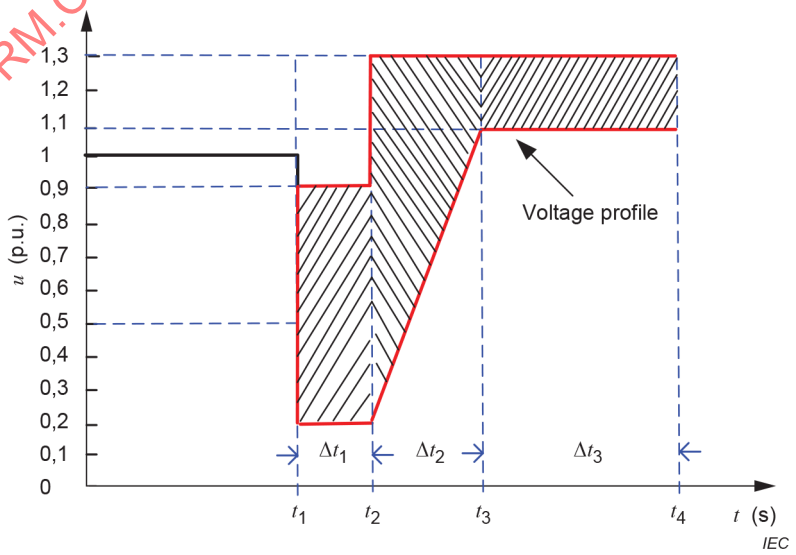

Figure 49 – Under/overvoltage ride-through curve

7.3.7 Active/reactive current support of inverter-based resource during fault

When the system fault causes the terminal voltage to drop, because the common control strategy of the doubly-fed wind turbine is to generate reactive power through the stator, and the reactive power of the grid-side converter control output is zero, the control of the dynamic reactive current can be directly considered to be the control of the absolute value of the stator reactive current during the fault:

$$\left|i_{q\_\text{stator}}^{\text{ref}}\right| \geq 1{,}5 \times (0{,}9 - U_{\text{T}})\, I_{\text{N}} \tag{99}$$

The relationship between the stator reactive current and the absolute value of the rotor reactive current is as follows:

$$\left|i_{q\_\text{stator}}\right| = \frac{U_{\text{S}}}{\omega_s L_s} + \frac{L_m}{L_s}\left|i_{q\_\text{rotor}}\right| \tag{100}$$

For the rotor current reference value, see Formula (101):

$$\left|i_{q\_\text{rotor}}^{\text{ref}}\right| \geq \frac{L_s}{L_m} 1{,}5 \times (0{,}9 - U_{\text{T}})\, I_{\text{N}} - \frac{U_s}{\omega_s L_m} \tag{101}$$

In the formula, U_{T} is the wind farm grid point voltage. When conducting the control strategy research, it is equivalent to the wind turbine motor terminal voltage. Since the terminal voltage is equal to the stator voltage, ie $U_{\text{T}} = U_{\text{S}}$, the above formula can be expressed as Formula (102):

$$\begin{aligned}
\left|i_{q_\text{rotor}}^{\text{ref}}\right| &\geq \frac{L_s}{L_m} 1{,}5 \times (0{,}9 - U_{\text{T}})\, I_{\text{N}} - \frac{U_T}{\omega_s L_m} \\
&\geq \frac{L_s}{L_m} 1{,}5 \times (0{,}9 - U_{\text{T}})\, I_{\text{N}} - \frac{U_T - 0{,}9}{\omega_s L_m} - \frac{0{,}9}{\omega_s L_m} \\
&\geq \left(\frac{L_s}{L_m} 1{,}5 \times I_{\text{N}} + \frac{1}{\omega_s L_m}\right)(0{,}9 - U_{\text{T}}) - \frac{0{,}9}{\omega_s L_m} \\
&\geq k(0{,}9 - U_{\text{T}}) - c
\end{aligned} \tag{102}$$

where:

$$k = \left(\frac{L_s}{L_m} 1{,}5 \times I_{\text{N}} + \frac{1}{\omega_s L_m}\right), \quad c = \frac{0{,}9}{\omega_s L_m}.$$

The rotor reactive current reference value $\left|i_{d\_\text{rotor}}^{\text{ref}}\right|$ is calculated according to Formula (102), and the rotor active current reference value $\left|i_{q\_\text{rotor}}^{\text{ref}}\right|$ is calculated on the premise that the active current is generated as much as possible under the premise of meeting the national standard reactive power injection. In the control, k can be set as a variable parameter, according to the actual situation, by adjusting the reactive current generated by the wind turbine, and compensating the error caused by U_{T} equivalent to the voltage of the wind turbine unit. The adjustment range is $k \geq (L_s / L_m)1{,}5 \times I_{\text{N}} + 1/(\omega_s L_m)$. Therefore, the formula of the rotor active/reactive current reference value is as follows, where $I_{\text{rotor}}^{\text{over}}$ is the maximum overcurrent that the wind turbine can withstand.

$$\begin{cases} \left|i_{q\_\text{rotor}}^{\text{ref}}\right| = k(0{,}9 - U_{\text{T}}) - c \\ \left|i_{d\_\text{rotor}}^{\text{ref}}\right| = \sqrt{\left(I_{\text{rotor}}^{\text{over}}\right)^2 - \left(i_{q\_\text{rotor}}^{\text{ref}}\right)^2} \end{cases} \tag{103}$$

7.4 Operating experiences

7.4.1 Operating experience – China

The installed capacity of wind power in Jiuquan area at the end of 2011 was 5 403 MW. Among them, the main wind farms with 330 kV integration are 4 100 MW, which are divided into Ganhekou wind area, Beidaqiao wind area, Changma wind area and Qiaowan wind area. Among them, the total was 1 600 MW wind power in the Ganhekou wind area, 1 300 MW in the Beidaqiao wind area, 600 MW in the Changma wind area, and 600 MW in the Qiaowan wind area. The diagram of the Jiuquan base wind farms is shown in Figure 50.

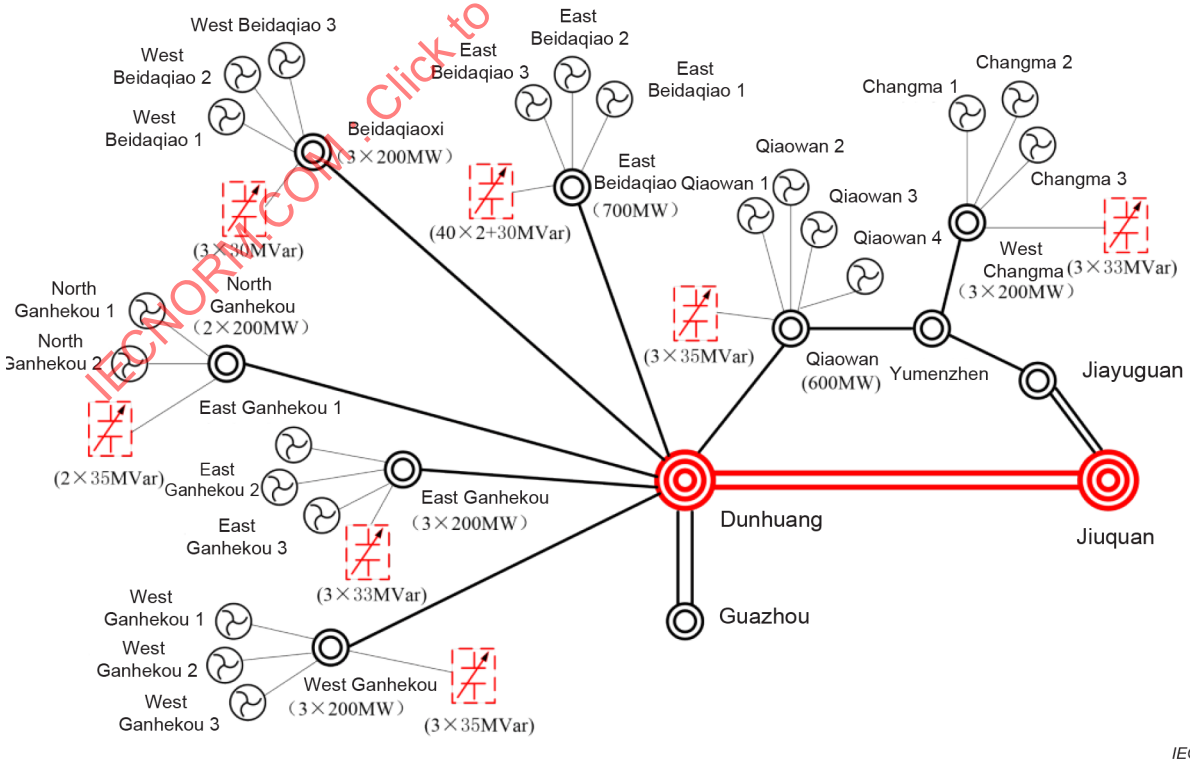

Figure 50 – Circuit diagram in Jiuquan

At 00:34 on February 24, 2011, the 35 kV side equipment of the first wind farm in Qiaoxi was faulty, causing the loss of Jiuquan wind power output to 777 MW, and the frequency of the whole network was reduced to 49,854 Hz. The accident occurred as shown in Figure 51.

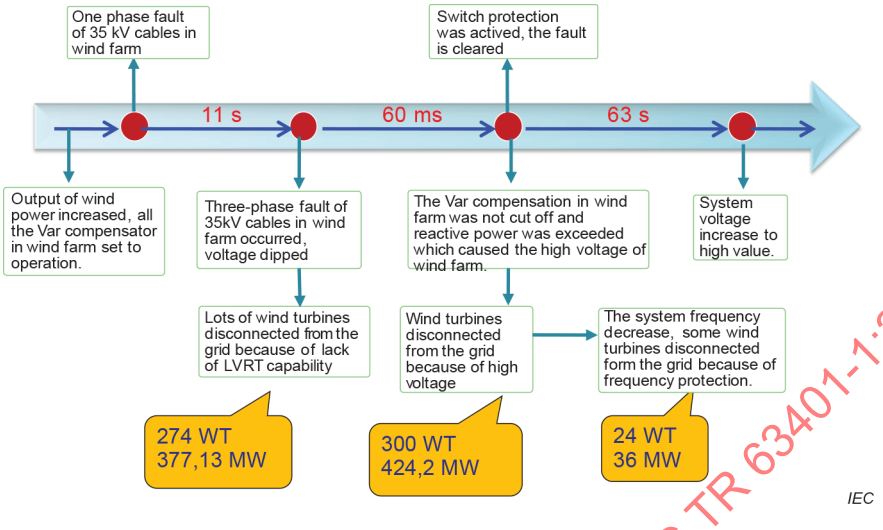

Figure 51 – Analysis of wind power disconnection incident

Before the failure, the base wind power was higher, and the reactive power compensation devices were all put into operation.

1) In the first stage, the C-phase breakdown of the 35 kV switchgear cable head of the Qiaoxi wind farm was broken. After 11 s, the single-phase short circuit developed into a three-phase fault, which caused the system voltage to drop. A large number of wind turbines in the wind power base that do not have low voltage ride-through capability were disconnected, and a total of 274 turbines were disconnected, and the loss power was about 400 MW.
2) In the second stage, after a large number of wind turbines were disconnected, the reactive devices did not operate in time, resulting in overvoltage caused by excess reactive power in the base. A large number of wind turbines were disconnected from the grid due to excessive voltage protection, and a total of 300 turbines were cut off, losing power of about 420 MW.
3) In the third stage, due to a large amount of power loss, the frequency of the system was reduced, and some turbines were disconnected due to the frequency limit. A total of 24 turbines were cut off, and the power loss was close to 40 MW.

7.4.2 Operating experience

Application of wind plants in weak systems can raise concerns about system stability, voltage regulation and post-fault power swings. Some connecting utilities require conditions such that wind plants shall not trip during faults and other system disturbances. Handling of post fault electromechanical swings in the power grid can be particularly challenging in weak grid applications. Subclause 7.4.2 reports on the experience of one manufacturer and how these challenges have been addressed.

The latest generation of wind turbine-generator controls can include wind farm management systems (WFMS) and low-voltage ride-through (LVRT) among other features. The addition of these control features to a wind plant applied in a weak grid location can provide much improved performance over previous generations of wind generation equipment.

Figure 52 shows the response of a wind plant, consisting of 108 GE 1,5 MW wind turbine generators, to 60 min of highly variable wind speed. This wind plant is connected to the grid by a dedicated 75 km 230 kV transmission line. The short circuit capacity at the remote point of grid interconnection is quite low compared to the rating of the wind plant, approximately 670 MVA, which is a short circuit ratio of approximately 4,1. At the wind plant collector system, the short circuit ratio is much lower, less than 2,5.

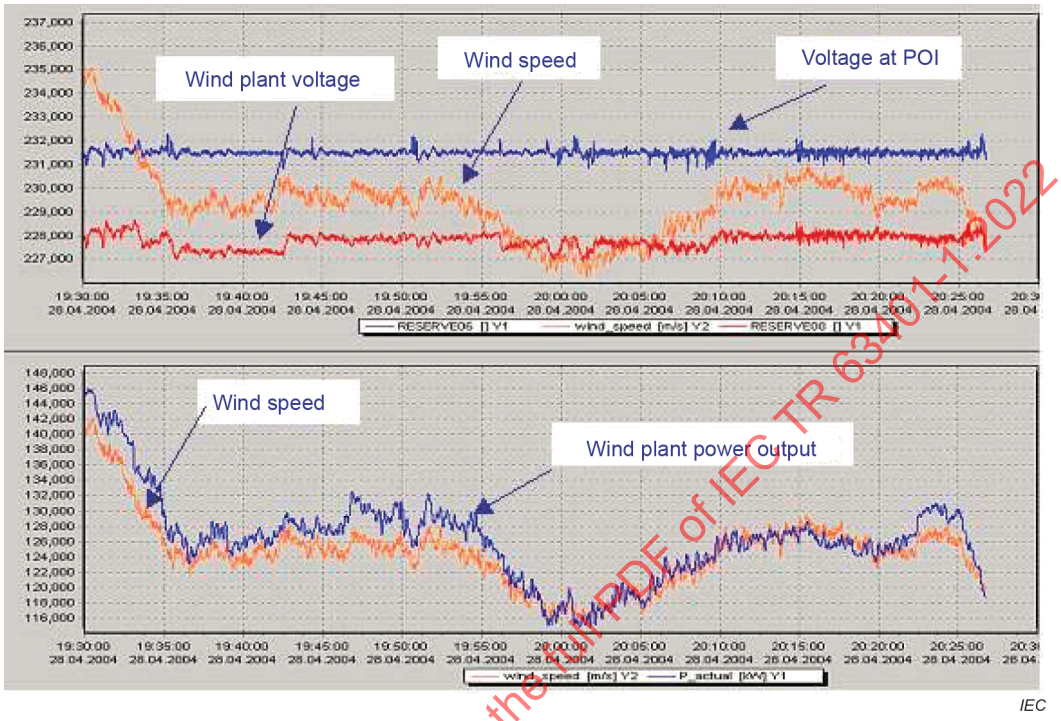

Figure 52 – Demonstration of voltage regulation performance during variable power output conditions

The specifications of this particular system required regulation of the voltage at a remote point of grid interconnection. To avoid dependence on telecommunications, the wind plant control system line drop compensating feature was used to synthesize the voltage at the point of interconnection, 75 km from the measurement points at the wind plant substation.

Despite the challenges of a very weak grid and the requirement of regulation of a remote voltage, performance of this system has been excellent. The upper chart of Figure 52 shows the wind plant voltage and the voltage at the point of grid interconnection. The wind velocity is also shown, but without a scale. In the lower chart of Figure 52, the same wind velocity is shown, along with the wind plant power output. Despite rather large variations in generated power, the voltage at the interconnection bus is quite invariant. The voltage flicker index, P_{st}, is less than 0,02 for this high stress condition – well within industry expectations. Most of the voltage variations are within a few hundred volts on the 230 kV system.

This example demonstrates that with proper control algorithms and coordination, in this case WFMS and UVRT, the performance of a wind plant can be improved even in weak grid applications.